© The Authors, 2011. Journal compilation © Australian Museum, Sydney, 2011
Records of the Australian Museum (2011) Vol. 63: 203–266. ISSN 0067-1975
doi:10.3853/j.0067-1975.63.2011.1586

Middle to Late Ordovician (Darriwilian-Sandbian) Conodonts from the Dawangou Section, Kalpin Area of the Tarim Basin, Northwestern China

YONG YI ZHEN[1]*, ZHIHAO WANG[2], YUANDONG ZHANG[2], STIG M. BERGSTRÖM[3], IAN G. PERCIVAL[4] AND JUNFENG CHENG[2]

[1] Australian Museum, 6 College Street, Sydney NSW 2010, Australia
yongyi.zhen@austmus.gov.au

[2] LPS, Nanjing Institute of Geology and Palaeontology, Chinese Academy of Sciences, Nanjing 210008, China
zhwang@nigpas.ac.cn · ydzhang@nigpas.ac.cn · cjfcjf1983@163.com

[3] School of Earth Sciences, Division of Earth History, The Ohio State University, Columbus, Ohio 43210, United States of America
stig@geology.ohio-state.edu

[4] Geological Survey of New South Wales, W B Clarke Geoscience Centre, 947–953 Londonderry Road, Londonderry NSW 2753, Australia
ian.percival@industry.nsw.gov.au

ABSTRACT. Forty-four conodont species are documented from the Dawangou section in the Tarim Basin, which spans the Darriwilian to Sandbian interval and is the global auxiliary stratotype for the base of the Upper Ordovician. Five conodont zones are recognized in this section, including the *Yangtzeplacognathus crassus*, *Histiodella holodentata* and *H. kristinae* zones in the upper part of the Dawangou Formation, the *Pygodus anserinus* Zone from the upper part of the Saergan Formation to the lower part of the Kanling Formation, and the *Baltoniodus alobatus* Zone in the upper part of the Kanling Formation. Presence of the *P. serra* Zone is based on occurrences of this species on shale bedding planes in the lower and middle Saergan Formation, but could not be confirmed in acid-leached samples studied from this interval. The Middle/Upper Ordovician boundary occurs within graptolitic black shale of the upper Saergan Formation. Although the boundary interval was intensively sampled, conodonts were very rare, probably due to stagnant or stratified basinal environments. This documentation of the conodont faunas and biostratigraphy of the Dawangou section is considered preliminary and more detailed conodont studies are required, but the remoteness of the site hinders the further extensive sample collection needed for this purpose.

ZHEN, Y. Y., Z. H. WANG, Y. D. ZHANG, S. M. BERGSTRÖM, I. G. PERCIVAL, AND J. F. CHEN. 2011. Middle to Late Ordovician (Darriwilian-Sandbian) conodonts from the Dawangou section, Kalpin area of the Tarim Basin, northwestern China. *Records of the Australian Museum* 63(3):203–266.

KEYWORDS: Conodonts, Ordovician, Darriwilian, Sandbian, biostratigraphy, Tarim, China

* author for correspondence

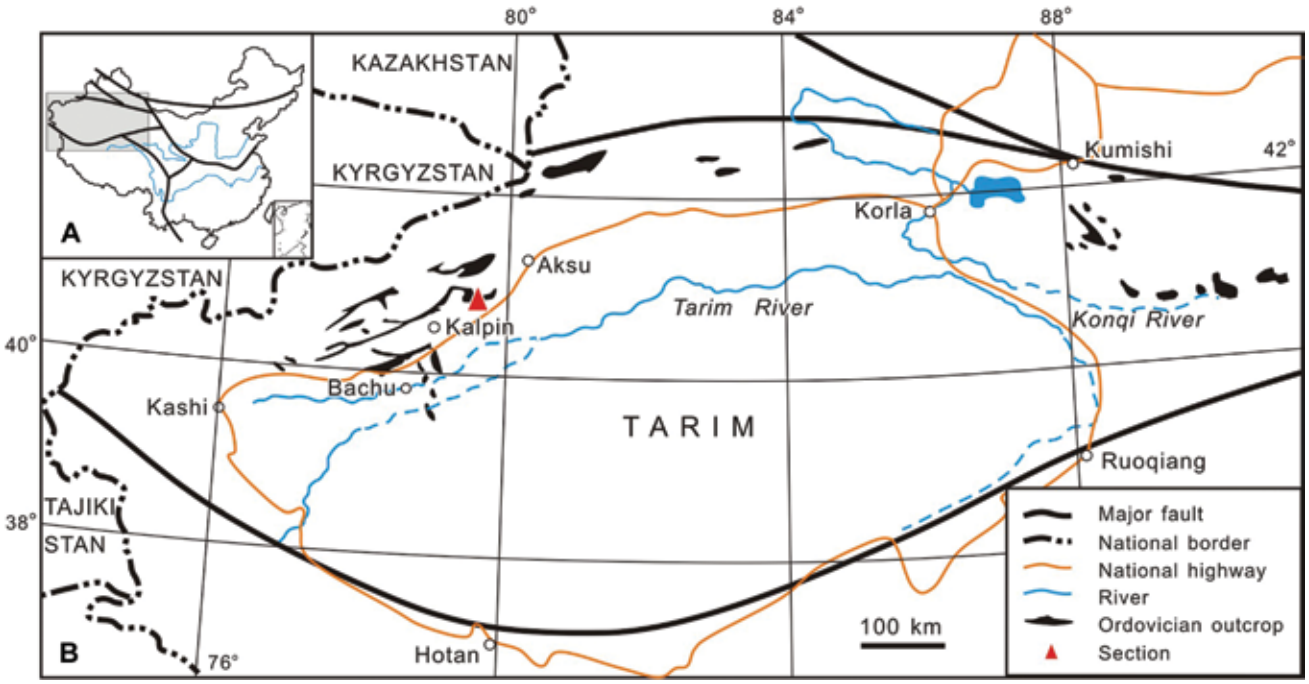

Figure 1. Locality map. ***A***, map of China showing the location of the Tarim Basin in northwestern China; ***B***, Map showing the outline of the Tarim Basin, outcrops of the Ordovician strata, and the location of the Dawangou section (red triangle), Kalpin, Xinjiang Autonomous Region, China.

Ordovician conodonts from the Dawangou section of the Tarim Basin were first reported by Zhou *et al.* (in Zhou & Chen, 1990, 1992, p. 66–79) who listed occurrences from the Dawangou Formation (Upper Qiulitag Group) to the Qilang Formation. They recognized eight conodont zones from the Dawangou Formation to the Kanling Formation (Zhou & Chen, 1992, fig. 3.2). Ordovician conodonts from this section were also reported briefly in several other publications (Gao, 1991; Bergström & Wang, 1998; Wang & Zhou, 1998; Bergström *et al.*, 1999; 2000; Wang, 2001), but no detailed systematic treatment of the conodont faunas from the Dawangou section has previously been published.

In the late 1990's, the Dawangou section was considered, along with the Fågelsång Section of southern Sweden and the Calera Section of USA, as potential GSSP candidates for the base of the Upper Ordovician (Bergström *et al.*, 1999). Through a world-wide assessment process organized by the Ordovician Subcommission of the International Commission on Stratigraphy, the Fågelsång Section was chosen as the global boundary stratotype (defined by the FAD of graptolite *Nemagraptus gracilis*), and the Dawangou section of the Tarim Basin was selected as an auxiliary stratotype (Bergström *et al.*, 2000). To fulfill its role as a standard reference assisting precise regional and international correlation of the Middle/Upper Ordovician boundary, detailed documentation of the conodont faunas from this level in the upper part of the Saergan Formation and lower part of the Kanling Formation is of great importance. This contribution, mainly based on collections made in 1987 by the Nanjing Institute of Geology and Palaeontology, supplemented by additional material collected on a field trip during 2008, addresses this imperative.

Regional geological and stratigraphic setting

Located in the central and southern part of the Xinjiang Autonomous Region of far northwestern China, the Tarim Basin (Fig. 1) is the largest inland sedimentary basin of China, covering an area of about 570,000 km^2 with the Tianshan Mountains bordering to the north and northwest, the Kunlun Mountains to the southwest and the Altun Mountains to the southeast. Much of the interior of the basin is covered by China's largest desert, the Taklamakan Desert. The Kunlun Mountains extending over 2,000 km represent a complex geological entity evolved through sedimentation, volcanism, deformations, subduction–accretions, collisions between Gondwana (or peri-Gondwanan terranes) and several Kunlun Terranes primarily during various orogenic episodes throughout the Palaeozoic and the Early Mesozoic, and the closure of the eastern parts of the Palaeo-Tethys Ocean (Yao & Hsü, 1994; Pan *et al.*, 1996). They are widely regarded as the "back bone" of today's China by joining the Pamir Mountains to the west and the Qilian Mountains to the east along the north edge of the Tibetan Plateau, with the Qinling Mountains further to the east. The Tianshan Mountains form an intracontinental mountain range stretching some 2,800 km eastward from Tashkent in Uzbekistan, that initially formed in the Late Palaeozoic following the collision and coalescence of the Tarim Plate and the Siberia-Kazakhstan plates (Windley *et al.*, 1990; Zhou & Chen, 1992). This region was reactivated in the Cenozoic during the Himalayan Orogeny (Molnar & Tapponnier, 1975), and remains active as a modern example of large-scale continental deformation resulting from the India-Eurasia convergence (Wang *et al.*, 2001).

The Tarim Basin is the remnant of an independent palaeo-plate with a long and complicated geological history, characterized by collisions, accretions and amalgamations, compressions, and intracontinental mountain building on its edges, which were mainly associated with the Indian Plate moving northward against Eurasia since the Mesozoic (Zhou & Chen, 1992; Zhou & Lin, 1995). It consists of basement comprising Proterozoic and Archaean metamorphic complexes, overlain by a very thick succession (locally exceeding 31 km) of shelf-marine-dominated Upper Proterozoic (Sinian) to Palaeozoic sediments, and predominantly non-marine deposits of the latest Palaeozoic (Late Permian) to Cenozoic (Wang *et al*., 1992, table 2).

Owing to the development of a huge overburden of the Taklamakan Desert that came into existence in the late Miocene, in association with the formation and depression of the basin, and the accumulation of thick successions of foreland deposits fringing the uplifted mountain ranges, Palaeozoic and older rocks are mainly exposed along the basin margins. Outcrops of Late Proterozoic (Sinian) and Early Palaeozoic strata are largely restricted to two areas on the western and northeastern margins of the Tarim Basin, whereas the Late Palaeozoic rocks are more widely distributed (Zhou & Chen, 1992).

During the Ordovician, the Tarim Basin, as a peri-Gondwanan palaeo-plate, was situated at low to middle latitudes of the Southern Hemisphere (Zhao *et al*., 1996; Huang *et al*., 2000; Li & Powell, 2001), and received carbonate-dominated marine shelf deposits with a total thickness up to 6000 m (He *et al*., 2007) that are now only exposed in western Tarim (Kalpin-Bachu areas) and in northeastern Tarim (Queerqueke-Uligezhitag areas; see Fig. 1). However, subsurface data revealed by petroleum boreholes and seismic stratigraphy indicate that Ordovician rocks are much more widely distributed underneath the extensive Cenozoic desert cover (Zhou & Chen, 1992; Zhao *et al*., 2000).

Analysis of the Ordovician lithofacies and biofacies (Zhou & Chen, 1992; He *et al*., 2007; Wang *et al*., 2007) indicated the existence of an intracratonic basin in the northeast part of Tarim Basin that extended further westward, crossing the entire northern Tarim plate on an east-west trend. It is characterized by turbidite successions with radiolarian siliciclastics (bathyal to abyssal), graptolitic black shale (shallow and stagnant basin), and rhythmically alternating sandstones, siltstones, shales and minor calcarenites (shallow trough; more than 2500 m in thickness in the Queerqueke area) (Zhong & Hao, 1990; Wang *et al*., 2008). The basinal facies is flanked on its southern side by a narrow and continuous zone of slope facies (Nileid trilobite biofacies). As the transitional zone between the basin (or trough) and the platform, the slope facies is mainly composed of argillaceous-laminated or nodular calcilutite, calcarenite and calcirudite intercalated with shale. The Mid-Tianshan Islands of Ordovician time, situated along the northern margin of the Tarim plate, and the uplifts on the southeastern margin of the basin, were subjected to erosion, and might be the major source regions of the terrigenous material, while the carbonate platform (occupying a vast area in the central-western part of the Tarim plate) received shallow marine carbonate deposits during the Ordovician. Spatial and temporal distribution patterns reflecting the expansion and contraction of these two contrasting sedimentary systems (or megafacies) throughout the Ordovician, namely the deeper siliciclastic basin or trough regime and the shallow carbonate platform regime, were largely controlled by sea level changes and regional transgressive and regressive events.

Ordovician rocks are well exposed along the Dawangou, a narrow but deep erosional stream-cut gorge on the western slope of the Tianshan Mountains, about 15 km northwest of the Yingan Village in Kalpin County, northwestern Tarim Basin (Fig. 1). Zhou & Chen (1992, p. 66–79, fig. 3–2) provided a detailed stratigraphic log of the section and faunal lists. Part of the material in the current study (39 samples with prefix Nj, see Fig. 2, Table 1) formed the basis of the conodont data presented by Zhou & Chen (1992). The Ordovician System at the Dawangou gorge conformably overlies the Late Cambrian Awatag Group and is itself disconformably overlain by the Early Silurian Kalpintag Formation. The Ordovician section consists of 26 Beds that are grouped into six lithostratigraphic units with a total thickness of 748.44 m. The area was located in a transitional facies zone, with the lower part of the succession (Early Ordovician Qiulitag Group) deposited in a shallow water carbonate platform setting, the Saergan Formation (late Darriwilian to early Sandbian age) and the Yingan Formation (Katian) accumulated in a basinal setting, whereas the Middle Ordovician Dawangou Formation and the Late Ordovician Kanling and Qilang formations were primarily deposited in a slope setting.

The stratotype of the Dawangou Formation proposed by Zhou *et al*. (1991; also see Zhao & Zhang, 1991, p. 66) is exposed on the north side of Yingan Mountain located to the northwest of the Yingan village (not far from the Dawangou section). It consists of 15.1 m of greyish medium- to thinly-bedded nodular biocalcilutites, with glauconitic algal-bound biocalcilutites in the middle part and irregular cherty bands in the basal part. In the Dawangou section, the Dawangou Formation is equivalent to Bed 10 of Zhou & Chen (1990, 1992; see Wang & Zhou, 1998, text-fig. 1; Zhou *et al*., 1998, text-fig. 2), and consists of 22 m of greyish medium- to thinly-bedded nodular biocalcilutites and biocalcarenites with glauconite and cherty masses and bands. It forms a lithologically distinctive unit that can be easily differentiated from the underlying mainly thick-bedded algal-laminated limestones of the upper part of the Upper Qiulitag Group, and from black shales of the overlying Saergan Formation. The Dawangou Formation, which is extensively exposed along the northwestern margin of the Tarim Basin, was deposited in a generally calm, upper slope environment with a depositional depth generally not much greater than 70 m (Zhou *et al*., 1998). A significant transgressive event occurred in the region during the late Middle Ordovician (Darriwilian) and earliest Late Ordovician, indicated by a conformable transition from the open, shallow water carbonate platform setting of the Upper Qiulitag Group, through the slope setting of the Dawangou Formation, to the basinal setting of the Saergan Formation.

The name Saergan Formation is derived from the Saergan Series that was initially proposed for all the Ordovician rocks above the Qiulitag Group. It was restricted to only about 14 m of black calcareous graptolitic shale with limestone lenses distributed in the Kalpin area (Chen *et al*., 1995). As one of the most important Ordovician source rocks for petroleum in the Tarim Basin, this condensed black shale unit with abundant pyrite and organic material (Cai *et al*., 2009) was likely deposited in an euxinic bottom

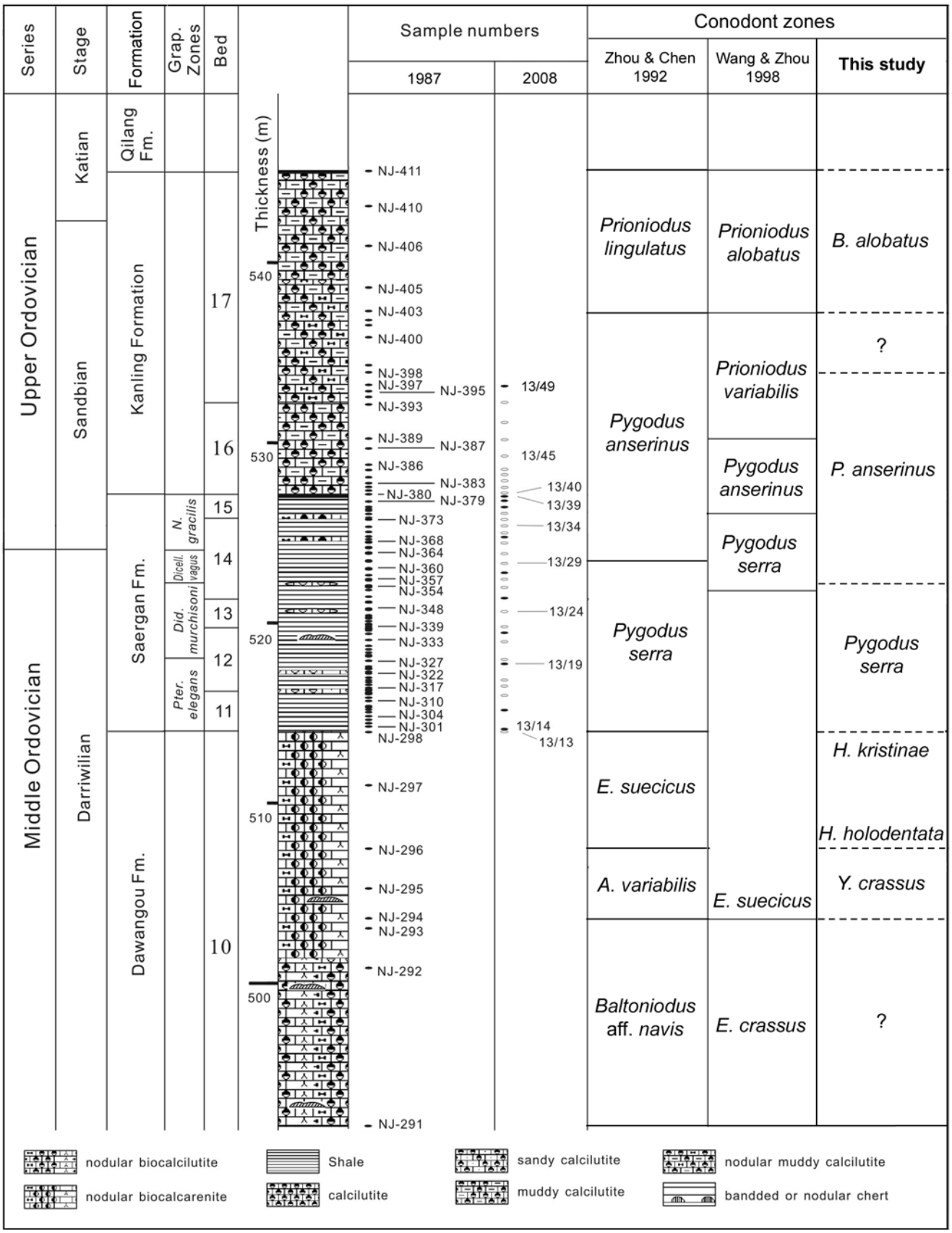

Figure 2. Stratigraphy and conodont sampling positions of the Dawangou section (Dawangou, Saergan and Kanling formations), Kalpin, Xinjiang Autonomous Region, China.

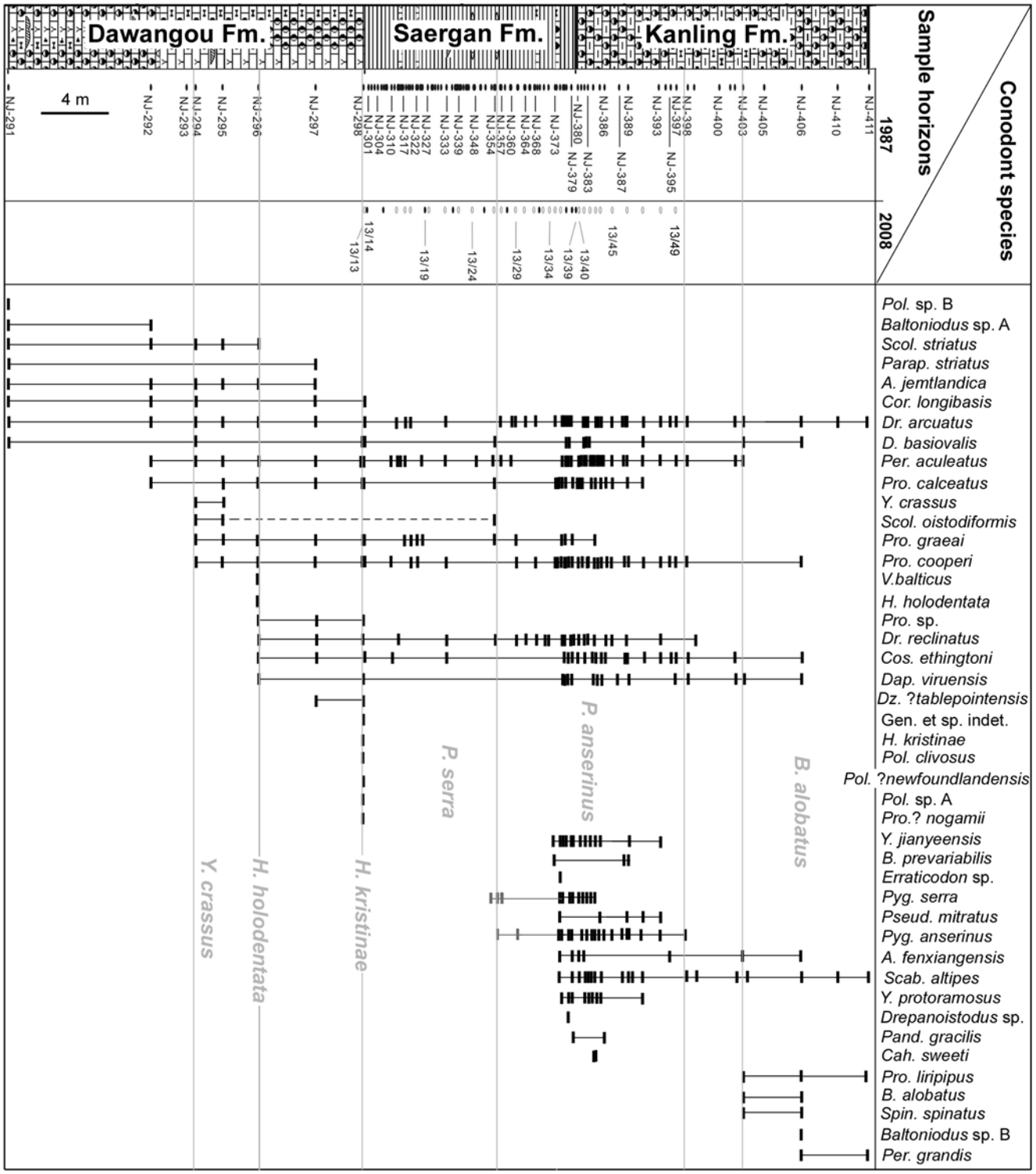

Figure 3. Conodont occurrences recorded in this study from the Dawangou section (Dawangou, Saergan and Kanling formations), Kalpin, Xinjiang Autonomous Region, China.

water environment of restricted circulation and stagnant or stratified conditions. The overlying Kanling Formation (Sandbian), consisting of 17–36 m of purplish red and greyish green to grey thin-to medium-bedded calcilutites, is widely exposed in the Kalpin area, with its stratotype located at Kanling, near Yingan Village, where it is also 18 m in thickness as in the Dawangou section (Fig. 2).

Systematic studies of the other fossil groups from the Dawangou section include the trilobites from the Dawangou Formation (Zhou *et al.*, 1998), chitinozoans from the Saergan Formation (Hennissen *et al.*, 2010), and acritarchs (Li *et al.*, 2006). A detailed monographic documentation of the trilobite faunas from this section is currently in preparation (Z. Y. Zhou pers. comm.).

Conodont biostratigraphy and regional correlation

Zhou & Chen (1990, 1992) recognized six informal conodont zones from the Dawangou Formation to Kanling Formation of the Dawangou section at Kalpin in the Tarim Basin (Fig. 2; also see Zhou & Chen, 1992, p. 80, fig. 3–2), which were further revised by Wang & Zhou (1998, fig. 1). Bergström *et al*. (1999) recognized two conodont zones (the *P. serra* and *P. anserinus* zones) in the Saergan Formation. In this study the conodont biostratigraphic framework proposed by previous authors was re-assessed, based on material collected from two field trips (Tables 1–2). Five conodont zones can now be recognized, although due to data limitation, their upper and lower boundaries are yet to be precisely defined (Fig. 2). As an auxiliary stratotype for the base of the Upper Ordovician, more detailed conodont studies are required, but the remoteness of the site hinders collection of the numerous samples needed for this purpose.

***Baltoniodus alobatus* Zone**: In the upper part of the Kanling Formation (from samples Nj 403 to Nj 411), Zhou & Chen (1992) recognized the *Prioniodus lingulatus* Zone with some 11 conodont species (authors' original identifications) recovered from this interval including *Dapsilodus mutatus, Prioniodus lingulatus, Protopanderodus liripipus, P. rectus, Periodon grandis, Scabbardella altipes, Spinodus spinatus*, *Drepanodus* sp., *Eoplacognathus* sp., *Panderodus* sp., and *Prioniodus* sp. Wang & Zhou (1998, text-fig. 1) referred to this interval as the *Prioniodus alobatus* zone and recorded the occurrence of 22 conodont species (authors' original identifications) from the Dawangou section, including *Ansella nevadensis*, *Cornuodus longibasis*, *Dapsilodus mutatus, Drepanoistodus venustus, D.* sp., *Eoplacognathus jianyeensis*, *E.* sp. B, gen. et sp. indet., *Paltodus*? *jemtlandicus*, *Periodon grandis, Protopanderodus cooperi*, *P. liripipus, P. rectus*, *P. robustus*, *P. varicostatus*, *Prioniodus alobatus*, *P. variabilis*, *P.* sp., *Scabbardella altipes, Spinodus spinatus*, and *Walliserodus ethingtoni*. Our re-examination of conodont specimens recovered from five samples through this interval has confirmed the occurrence of the following 13 species (Fig. 3): *Ansella fenxiangensis, Baltoniodus alobatus, B.* sp. B, *Costiconus ethingtoni, Dapsilodus viruensis, Drepanodus arcuatus, Drepanoistodus basiovalis, Periodon aculeatus, P. grandis, Protopanderodus cooperi, P. liripipus, Scabbardella altipes,* and *Spinodus spinatus*.

Prioniodus lingulatus An, 1987 is considered herein as a junior synonym of *Baltoniodus alobatus* (Bergström, 1971) (see further discussion under Systematic Palaeontology section). This morphologically distinctive species with a wide platform-like posterior process has been widely reported in Europe (Bergström, 1971; Dzik, 1994), North America (Kennedy *et al*., 1979; Nowlan, 1981; Leslie, 2000), Precordilleran Argentina (Ortega *et al*., 2008), Tarim (Zhong, 1990; Wang & Zhou, 1998; Zhao *et al*., 2000; Xiong *et al*., 2006; this study), South China (An, 1981; Zeng *et al*., 1983; An, 1987; Chen *et al*., 2011) and southeast Asia (Agematsu *et al*., 2006, 2008a). Based on a collection of more than 100,000 identified conodont specimens from some 40 stratigraphic sections of the Swedish Middle-Upper Ordovician, Bergström (1971) established the conodont biostratigraphic zonal succession (including five zones and ten subzones) for Baltoscandia, and recognized *B. alobatus* as the index species for the upper Subzone of the *Amorphognathus tvaerensis* Zone of the Upper Ordovician. The *B. alobatus* Subzone, with its base marked by the first appearance (FAD) of *B. alobatus* and with top defined by the first appearance (FAD) of *Amorphognathus superbus* (Rhodes), was originally correlated with the upper part of the British graptolite *Diplograptus multidens* zone (Bergström, 1971, p. 101), equivalent to the *C. bicornis* Zone of late Sandbian age (Webby *et al*., 2004; Bergström *et al*., 2009). The upper boundary of the *B. alobatus* Subzone (*A. tvaerensis* Zone) is generally correlated with the basal part of the *Belodina confluens* Zone of the North American Midcontinent succession (Webby *et al*., 2004; Bergström *et al*., 2010, fig. 3).

The *B. alobatus* Subzone spanned the interval when enormous explosive volcanic eruptions took place in the Iapetus Ocean with volcanic ash layers (K-bentonites) widespread over much of eastern and central North America (Millbrig) and in Baltoscandia (Kinnekulle), representing the largest volcanic ash falls in the Earth's Phanerozoic history (Bergström *et al*., 2004). In Baltoscandia, the Kinnekulle K-bentonite Bed forms a prominent stratigraphical marker defining the base of the Keila Stage (Hints & Nõlvak, 1999). Biostratigraphic studies suggest a correlation of the North American Millbrig K-bentonite with the upper part of the *Phragmodus undatus* conodont Zone (upper *C. bicornis* graptolite Zone). The Baltoscandian Kinnekulle K-bentonite Bed is in the upper part of the *D. foliaceus* (formerly *multidens*) graptolite Zone (Huff *et al.*, 1992; Bergström *et al*., 2004), which was correlated with the *B. alobatus* conodont Subzone (Webby *et al*., 2004).

In the Tarim Basin, *B. alobatus* was reported from the Queerqueke Formation of the northeastern part of the Tarim Basin (Zhong, 1990), the Qiaerbake Formation in Bachu (Xiong *et al*., 2006), the Tumuxiuk Formation in subsurface core (Zhao *et al*., 2000), and from the upper part of the Kanling Formation near Kalpin (Zhou & Chen, 1992; Wang & Zhou, 1998; Zhao *et al*., 2000; this study). In South China, An (1987) proposed the *P. lingulatus* Zone based on the conodont assemblage from the upper part of the Datianba Formation of Guizhou and Jiangsu, with the holotype of *P. lingulatus* recovered from the top Datianba Formation in the Ganxi Section of Yanhe County, Guizhou (An, 1987, p. 35, pl. 25, fig. 17) in association with *Belodella* sp., *Drepanoistodus* sp., *Panderodus gracilis, Prioniodus* sp. and *Scabbardella similaris* (An's original identifications). In the lower part of the Datianba Formation the *Eoplacognathus jianyeensis* Zone includes the nominate species associated with *Complexodus pugionifer*, *Panderodus gracilis, Periodon aculeatus*, *Prioniodus alobatus*, *P. variabilis*, *P.* sp., and *Protopanderodus* sp. An (1987, table 3) correlated the *P. lingulatus* Zone with the *B. alobatus* Subzone of the North American Midcontinent succession. As *B. lingulatus* is now considered a junior synonym of *B. alobatus* (see discussion under Systematic Palaeontology Section), the *B. alobatus* Subzone should then be correlated with the entire 3.4 m thick Datianba Formation in the Ganxi section in Guizhou. However, in the Dawangou section of the Tarim Basin, *Y. jianyeensis* occurs in a stratigraphically slightly lower interval (in the top part of the Saergan Formation and the lower part of the Kanling Formation) in association with *P. anserinus* and others, an assemblage similar to that documented from the top part of the Datianba Formation in Hunan, South China (Zhang, 1998c).

Protopanderodus liripipus is a widely distributed species with a relatively long stratigraphic range from the upper *A. tvaerensis* Zone to *A. ordovicicus* Zone (Sweet, 1988), reported from North America (Kennedy *et al*., 1979; McCracken, 1989; Leslie, 2000; Pyle & Barnes, 2001), Europe (Bergström, 1990, 2007; Dzik, 1994), Australia (Burrett *et al*., 1983; Trotter & Webby, 1994; Zhen *et al*., 1999), North China (Wang & Lou, 1984; An & Zheng, 1990), Tarim Basin (Gao, 1991; Zhao *et al*., 2000; Wang, 2001; Wang & Qi, 2001), South China (An *et al*., 1981; An *et al*., 1985; An, 1987; Ding *et al*. in Wang, 1993) and southeast Asia (Agematsu *et al*., 2007, 2008a). *Periodon grandis* also had a wide distribution globally, with first appearance in the *undatus* Zone and disappearing in the upper part of the *A. superbus* Zone (Webers, 1966), a level slightly younger than the *velicuspis* Zone in the North American Midcontinent succession.

***Pygodus anserinus* Zone**: This zone is represented by the whole range of *P. anserinus* from the upper part of the Saergan Formation with the lowest level represented by the specimens from acid residue (from sample 96B50-6) to the lower part of the Kanling Formation (sample Nj 398). It is associated with two other biostratigraphically important species, *Y. jianyeensis* (from sample Nj 374 to Nj 389) and *P. serra* (from sample Nj 375 to AFT-X-K14/43; specimens observed on shale bedding surface at the levels equivalent to samples Nj359, Nj356, and Nj353, see Bergström *et al*., 1999; see also Tables 1–2).

Zhou & Chen (1992, p. 74) and Bergström *et al*. (1999) reported the lowest occurrence of *P. anserinus* on the bedding surface of shale at the same stratigraphic level as sample Nj 362, and suggested this represented the lower boundary of this zone (see Figs 2, 3). However, as this bedding plane specimen of *P. anserinus* has been lost, Wang & Zhou (1998) considered sample Nj 375 as the base of the *P. anserinus* Zone. As the most diverse assemblage in the Dawangou section, this sample yields 21 species including *Ansella fenxiangensis, Baltoniodus prevariabilis, Cahabagnathus sweeti, Costiconus ethingtoni, Dapsilodus viruensis, Drepanodus arcuatus, D. reclinatus, D.* sp., *Drepanoistodus basiovalis, Erraticodon* sp., *Panderodus gracilis, Periodon aculeatus, Protopanderodus calceatus, P. cooperi, P. graeai, Pseudooneotodus mitratus, Pygodus anserinus, P. serra, Scabbardella altipes, Yangtzeplacognathus jianyeensis* and *Y. protoramosus*. *Cahabagnathus sweeti* and *Baltoniodus prevariabilis* are two other distinctive species of the *P. anserinus* Zone in Sweden (Bergström, 1971). Sample 96B50-6 was collected by Bergström in 1996 from a limestone lens exposed 4.6 m below the top of the Saergan Formation (about the same stratigraphical level as sample Nj355, see Figs 2–3). *Pygodus serra* and an early form of *P. anserinus* (with only a couple of nodes in a weakly developed fourth row directly comparable with Lindström's holotype from Sweden) were recovered from this sample. Such early forms of *P. anserinus* are found right at the base of the *P. anserinus* Zone in Sweden. Therefore, it would be appropriate to move the base of the *P. anserinus* Zone to the level 4.6 m below the top of the Saergan Formation.

Yangtzeplacognathus jianyeensis is a highly distinctive platform species with a stratigraphic range confined to the *P. anserinus* Zone, and has not been reported outside of China (see Systematic Palaeontology Section) where its species definition and stratigraphic range have been subject to debate among Chinese authors. An *et al.* (1981) established the *P. miaopoensis* (= *Y. jianyeensis*) Zone in the lower part of the Miaopo Formation in Hubei. Chen & Zhang (1984b) proposed the *P. anserinus–Y. jianyeensis* Zone for the conodont assemblage recovered from the middle part of the Datianba Formation in Jiangsu Province, and considered it equivalent to the *P. anserinus* Zone in Sweden. This view was accepted by Zhang (1998c) in defining the base of the *P. anserinus–Y. jianyeensis* Zone by the first appearance of both *P. anserinus* and *Y. jianyeensis*. However, An *et al*. (1985, p. 31) defined the *Y. jianyeensis* Zone for the conodont assemblage of the Miaopo Formation in Hubei, South China and correlated it with the upper part of the *P. serra* Zone to lower part of the *A. tvaerensis* Zone of the Swedish succession. Later, An (1987, tables 2–3) revised the *Y. jianyeensis* Zone with its base marked by the disappearance of *P. anserinus* and the top by the first appearance of his *P. lingulatus*, and correlated the *Y. jianyeensis* Zone with the lower and middle parts of the *A. tvaerensis* Zone of the Swedish succession (= *variabilis* + *gerdae* subzones). Co-occurrence of *Y. jianyeensis* and *P. anserinus* in the upper part of the Saergan Formation and the lower part of the Kaling Formation supports the definition given by Zhang (1998c).

Pygodus anserinus is a morphologically distinctive species with a stratigraphic range spanning the *P. anserinus* Zone and the lower *A. tvaerensis* Zone (Sweet, 1988, p. 192). In Swedish sections, the *P. anserinus* Zone has a thickness of 10 to 15 metres with the base defined by the first appearance of *P. anserinus*, and the top by the first appearance of *A. tvaerensis*, and was correlated with the upper part of the *H. teretiusculus* and the lower part of the *N. gracilis* graptolite zones (Bergström, 1971, pp. 97–98; Bergström *et al*., 2000, fig. 6). Bergström (1971, p. 98) subdivided the *P. anserinus* Zone into two informal subzones, subsequently naming these as the *A. inaequalis* Subzone and *A. kielcensis* Subzone (Bergström, 1983, fig. 1). The primary marker to define the Middle/Upper Ordovician Boundary is the first appearance datum (FAD) of the graptolite *N. gracilis*, which is within the conodont *P. anserinus* Zone. Efforts to subdivide the *P. anserinus* Zone in the Dawangou section have been largely hindered by the fact that the boundary level is condensed (similar to the GSSP stratotype section at Fågelsång in southern Sweden), and the graptolitic shale contains only several intercalated (temporally discontinuous) carbonate bands or nodules, from which only a low diversity conodont fauna dominated by long ranging species can be extracted. It is anticipated that detailed sampling in the Dawangou Formation of the Yangjikan Section (also in Kalpin) will have high potential for resolving this biostratigraphic problem, because in this section, the Middle/Upper Ordovician boundary level lies within the carbonates of the Dawangou Formation, which are age equivalent to the black shale of the Saergan Formation in the Dawangou section.

Wang & Zhou (1998, fig. 1) established the *B. variabilis* Zone in the middle part of the Kanling Formation based on the occurrence of *Baltoniodus variabilis* (Bergström, 1962) in the middle and upper part of the Kanling Formation, but both figured specimens (Wang & Zhou, 1998, pl. 1, figs 4, 6) were from sample Nj 406 and cannot be confidently assigned to *B. variabilis*. Moreover, no specimens are currently recognized from sample Nj 389 as belonging to *B. variabilis*, although Wang & Zhou (1998, fig. 1) reported its occurrence in this sample. Therefore, more detailed collecting is required

to confirm the occurrence of the *B. variabilis* Zone in this section (Fig. 2).

***Pygodus serra* Zone:** Zhou & Chen (1992, fig. 3–2) considered the lower and middle part of the Saergan Formation (beneath Nj 362, where the occurrence of *P. anserinus* was reported on a bedding surface) as belonging to the *P. serra* zone. Bergström *et al*. (1999, p. 71) also indicated the occurrence of *P. serra* at the level of 8.87 m above the base of the Saergan Formation, based on samples collected in 1996 (that unfortunately were not able to be relocated for the current study). Our extensive sampling of every calcareous bed in this interval has produced a low diversity assemblage including *Costiconus ethingtoni, Dapsilodus viruensis, Drepanodus arcuatus, D. reclinatus, Drepanoistodus basiovalis, Periodon aculeatus, Protopanderodus calceatus, P. cooperi, P. graeai,* and *Scolopodus*? *oistodiformis*, which are all long ranging species of little use in defining this zone (Tables 1–2, Figs 2–3). However, occurrence of *Histiodella kristinae* at the top of the Dawangou Formation suggests that this interval (middle and lower part of the Saergan Formation) may correlate with the *P. serra* Zone and possibly part of the *E. suecicus* Zone. Occurrence of *Pygodus anitae* on shale bedding surfaces in the lower Saergan Formation (Goldman & Leslie, personal comm. to Bergström) also supports this correlation.

The graptolite zonation for the lower and middle part of the Saergan Formation has been recently redefined to include three zones in ascending order, the *Pterograptus elegans*, the *Didymograptus murchisoni*, and the *Dicellograptus vagus* zones (Chen *et al*., 2008; Chen *et al.*, in press; Fig. 2). The *Dicellograptus vagus* Zone, with its base placed at the FAD (first appearance datum) of the eponymous species, replaces the poorly-defined *Hustedograptus teretiusculus* Zone, which was conventionally recognized by the disappearance of *Didymograptus murchisoni* together with the common occurrence of *H. teretiusculus*. However, the FAD of *Dicellograptus vagus* is slightly higher than the LAD (last appearance datum) of *Didymograptus murchisoni* in the Dawangou section, leaving a short interval below the boundary lacking stratigraphically diagnostic species.

***Histiodella kristinae* zone:** This level is represented by a diverse assemblage recovered from the top of the Dawangou Formation, and includes 18 species, *Cornuodus longibasis*, *Costiconus ethingtoni, Dapsilodus viruensis, Drepanodus arcuatus, D. reclinatus, Drepanoistodus basiovalis, Dzikodus tablepointensis,* gen. et sp. indet., *Histiodella kristinae, Periodon aculeatus, Polonodus clivosus, P. newfoundlandensis, P.* sp. A*, Protopanderodus calceatus, P. cooperi, P. graeai, P*. sp. and *P.? nogamii* (Fig. 3). *H. kristinae* Stouge, 1984 is the most distinctive species of this assemblage, along with several pectiniform species including *Dzikodus tablepointensis*, *Polonodus clivosus, P. newfoundlandensis,* and *P.* sp. A. Based on the inferred phylogeny of *Histiodella* species recovered from the Table Head Formation of western Newfoundland, Stouge (1984, table 3) proposed two conodont zones, namely the *H. tableheadensis* (= *H. holodentata*) Zone in the lower Table Head Formation and the *H. kristinae* Zone in the upper Table Head Formation, correlating the latter with the *E. suecicus* Zone of the Baltoscandian succession. *Histiodella kristinae* is widely distributed in North America (Barnes & Poplawski, 1973; Landing, 1976; Stouge, 1984; Nowlan & Thurlow, 1984), Europe (Dzik, 1994; Rasmussen, 2001; Löfgren, 2004), Argentine Precordillera (Heredia *et al*., 2005; Heredia, pers. com., 2010), South China (Ni, 1981; Ding *et al*. in Wang, 1993; Zhang, 1998c), North China (Wang & Lou, 1984; An & Zheng, 1990), and the Tarim Basin (Wang & Zhou, 1998; Zhao *et al*., 2000; Du *et al*., 2005; this study). Based on a large collection of *Histiodella* species from the Yangjikan section and other localities of the Tarim Basin, Du *et al*. (2005) recognized four conodont zones in ascending order: *H. sinuosa* Zone, *H. holodentata* Zone, *H. kristinae* Zone, and *H. bellburnensis* Zone, and correlated the *H. kristinae* Zone with the uppermost *A. variabilis* Zone and the lower part of the *E. suecicus* Zone. However, Bergström *et al*. (2009) suggested that the top of the *H. kristinae* Zone could approximate the base of the *P. serra* Zone, indicating a correlation of the *H. kristinae* Zone with the *E. suecicus* Zone of the Baltoscandian succession.

***Histiodella holodentata* zone**: This assemblage recovered from sample Nj 296 is characterized by the occurrence of *H. holodentata* Ethington & Clark, 1982 along with 15 other species including *Ansella jemtlandica, Cornuodus longibasis, Costiconus ethingtoni, Dapsilodus viruensis, Drepanodus arcuatus, D. reclinatus, Drepanoistodus basiovalis, Parapanderodus striatus, Periodon aculeatus, Protopanderodus calceatus, P. cooperi, P. graeai, P*. sp., *Scolopodus striatus*, and *Venoistodus balticus* (Fig. 3). *Histiodella holodentata* is a widely distributed and biostratigraphically useful species reported from North America (Ethington & Clark, 1982; Nowlan & Thurlow, 1984; Stouge, 1984; Johnston & Barnes, 2000; Bauer, 2010), Kazakhstan (Zhylkaidarov, 1998), Argentine Precordillera (Albanesi & Ortega, 2003; Heredia, pers. com., 2010), Australia and New Zealand (Zhen *et al*., 2004a, 2009b; Percival & Zhen, 2007), North Europe (Rasmussen, 2001), South China (An *et al.*, 1985; An, 1987; Zhang, 1998c), North China (An *et al*., 1983; An & Zheng, 1990), Tarim Basin (Gao, 1991; Wang & Zhou, 1998; Zhao *et al*., 2000; Du *et al.*, 2005), and southeast Asia (Agematsu *et al.*, 2006, 2008b).

Ethington & Clark (1982) proposed two informal conodont zones with *H. sinuosa* and *H. holodentata* as the index species based on their occurrences in the Ibex area of Utah, which were later recognized as the two formal conodont zones within the Whiterockian of the North American Midcontinent succession (Sweet, 1988, chart 1, p. 190). However, correlations of the *H. holodentata* Zone, with its base defined by the first appearance of *H. holodentata*, with the Baltoscandian succession were debated among conodont biostratigraphers. For instance, Stouge (1984, table 3) correlated this zone with the upper part of the *Lenodus variabilis* Zone, whereas Harris *et al*. (1995) suggested a correlation with the upper *L. variabilis* Zone to the lower *E. suecicus* Zone. Rasmussen (2001) correlated the base of the *H. holodentata* Zone with the basal *L. variabilis* Zone, and Webby *et al.* (in Webby *et al*., 2004, fig. 2.2) considered the *H. holodentata* Zone as the time equivalence of the *L. variabilis* Zone. Based on study of the Tarim material, Du *et al.* (2005, table 11) preferred a correlation with the middle part of the *L. variabilis* Zone.

Bergström (1971) subdivided the *Pygodus serra* conodont Zone into five subzones with *E. suecicus* as

the zonal index species for the lowermost subzone, and defined its base by the first appearance (FAD) of *P. serra* and the top by the disappearance of *E. suecicus* and the appearance of *Y. foliaceus*. Lindström (1971) established the *Amorphognathus variabilis* Zone for the conodont fauna from the Kundan Stage. Subsequent studies of conodonts from the middle Darriwilian of Baltoscandia and South China have supported recognition of these as two formal conodont zones. Furthermore, significant taxonomic revisions of both *E. suecicus* and *L. variabilis* have resulted in the recognition of two more conodont zones (the *E. pseudoplanus* Zone and the *Y. crassus* Zone) between the revised *E. suecicus* and *L. variabilis* zones (Viira, 1974; An *et al.*, 1985; Zhang, 1998c, 1998d; Löfgren & Zhang, 2003; Löfgren, 2003, 2004). The *E. suecicus* Zone was then subdivided into the *Pygodus anitae* Subzone and *P. lunnensis* Subzone and correlated to the Aserian Stage, and the *L. variabilis* Zone was restricted to an interval more or less corresponding to the middle-upper part of the Hunderum Substage of the Kundan (Zhang, 1998a; Löfgren & Zhang, 2003).

Löfgren, (2004, fig. 1) correlated both the *H. kristinae* Zone and *H. holodentata* Zone of the North American Midcontinent succession to the *E. pseudoplanus* Zone of the Baltoscandian succession. Considering that in the Dawangou section, *H. holodentata* occurs above the range of *Y. crassus*, it is best to correlate the occurrence of *H. holodentata* in the Dawangou Formation to only part of the *E. pseudoplanus* Zone. However, due to environmental changes resulting from a significant transgressive event in the late Darriwilian, occurrences of these zonal index species as recorded in the Dawangou section (Figs 2–3) clearly do not represent their full stratigraphic ranges, and their boundaries are still poorly defined (Fig. 2).

***Yangtzeplacognathus crassus* Zone:** *Y. crassus* was recovered from two samples (Nj294 and Nj 295) in the middle part of the Dawangou Formation associated with 10 other species including *Ansella jemtlandica, Cornuodus longibasis, Drepanodus arcuatus, Drepanoistodus basiovalis, Periodon aculeatus, Protopanderodus calceatus, P. cooperi, P. graeai, Scolopodus*? *oistodiformis*, and *S. striatus* (Table 1, Fig. 3). The distinctive pectiniform species, *Y. crassus*, has a wide distribution in the lower Darriwilian in South China (An, 1981, 1987; An *et al*., 1985; Ni & Li, 1987; Chen & Zhang, 1989; Wang, 1993; Zhang, 1997, 1998c; Wang & Bergström, 1999a, 1999b), Tarim (Wang *et al*., 1996; Bergström & Wang, 1998; Wang & Zhou, 1998), Baltoscandia (Viira, 1974; Stouge & Bagnoli, 1990; Wang, 1997; Viira *et al*., 2001; Löfgren, 2003; Löfgren & Zhang, 2003) and Poland (Podhalańska, 1979; Dzik, 1994). Prior to its formal recognition by Chen & Zhang (in Wang, 1993, pl. 37, figs 12–17) based on type material recovered from the Guniutan Formation near Tangshan of Nanjing, it was reported from the Guniutan Formation in Jiangsu (An, 1981, 1987), Hubei (Ni & Li, 1987; An *et al*., 1985), and Anhui (Chen & Zhang, 1989), and also from basal Hulo Formation of the Huangnitang Section of Changshan, west Zhejiang (Wang & Bergström, 1995; Zhang *et al*., 2007) and the Dawangou Formation of the Dawangou section near Kalpin, Tarim Basin (Wang *et al*., 1996), but assigned to different species names (see synonymy lists of Zhang, 1997 and Löfgren & Zhang, 2003). Detailed taxonomic studies of this species (Zhang, 1997, 1998c; Löfgren & Zhang, 2003) have made it one of the best documented conodont species in the lower Darriwilian, and biostratigraphically useful for regional correlations (Bergström & Wang, 1998).

The *Y. crassus* Zone was defined as a range zone marked by the occurrence of *Y. crassus* (Zhang, 1998c, table 2) in the Guniutan Formation of Hubei (Fenxiang Section—the type section of the Guniutan Formation) and Hunan (Cili and Maocaopu sections) provinces, South China, and correlated with the lower part of the Valaste Substage of the Baltic successions (Löfgren, 2003). Bergström & Wang (1998, fig. 1) suggested a correlation with the middle part of the *A. ellesae* graptolite Zone (Pacific Province) or *D. artus* graptolite Zone (Atlantic Province). Wang & Bergström (1995) and Zhang *et al*. (2007) reported the occurrence of *Y. crassus* in the lower part of the Hulo Formation at the Huangnitang Section, Changshan, west Zhejiang, and equated the *Y. crassus* Zone with the mid-upper part of the *A. ellesae* graptolite Zone. In the Maocaopu Section of Hunan Province, *H. holodentata* first appears in the upper part of the *Y. crassus* Zone (Zhang, 1998c, fig. 22), suggesting that the lowest part of the *H. holodentata* Zone overlaps with the uppermost part of the *Y. crassus* Zone (if the latter is retained as a range zone).

Material and methods

This study is based on a large collection of nearly twenty thousand identifiable, well-preserved (CAI 2-3) conodont specimens recovered from 63 samples collected during two separate field trips, in 1987 and in 2008 (Tables 1–2). Thirty-nine conodont samples collected in 1987 were processed with acetic acid (10%) and picked by one of the authors (ZHW) at the Nanjing Institute of Geology and Palaeontology, Chinese Academy of Sciences. He subsequently briefly reported identifications of the fauna in several publications, particularly important amongst which is a detailed listing of conodont species identified from each sample in a biostratigraphic description of the Dawangou section (in Zhou & Chen, 1992, pp. 71–78). Three of the authors (YYZ, YDZ, and JFC) participated in the 2008 field work, during which 24 conodont samples (about 5kg each) were collected from the top of the Dawangou Formation to the lower part of the Kanling Formation with particular focus on the carbonate or calcareous lenses within the black shale of the Saergan Formation. These 24 samples were each split into two halves, one of which was processed at the Nanjing Institute of Geology and Palaeontology and picked to completion by lab contractors. The other half of each of the 24 samples was acid leached (10% acetic acid) and the residues were separated and concentrated by using sodium polytungstate at the Londonderry laboratory of the Geological Survey of New South Wales; these residues were sorted and picked by the senior author at the Australian Museum. Interestingly, those samples processed in Australia had a much higher yield in comparison with the other halves processed in Nanjing, where they were not subjected to heavy-liquid separation techniques. One of the most productive samples from the top of the Dawangou Formation yielded nearly ten thousand specimens (Table 2).

All photographic illustrations shown in Figs 4 to 32 are SEM photomicrographs captured digitally (numbers with the prefix IY are the file names of the digital images).

Table 1. Distribution of conodont species recovered from 39 samples collected from the Dawangou, Saergan and Kanling formations of the Dawangou section, near Kalpin, Tarim Basin in 1987 field work.

	Nj 411	Nj 410	Nj 406	Nj 403	Nj 402	Nj 399	Nj 398	Nj 395	Nj 389	Nj 388	Nj 386	Nj 385	Nj 384	Nj 383	Nj 382	Nj 379	Nj 378	Nj 377	Nj 376	Nj 375	Nj 368	Nj 364	Nj 362	Nj 360	Nj 357	Nj 354	Nj 348	Nj 325	Nj 323	Nj 316	Nj 314	Nj 310	Nj 298	Nj 297	Nj 296	Nj 295	Nj 294	Nj 292	Nj 291	total
Ansella jemtlandica																																	3	4	36	65	3	3	114
Ansella fenxiangensis			2	6				2								2				3																			15
Baltoniodus alobatus			21	15																																			36
Baltoniodus prevariabilis									1	3																													4
Baltoniodus sp. A																																					2	1	3
Baltoniodus sp. B			2																																				2
Cahabagnathus sweeti													1																										1
Cornuodus longibasis																																	6			1	1	1	9
Costiconus ethingtoni			27		1		1	4	6	6	1	5			7	16	27	9	12												1	4	15	4					146
Dapsilodus viruensis			3				1	5	4	3	1	6	5			20	8	1	4	4														1					66
Drepanodus arcuatus	9	1	68	5	3		3	6	8	8		21		4	9	51	32	4	15	42	2	2		4	2							23	91	12	21	8	5	6	465
Drepanodus reclinatus						7							9			3	4		3	4		2				2				2		4	8	1					49
Drepanoistodus basiovalis	11			3												20	14									1						4			1		3	57
Drepanoistodus sp.																	1																						1
Dzikodus ?tablepointensis																																	29						29
Histiodella holodentata																																		3					3
Panderodus gracilis											1					3																							4
Parapanderodus striatus																																	5				2		7
Periodon aculeatus				2	8		3		15	19	2	21	6	12	18	49	189	13	43	13				1	2		6	5		2	10	3	62	1437	4	153	1255	1		3354
Periodon grandis	7		101																																				108
Polonodus sp. B																																					2		2
Protopanderodus calceatus															1	3			3	3													1	6	5	1		4		27
Protopanderodus cooperi			6				3	4	7	16	2	13	11	2	5	64	98	12	35	6	2		1						1		1	31	18	3	18	19			378
Protopanderodus graeai													4			10	3	3	7	4			3			2?		2	4			25	79	27	22	80			273
Protopanderodus liripipus	7		13	6																																			26
Protopanderodus sp.																																	3	1					4
Pseudooneotodus mitratus																				1																			1
Pygodus anserinus							5		1	93	29	43	177	75	57	59	5		11	2																			557
Pygodus serra															2?	57	4		12	255																			328
P. serra+anserinus (Pb and S)																357	215	128	145																				845
Scabbardella altipes	20	1	15	21	10	23	5		17	7	3		29			1																							152
Scolopodus striatus																																		2?	10	18	6	3	37
Scolopodus? oistodiform																																			1	4			5
Spinodus spinatus			6	1																																			7
Venoistodus balticus																																		2					2
Yangtzeplacognathus crassus																																			14	49			63
Yangtzeplacognathus jianyeensis									1							11	5?		1	9																			22
Yangtzeplacognathus protoramosus																6	3			1																			10
Total	43	2	275	59	22	30	21	21	60	155	39	109	242	93	97	732	603	170	291	347	4	4	4	5	4	3	6	7	5	2	12	5	154	1700	67	276	1500	22	21	7212

Table 2. Distribution of conodont species recovered from 24 samples collected from the Dawangou, Saergan and Kanling formations of the Dawangou section, near Kalpin, Tarim Basin in 2008 field work.

total	AFT-X-K13/49	AFT-X-K13/48	AFT-X-K13/47	AFT-X-K13/46	AFT-X-K13/45	AFT-X-K13/44	AFT-X-K13/43	AFT-X-K13/42	AFT-X-K13/41	AFT-X-K13/40	AFT-X-K13/36	AFT-X-K13/35	AFT-X-K13/34	AFT-X-K13/33	AFT-X-K13/31	AFT-X-K13/30	AFT-X-K13/29	AFT-X-K13/27	AFT-X-K13/26	AFT-X-K13/21	AFT-X-K13/18	AFT-X-K13/17	AFT-X-K13/16	AFT-X-K13/13	total
Ansella fenxiangensis									5	10															15
Baltoniodus prevariabilis												5													5
Cahabagnathus sweeti							7																		7
Cornuodus longibasis																								6	6
Costiconus ethingtoni	10	6	18	8		28	35	8	8	2										1				204	328
Dapsilodus viruensis	1			2																				5	8
Drepanodus arcuatus	2	6	13	53	6	25	81	12	16	48	12					2		4		4	1	1	4	103	393
Drepanodus reclinatus		1		6	2	3		6	5	3			1	2	4		2		2	4				26	67
Drepanoistodus basiovalis			5				17	13	12															6	53
Dzikodus ?tablepointensis																								2	2
Erraticodon sp.											5														5
Gen. et sp. indet.																								1	1
Histiodella kristinae																								30	30
Periodon aculeatus		38	50	91	3	142	78	75	85	2								2	9	63		3	11	6400	7052
Polonodus clivosus																								2	2
Polonodus newfoundlandensis																								36	36
Polonodus sp. A																								1	1
Protopanderodus calceatus			3	19	4	1	9	1	8	16	10	1							1					147	220
Protopanderodus cooperi	3	5	30	83	8	145	135	30	62	23	3	1								10	1			159	698
Protopanderodus graeai																					1	1		974	976
Protopanderodus? nogamii																								37	37
Protopanderodus sp.																								1	1
Pseudooneotodus mitratus		3	1	2		2																			8
Pygodus anserinus		47	125	640	9	293	107	9	24	5															1259
Pygodus serra							212	45	117	137															511
P. serra + *P. anserinus* (Pb+S)							327	87	162	97															673
Scabbardella altipes			13	2		48		8	5	2	2														80
Scolopodus? oistodiform																			1						1
Yangtzeplacognathus jianyeensis		6				97	24	6	6	14		1													154
Yangtzeplacognathus protoramosus			3			2	4	4	1																14
Total	16	112	261	906	32	786	1036	304	516	359	32	8	1	2	4	2	2	6	13	82	3	5	15	8140	12643

Figured specimens bearing the prefix NIGP are deposited in the collections of the Nanjing Institute of Geology and Palaeontology, Chinese Academy of Sciences in Nanjing, China. Fourteen topotype specimens of *Protopanderodus varicostatus* and *P. cooperi* from the Pratt Ferry Formation of Alabama are illustrated in Fig. 20 and Fig. 22 for comparison, and these (bearing the prefix OSU 53802 to OSU 53815 inclusive) are housed at the Orton Geological Museum, Ohio State University, Columbus, Ohio, USA.

Synonymy lists of the species documented in this contribution have emphasis on the Chinese literature in order to provide complete data for the distribution of the species in China. Fifteen species, including *Ansella fenxiangensis* (An, Du, Cao, Chen & Lee, 1981), *Baltoniodus* sp. A, *Baltoniodus* sp. B, *Cornuodus longibasis* (Lindström, 1955a), *Drepanoistodus* sp., *Erraticodon* sp., *Panderodus gracilis* (Branson & Mehl, 1933), *Periodon grandis* (Ethington, 1959), *Polonodus* sp. A, *Polonodus* sp. B, *Protopanderodus*? *nogamii* (Lee, 1975), *Protopanderodus* sp., *Spinodus spinatus* (Hadding, 1913), *Venoistodus balticus* Löfgren, 2006, and gen. et sp. indet. (a single quadriramate ramiform element), are documented by illustration only, as they are either represented by insufficient material to warrant an appropriate taxonomic treatment, or have lesser biostratigraphic significance. Conventional conodont terminology and notation as defined in the Treatise Part W (Clark *et al.* 1981) is employed in this contribution, except for the M elements (makellate), whose orientation, morphology and terminology was introduced by Nicoll (1990, 1992).

Systematic Palaeontology

Class Conodonta Pander, 1856

Ansella Fåhraeus & Hunter, 1985

Type species. *Belodella jemtlandica* Löfgren, 1978.

Ansella jemtlandica (Löfgren, 1978)

Fig. 4A–O

Roundya n. nov. Sweet & Bergström, 1962: 1244–1245, text-fig. 5.

Belodella jemtlandica Löfgren, 1978: 46, pl. 15, figs 1–8, fig. 24A–D; An *et al*., 1983: 77, pl. 25, figs 8–12; Zhao *et al*., 1984: 210, pl. 90, figs 1, 4, 11, 14; An & Zheng, 1990: pl. 10, figs 4–7.

Belodella? *jemtlandica* (Löfgren).–Ding *et al*. in Wang, 1993: 165, pl. 30, figs 9, 11, 14, 19.

Ansella jemtlandica (Löfgren).–Fåhraeus & Hunter, 1985: 1173, pl. 1, figs 1–5, 9, pl. 2, fig. 12, Fig. 1 (*cum syn.*); Ding, 1987: pl. 5, figs 11–12; Ni & Li, 1987: 396, pl. 60, figs 21–22, 24–25; An & Zheng, 1990: pl. 10, figs 4–7; Gao, 1991: 128, pl. 11, figs 3–6; Pohler, 1994: pl. 1, figs 15–16; Lehnert, 1995: 70, pl. 9, figs 1, 2, 5; pl. 10, fig. 8, pl. 12, fig. 1, pl. 13, fig. 1; Albanesi in Albanesi *et al*., 1998:160–161, pl. 1, figs 18–23, text-fig. 27; Zhang, 1998c: 50, pl. 1, figs 5–9; Zhao *et al*., 2000: 188, pl. 35, figs 13, 14; Rasmussen, 2001: 51, pl. 1, figs 4–9; Wang & Qi, 2001: pl. 1, figs 10, 12; Pyle & Barnes, 2002: 57, pl. 19, figs 1, 2; Pyle & Barnes, 2003: fig. 11.1–11.4; Zhen & Percival, 2004a: 84–86, fig. 5A–Q (*cum syn.*); Zhen & Percival, 2004b: fig. 4A–G; Zhen *et al*., 2009b: 32, fig. 2A–I; Bauer, 2010: pl. 1, figs 1–2, 4–5.

Material. 114 specimens from six samples of the Dawangou Formation (see Table 1).

Remarks. Several species of *Ansella* introduced in the Chinese literature, including *A. fenxiangensis* (An, Du, Gao, Chen & Li, 1981) = *Belodella guniutanensis* Ni *in* Ni & Li, 1987, *A. longicuspica* Zhang, 1998c, *A. rigida* (An *in* An *et al*., 1983) and *A. baotaensis* Ni *in* Ni & Li, 1987, show close morphological similarities to *A. jemtlandica.* They were differentiated from the latter mainly based on the depth of the basal cavities in the P elements (An *et al*., 1983, p. 78; Zhang, 1998c, text-fig. 25). Zhang (1998c) suggested a possible evolutionary lineage from oldest *A. longicuspica* with a shallower basal cavity (about half of the P element length) to intermediate *A. jemtlandica* (basal cavity about three-fourths of the P element length), and then to the most derived *Ansella fenxiangensis* (see Fig. 5A–C) with a deep basal cavity (four-fifths to five-sixths of total P element length). Although in theory, recognition of these species with their shorter stratigraphical ranges might be more useful than a broad concept of the long ranging *A. jemtlandica*, in practice it may be difficult to correctly assign the material to a species based solely on the depth of the basal cavity in the P elements.

Baltoniodus Lindström, 1971

Type species. *Prioniodus navis* Lindström, 1955a.

Baltoniodus alobatus (Bergström, 1971)

Figs 5L, Q, 8M–N

Prioniodus alobatus Bergström, 1971: 145, pl. 2, figs 4–5; Zeng *et al*., 1983: pl. 12, fig. 33; An, 1987: 169–170, pl. 25, figs 7–9 (*cum syn.*); Zhong, 1990: 150, pl. 17, figs 1–2; Wang & Zhou, 1998: pl. 1, figs 11–13.

Prioniodus lingulatus An, 1987: 170–171, pl. 25, figs 10–17 (*cum syn.*).

Baltoniodus alobatus (Bergström).–Dzik, 1994: 83, fig. 14d; Leslie, 2000: 1127, fig. 7.2–7.13 (*cum syn.*); Zhao *et al*., 2000: 189, pl. 34, figs 11–13, pl. 39, figs 16–20, 23 (*cum syn.*); Xiong *et al*., 2006: 368, pl. 1, figs 2–3; Agematsu *et al*., 2008a: 967, fig. 11.1–11.21; Ortega *et al*., 2008: fig. 6.1.

Prioniodus cf. *P. alobatus* Bergström.–An, 1981: pl. 4, fig. 9a–b.

Baltoniodus sp. cf. *B. variabilis* (Bergström).–Agematsu *et al*., 2007: 33–35, fig. 10.1–10.17.

Material. Thirty-six specimens from two samples of the Kanling Formation (see Table 1).

Remarks. Bergström (1971, pl. 2, figs 4–5) described and illustrated only the amorphognathiform element of *Prioniodus alobatus* represented by the holotype, indicating that the other five or six types of elements comprising the apparatus were closely similar to those of *B. variabilis* (Bergström, 1962). According to the original description, the most distinctive feature of its amorphognathiform (Pa herein) element was “a wide, but low, platform-like posterior process” (Bergström, 1971, p. 145). More recently, Leslie (2000) fully described and illustrated this species as consisting of a seximembrate apparatus including geniculate M, alate ramiform Sa, bipennate Sc, quadriramate Sd, pastinate Pa and Pb elements.

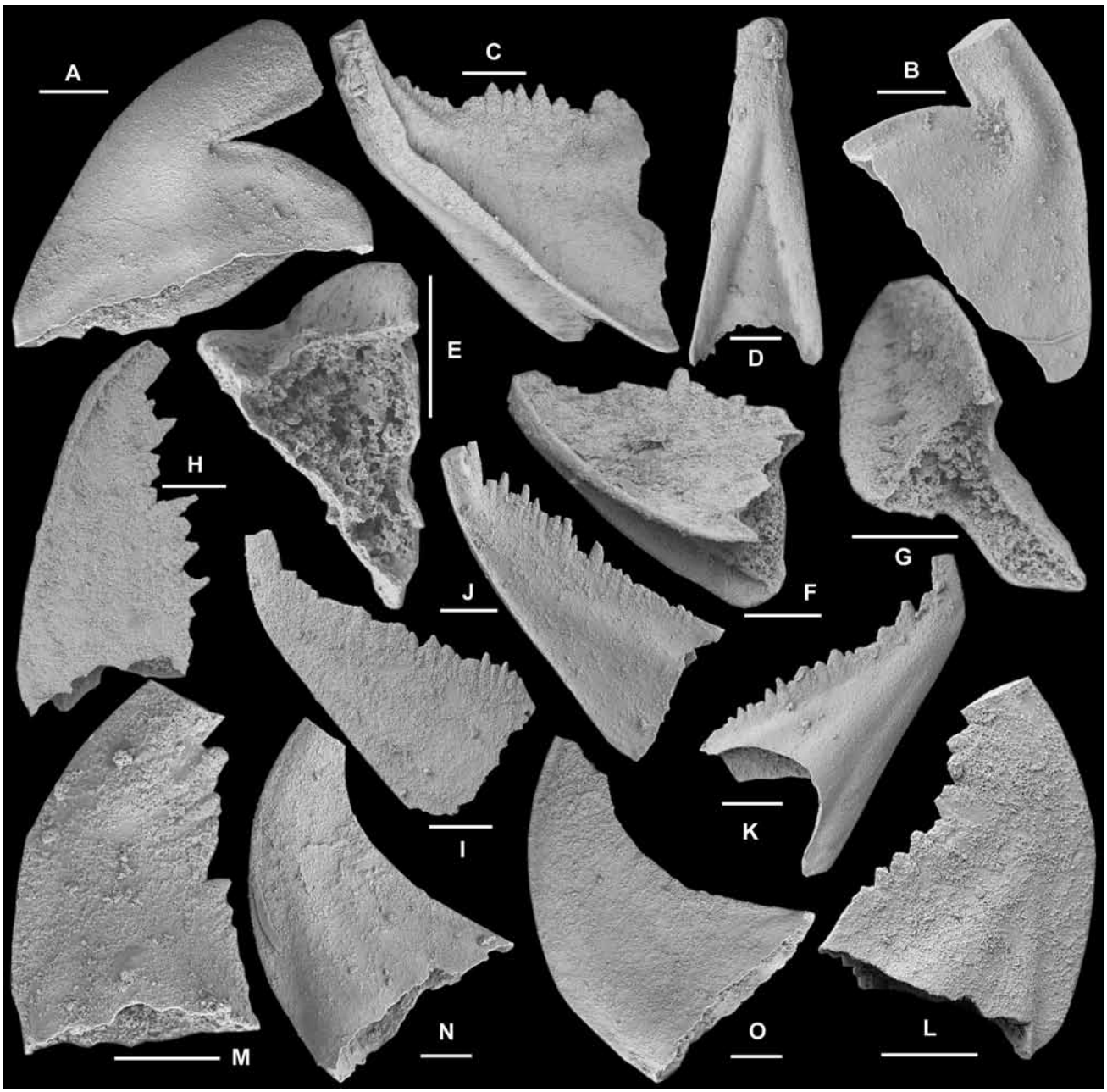

Figure 4. *Ansella jemtlandica* (Löfgren, 1978). A, B, M element; ***A***, NIGP 152839, anterior view (IY147-004); ***B***, NIGP 152840, posterior view (IY147-005). C–F, Sa element; ***C–D***, NIGP 152841, C, lateral view (IY146-040), D, anterior view (IY146-039); ***E–F***, NIGP 152842, E, basal view (IY147-006), F, lateral view (IY147-008). ***G–H***, Sb element, NIGP 152843, G, antero-basal view (IY147-010), H, inner lateral view (IY147-011). I–K, Sc element; ***I***, NIGP 152844, outer lateral view (IY147-012); ***J***, NIGP 152845, inner lateral view (IY147-013); ***K***, NIGP 152846, outer lateral view (IY146-043). L–M, Pa element; ***L***, NIGP 152847, outer lateral view (IY147-003); ***M***, NIGP 152848, inner lateral view (IY148-001). N–O, Pb element; ***N***, NIGP 152849, inner lateral view (IY147-002); ***O***, NIGP 152850, outer lateral view (IY147-001). All from sample Nj294; scale bars 100 μm.

The illustrated Pa element (Fig. 8N) from the upper part of the Kanling Formation is a broken specimen with only the posterior process preserved. Similar specimens with a wide platform and a centrally positioned row of denticles were also reported as *B. alobatus* from subsurface core samples of the Yingmai-10 well (Zhao *et al*., 2000, pl. 39, fig. 18), from the Tumuxieke Formation of Bachu (Wang & Zhou, 1998, pl. 1, fig. 11), from the Qiaerbake Formation in Bachu (Xiong *et al*., 2006, pl. 1, figs 2–3), and from the same sample (Nj406) of the Kanling Formation of the Dawangou section (Wang & Zhou, 1998, pl. 1, fig. 13). The illustrated Pb element (Fig. 5Q) is identical with the specimen previously illustrated as *B. alobatus* by Wang & Zhou (1998, pl. 1, fig. 12) from a slightly higher level (sample Nj406) in the Kanling Formation of the same section, and also corresponds exactly to the ambalodiform (Pb herein) element of *Prioniodus lingulatus* (An, 1987, pl. 25, fig. 12) from the Datianba Formation of Ganxi, Guizhou Province.

The illustrated Pa element (Fig. 8N) is also identical with the holotype of *B. lingulatus* An, 1987, which was defined as consisting of a seximembrate apparatus including amorphognathiform, ambalodiform, cordylodiform,

tetraprioniodiform, trichonodelliform and oistodiform elements. An (1987) suggested that *B. lingulatus* was closely similar to *B. alobatus*, but the posterior process in the amorphognathiform element of the latter had a more convex upper surface, which was undulose in lateral view. One illustrated specimen of the Pa element of *P. lingulatus* (An, 1987, pl. 25, fig. 15) from the Datianba Formation of Jiangsu is identical with the specimen illustrated by Leslie (2000, fig. 7.3) as the Pa element of *B. alobatus* in having a distinctive inner-lateral lobate expansion on the posterior process. Leslie (2000, p. 1127) indicated that this feature was seen in many of the specimens referred to as the Pa element of *B. alobatus*. Based on his description, one of the most distinctive features of *B. alobatus* is that its S elements have small closely spaced denticles intercalated with several much larger denticles, particularly on the posterior process of the Sc element (Fig. 5L; see also Leslie, 2000, fig. 7.9). This feature is also developed in the type specimens of *Prioniodus lingulatus* An, 1987 (pl. 25, fig. 13), indicating that the latter, if not conspecific with *B. alobatus*, is certainly closely related to it. However, some specimens from a stratigraphically slightly lower level (Nj388, Fig. 5H–I) that are assigned to *B. prevariabilis* also show a similar denticle pattern on the posterior process.

Specimens representing the Pa element of *B. alobatus* recorded from the Tarim Basin (Fig. 8N; also see Wang & Zhou, 1998; Xiong *et al*., 2006) are more comparable with the holotype of *P. lingulatus* in having a wider posterior platform than the holotype of *B. alobatus*. Considering that the width and the shape of the posterior platform varies significantly amongst the type material of *B. lingulatus*, that species is regarded herein as a junior synonym of *B. alobatus* as indicated by Zhao *et al*. (2000, p. 189). The Sc element of *B. alobatus* (Fig. 5L) differs from the corresponding element of the stratigraphically slightly older species *B. prevariabilis* (Fig. 5O–P) in having smaller denticles intercalated with a number of larger denticles on the posterior process, and the same feature is also observed in the Sd element (Fig. 8M). The specimens of *B. alobatus* assigned by Agematsu *et al*. (2007, fig. 10) to *B*. sp. cf. *B. variabilis* are similar to the Tarim form. Their M element has an unusually long inner lateral process compared to the Swedish specimens (although those are usually broken).

The Pa element representing *Baltoniodus* sp. B (Fig. 8I–L) that co-occurs with *B. alobatus* in sample Nj406 has a platform-like anterior process (rather than posterior process), which is narrower with the row of denticles near the outer lateral margin (Fig. 8J–K). Furthermore, the anterior process is straight, extending downward in lateral view (Fig. 8I) in comparison to the posterior process of *B. alobatus*. It shows some resemblance to *B. variabilis*, but the Pa element of the latter has a "triangular lateral expansion of the inner side of the posterior process" (Bergström, 1971, p. 148, pl.2, fig. 2).

Baltoniodus prevariabilis (Fåhraeus, 1966)

Fig. 5H–K, M–P, ?R

Prioniodus prevariabilis Fåhraeus, 1966: 29, pl. 4, fig. 5a–b; Bergström, 1971: 146, pl. 2, fig. 1.

Prioniodus (Baltoniodus) prevariabilis prevariabilis Fåhraeus.–Löfgren, 1978: 87, pl. 12, figs 37–43 (*cum syn.*).

Baltoniodus prevariabilis Fåhraeus.–Lindström, 1971: 56 *partim*; An & Ding, 1982: pl. 5, figs 1–3, 7; An *et al.*, 1985: pl. 7, figs 15, 18–19, pl. 16, figs 1–13; An, 1987: 127–128, pl. 20, figs 21–25, pl. 21, figs 1–7; Chen & Zhang, 1989: pl. 1, figs 10–14; Gao, 1991: 127, pl. 9, figs 1–3, 6; Ding *et al*. in Wang, 1993: 163, pl. 26, figs 1–17; Dzik, 1994: 82, pl. 18, figs 17–22, text-fig. 14b; Bednarczyk, 1998: pl. 1, figs 9–10, 12–13; Zhang, 1998c: 54, pl. 3, figs 1–8; Zhao, *et al.*, 2000: 189, pl. 34, fig. 15, pl. 39, figs 1–6; Viira, 2011: fig. 6D–F, H, K, M–N, Q–S.

Material. Nine specimens from three samples (see Tables 1–2).

Remarks. *Prioniodus prevariabilis* was erected as a form species with the only figured specimen (holotype) exhibiting straight, denticulated posterior and outer lateral processes and a denticulated, inner laterally deflected anterior process (Fåhraeus, 1966, pl. 4, fig. 5a–b). It represents the ambalodiform element in the multielement species apparatus that was first proposed by Löfgren (1978) to include the oistodiform (M), trichonodelliform (Sa herein), belodiform (Sb herein), tetraprioniodiform (Sd herein), amorphognathiform (Pa herein) and ambalodiform (Pb herein) elements. The cordylodiform (Sc herein) was also included in the species apparatus to form a septimembrate apparatus (An & Ding, 1982; An *et al.*, 1985; Zhang, 1998c). Specimens referable to *B. prevariabilis* are rare in the Dawangou samples, and only Sa, Sc, Pa and Pb elements of this species are recovered from the Kanling Formation and the upper part of the Saergan Formation. The Sa element is alate with a long denticulate posterior process and a denticulate, downward-extending lateral process on each side (Fig. 5H–I); the Sc element is bipennate with a long denticulate posterior process and a long, adenticulate anticusp-like anterior process (Fig. 5O–P); the Pa element has low and long denticulate posterior and anterior processes (Fig. 5J–K), and the Pb element displays a long denticulate, inner laterally curved, and strongly downward-extending anterior process (Fig. 5M–N). These specimens are comparable with those documented from Jämtland of northern Sweden (Löfgren, 1978) and from the Guniutan Formation of South China (Zhang, 1998c).

Several specimens recovered from the upper part of the Dawangou Formation are assigned to *Baltoniodus* sp. A (Fig. 5D–G). It is characterized by the Pa element (Fig. 5G) having the straight anterior and outer lateral processes adjoining at approximately right angles, and a Pb element (Fig. 5E) with an inner laterally deflected anterior process and a posteriorly curved outer lateral process, which are remarkably different from that of *B. prevariabilis*. The denticulate lateral processes of this species are also higher and more laterally extended (Fig. 5D) compared with *B. prevariabilis*.

Cahabagnathus Bergström, 1983

Petalognathus Drygant, 1974b (a junior homonym of *Petalognathus* Duméril & Bibron, 1854, a reptile, see Clark *et al*., 1981, p. W129).

Type species. *Polyplacognathus sweeti* Bergström, 1971.

Figure 5. A–C, *Ansella fenxiangensis* (An, Du, Cao, Chen & Lee, 1981). ***A***, M element, NIGP 152851, Nj403, posterior view (IY161-019); ***B***, Sb element, NIGP 152852, Nj403, outer lateral view (IY161-020); ***C***, P element, NIGP 152853, Nj403, outer lateral view (IY161-018). D–G, *Baltoniodus* sp. A. ***D***, Sa element, NIGP 152854, Nj292, posterior view (IY158-019); ***E–F***, Pb element, NIGP 152855, Nj292, E, upper view (IY158-016), F, inner lateral view (IY158-015); ***G***, Pa element, NIGP 152856, Nj294, upper view (IY158-030). H–K, M–P, *Baltoniodus prevariabilis* (Fåhraeus, 1966). ***H–I***, Sa element, NIGP 152857, Nj388, H, lateral view (IY162-002), I, upper view (IY162-001); ***J–K***, Pa element, NIGP 152858, Nj388, J, inner lateral view (IY162-003), K, outer lateral view (IY162-006); ***M***, Pb element, NIGP 152860, Nj403, outer lateral view (IY161-016); ***N***, Pb element, NIGP 152861, AFT-X-K13/35, outer lateral view (IY163-022); ***O***, Sc element, NIGP 152862, AFT-X-K13/35, outer lateral view (IY163-20); ***P***, Sc element, NIGP 152863, AFT-X-K13/35, inner lateral view (IY163-021). L, Q, *Baltoniodus alobatus* (Bergström, 1971). ***L***, Sc element, NIGP 152859, Nj403, outer lateral view (IY161-017); ***Q***, Pb element, NIGP 152864, Nj403, outer lateral view (IY161-015). ***R***, *Baltoniodus prevariabilis*? (Fåhraeus, 1966). M element, NIGP 152865, AFT-X-K13/35, anterior view (IY163-029). Scale bars 100 μm.

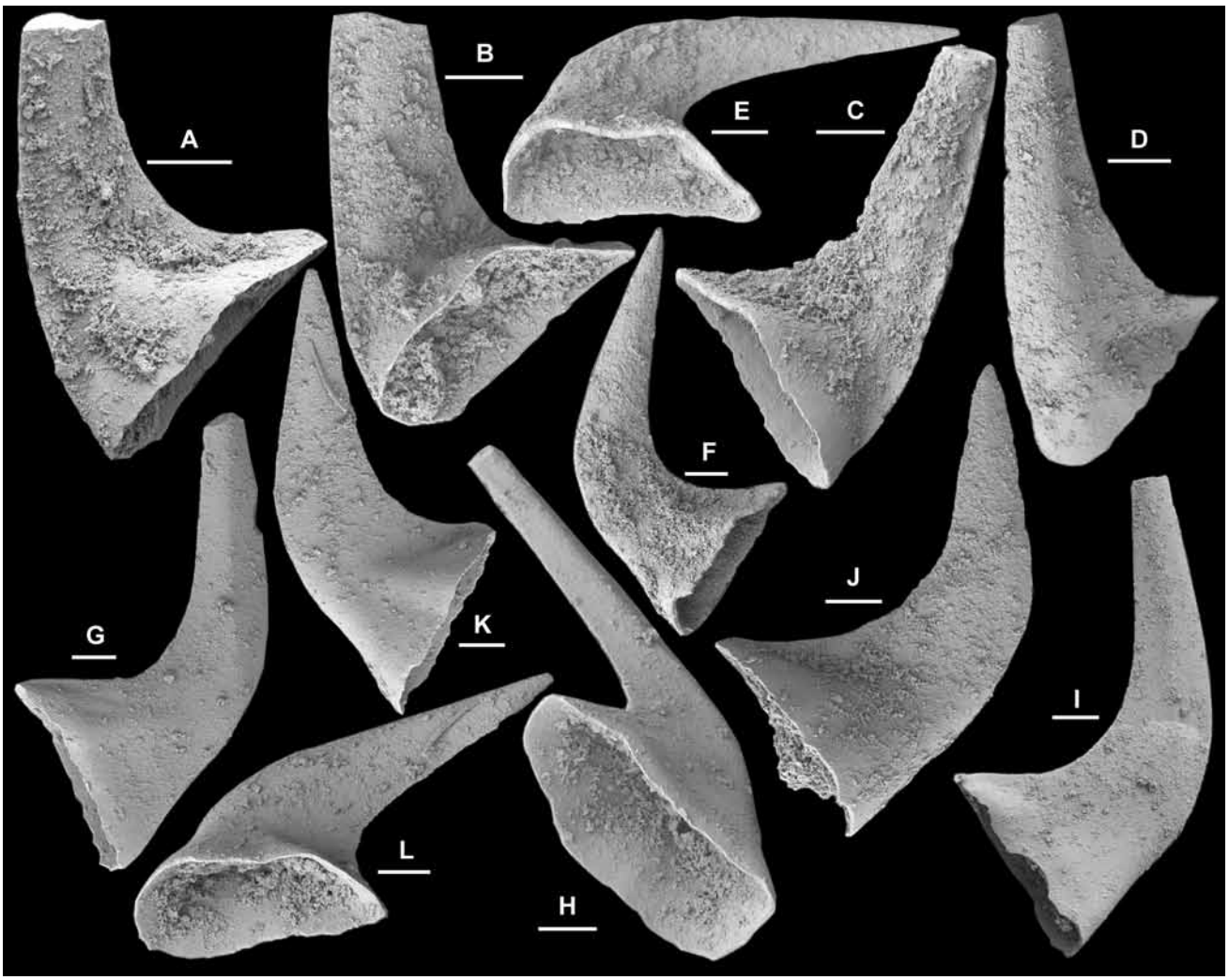

Figure 6. *Costiconus ethingtoni* (Fåhraeus, 1966). A–D, M element; ***A–B***, NIGP 152866, A, posterior view (IY166-016), B, basal-posterior view (IY166-017); ***C***, NIGP 152867, posterior view (IY166-008); ***D***, NIGP 152868, anterior view (IY166-015). E–I, Pb element; ***E–F***, NIGP 152869, E, basal view (IY166-002), F, inner lateral view (IY166-001); ***G–H***, NIGP 152870, G, outer lateral view (IY166-013), H, basal view (IY166-014); ***I***, NIGP 152871, outer lateral view (IY166-009). J–L, Pa element; ***J***, NIGP 152872, inner lateral view (IY166-010); ***K–L***, NIGP 152873, K, inner lateral view (IY166-004), L, inner-basal view (IY166-003). All from sample AFT-X-K13/13, scale bars 100 μm.

Remarks. Eight species belonging to *Cahabagnathus* are known in the literature, ranging in age from the early *P. serra* Zone to early *A. tvaerensis* Zone. Seven of these (the exception being *C. sweeti*) are recorded only from Laurentia, primarily in warm, shallow water facies (Leslie & Lehnert, 2005, Table 1). Leslie & Lehnert (2005) indicated that episodes of wider dispersals of this genus, dominated by endemic species and centered in Laurentia, were associated with major sea level transgressions. *Cahabagnathus sweeti* represents the acme of the cahabagnathid development at or near the Middle/Late Ordovician transition, when it became more cosmopolitan and also invaded deeper and cooler water environments.

Cahabagnathus sweeti (Bergström, 1971)

Fig. 8A–H

Polyplacognathus sweeti Bergström, 1971: 143–144, pl. 1, figs 1–2, text-fig. 14C–D; Harris *et al*., 1979: pl. 2, figs 12–13; Wang & Lou, 1984: 257, pl. 11, fig. 20, pl. 12, figs 5–6.

Petalognathus bergstroemi Drygant, 1974b: 54, pl. 1, figs 1–2.

Cahabagnathus sweeti (Bergström).–Bergström, 1983: 51, fig. 6I–J; Bauer, 1990: pl. 1, figs 16–17; Bergström, 1990: pl. 1, fig. 18; Gao, 1991: 128, pl. 8, figs 4–6; Bauer, 1994: pl. 4, figs 1–3; Wang *et al*., 1996: pl. 1, figs 24, 27, pl. 4, fig. 11; Zhang, 1998b: fig. 9G–H; Wang & Zhou, 1998: pl. 1, fig. 1; Lehnert *et al*., 1999: pl. 3, fig. 11; Zhao *et al.*, 2000: 192, pl. 29, figs 7–10; Leslie & Lehnert, 2005: figs 1–2; Bergström, 2007: fig. 3C.

Material. Eight specimens from two samples of the lower Kanling Formation (see Tables 1–2).

Description. This species is rare in the Dawangou samples, being represented by only a few specimens. It has a bimembrate apparatus consisting of paired (sinistral and dextral) stelliplanate Pa and pastiniplanate Pb elements. Both elements bear an indistinct cusp and four processes (anterior, posterior, antero-lateral and postero-lateral) with a central row of nodes on each one. The sinistral and dextral elements

Figure 7. *Costiconus ethingtoni* (Fåhraeus, 1966). A–E, Sa element; ***A–C***, NIGP 152874, Nj379, A–B, lateral views (IY154-010, IY154-011), C, basal view (IY154-009); ***D–E***, NIGP 152875, 14/45, lateral views (IY155-032, IY155-033). ***F–G***, Sb element, NIGP 152876, 13/40, F, basal view (IY155-022), G, inner lateral view (IY155-021). H–L, Sc element; ***H***, NIGP 152877, Nj388, inner lateral view (IY162-010); ***I–J***, NIGP 152878, Nj378, I, inner lateral view (IY160-016), J, outer lateral view (IY160-015); ***K–L***, NIGP 152879, Nj297, K, outer lateral view (IY159-008), L, inner lateral view (IY159-009). M–T, Sd element; ***M–O***, NIGP 152880, Nj298, M, upper view (IY151-001), N, outer lateral view (IY151-002), O, inner lateral view (IY151-003); ***P–S***, NIGP 152881, Nj379, P–Q, lateral views (IY154-016, IY154-014), R, basal view (IY154-015), S, posterior view (IY154-017); ***T***, NIGP 152882, 13/45, posterior view (IY155-034). ***U***, Pa element, NIGP 152883, Nj388, inner lateral view (IY162-013). Scale bars 100 μm.

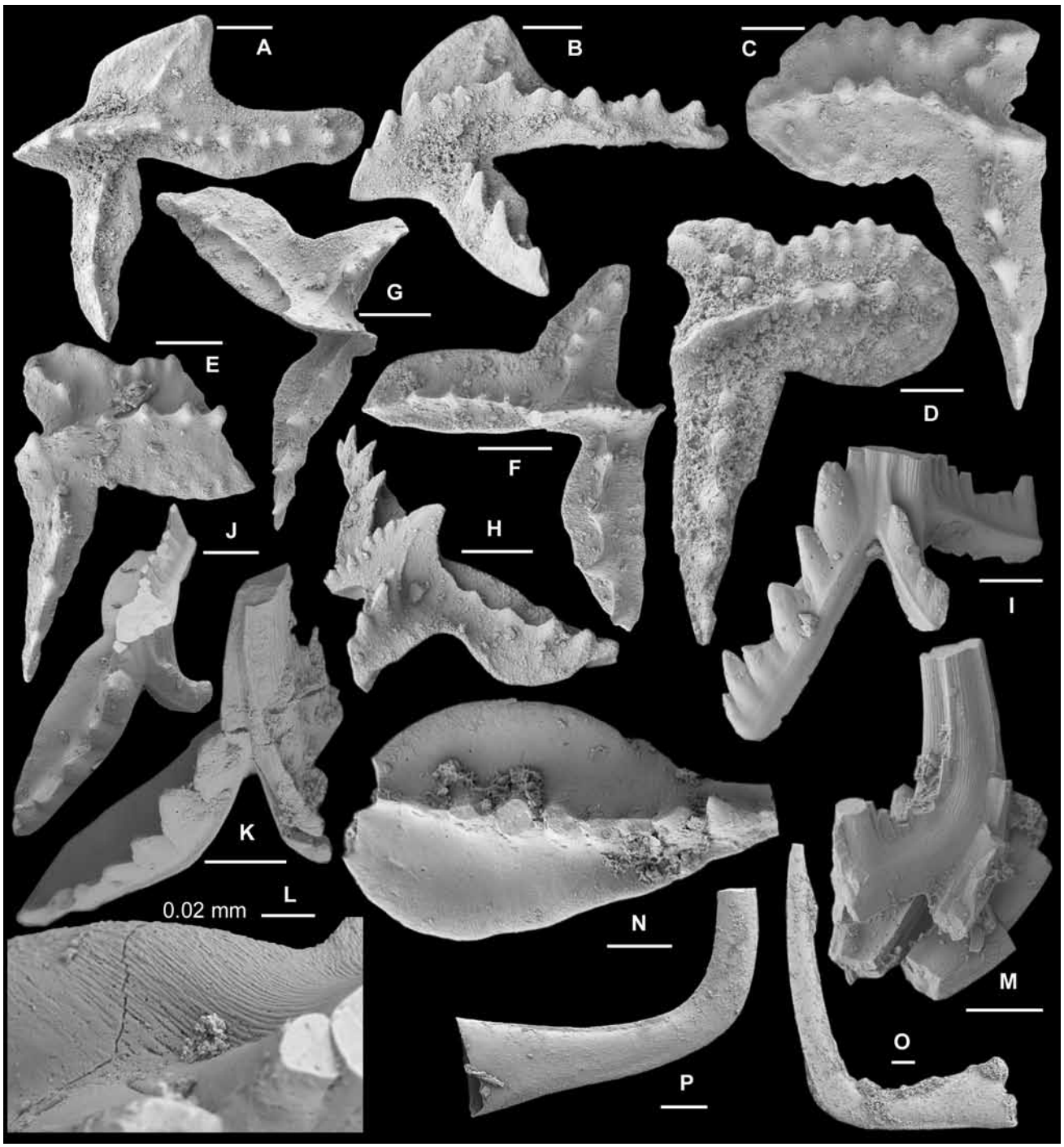

Figure 8. A–H, *Cahabagnathus sweeti* (Bergström, 1971). ***A–B***, sinistral Pa (stelliplanate) element, NIGP 152884, Nj384, A, upper view (IY154-019), B, upper-lateral view (IY154-020); ***C***, dextral Pb (pastiniplanate) element, NIGP 152885, AFT-X-K13/43, upper view (IY164-019); ***D***, sinistral Pb (pastiniplanate) element, NIGP 152886, AFT-X-K13/43, upper view (IY164-020); ***E***, sinistral Pb (pastiniplanate) element, NIGP 152887, AFT-X-K13/43, upper view (IY164-021); ***F***, dextral Pa (stelliplanate) element, NIGP 152888, AFT-X-K13/43, upper view (IY164-022); ***G–H***, dextral Pa (stelliplanate) element, NIGP 152889, AFT-X-K13/43, G, upper view (IY164-024), H, lateral view (IY164-026). I–L, *Baltoniodus* sp. B. ***I–J***, ***L***, Pa element, NIGP 152890, Nj406, I, outer lateral view (IY155-011), J, upper view (IY155-012), L, upper view, close up showing fine striation on the upper surface (IY155-013); ***K***, Pa element, NIGP 152891, Nj406, antero-outer lateral view (IY161-012). M–N, *Baltoniodus alobatus* (Bergström, 1971). ***M***, Sd element, NIGP 152892, Nj406, postero-lateral view (IY161-010); ***N***, Pa element, NIGP 152893, Nj406, upper view (IY161-009). O–P, *Cornuodus longibasis* (Lindström, 1955). ***O***, Sb element, NIGP 152894, AFT-X-K13/13, outer lateral view (IY167-001); ***P***, Sa element, NIGP 152895, Nj291, lateral view (IY158-004). Scale bars 100 μm, unless otherwise indicated.

form mirror-images of each other (Fig. 8C–D). Pa element has a short, blade-like anterior process nearly linear with the longer posterior process; antero-lateral process narrower and longer, being nearly perpendicular to the anterior and posterior processes; postero-lateral process shorter with a wider platform, forming an obtuse angle (about 110°) with the anterior process (Fig. 8A–B). A couple of specimens from the same sample have a rather prominent cusp, and their postero-lateral process has a narrower platform and forms a narrower angle (about 60°) with the anterior process (Fig. 8F–G), hence they are only questionably included in this species. Pb element with a short anterior process and a long posterior process represented by a row of nodes arranged more or less in straight line across the centre of the platform; posterior process with a wide and rounded platform in upper view; antero-lateral process long and tapering distally with the mid-row of nodes approximately perpendicular to the row of nodes on the anterior or posterior process; postero-lateral process shorter, with central row of nodes forming an angle of about 130° with the row of the nodes on the posterior process; nodes also developed along the platform margins of posterior and postero-lateral processes (Fig. 8C–E).

Remarks. Bergström (1983) suggested that five distinctive species of *Cahabagnathus* occurring in successive stratigraphic order in North America formed an evolutionary lineage from the oldest *C*. sp. A (=*C. directus* Bauer, 1987) of mid-late Darriwilian age (early *P. serra* Zone) to the youngest *C. carnesi* in the early Sandbian (early *A. tvaerensis* Zone). He proposed the generic name *Cahabagnathus* for this group and indicated that its direct ancestor might be a species of *Eoplacognathus*, such as *E. foliaceus* and *E. reclinatus*. Bergström (1983, p. 41) and Zhang (1998b, p. 14–15) also discussed in detail the evolutionary trends and character transformations through several recognized stages of the *Cahabagnathus* lineage. Within the eight known species of *Cahabagnathus*, Leslie & Lehnert (2005) recognized two lineages that shared an unknown common ancestor, and suggested that their dispersals and speciation were largely influenced by the transgressive and regressive events of sea level changes.

Cahabagnathus sweeti differs from *C. carnesi* Bergström, 1983 in having the short anterior process in the Pb element more or less extending straight, rather than bending towards the antero-lateral process as in the Pb element of *C. carnesi*. In China, *C. sweeti* has only been recorded from the Kanling Formation (Gao, 1991; Wang *et al*., 1996; Wang & Zhou, 1998) and subsurface age equivalents (Zhao *et al.*, 2000) of the Tarim Basin, and from the Sandaogou Formation of Longxian County, Shaanxi Province in North China (Wang & Lou, 1984; Wang *et al*., 1996).

Costiconus Rasmussen, 2001

Type species. *Panderodus ethingtoni* Fåhraeus, 1966.

Costiconus ethingtoni (Fåhraeus, 1966)

Figs 6–7

Panderodus ethingtoni Fåhraeus, 1966: 26, pl. 3, fig. 5a–b.
Walliserodus ethingtoni (Fåhraeus).–Bergström *et al.*, 1974: pl. 1, fig. 12; An & Ding, 1982: pl. 2, figs 7–8; An *et al*., 1983: 162, pl. 26, figs 16–18; An & Xu, 1984: pl. 2, fig. 6; Wang & Lou, 1984: 288, pl. 3, figs 1–5; An *et al*., 1985: pl. 10, figs 19–22; Ding, 1987: pl. 5, fig. 24; Chen & Zhang, 1989: pl. 5, fig. 24; Pohler & Orchard, 1990: pl. 2, fig. 19; Ding *et al*. in Wang, 1993: 213, *partim* only pl. 18, figs 4–6, 9, 11; Chen & Bergström, 1995: pl. 8, figs 13–14; Wang *et al*., 1996: pl. 1, fig. 15; Albanesi in Albanesi *et al*., 1998: 114, pl. 14, figs 20–25, text-fig. 8; Zhang, 1998c: 95–96, pl. 18, figs 10–15; Wang & Bergström, 1999a: 344, pl. 3, figs 6–7; Lehnert *et al*., 1999: pl. 2, fig. 6; Wang & Qi, 2001: pl. 2, fig. 27; Wang, 2001: pl. 1, figs 25–26; Pyle & Barnes, 2002: pl. 22, figs 19–22.
Costiconus ethingtoni (Fåhraeus).–Rasmussen, 2001, 62–64, pl. 3, figs 16–18 (*cum syn.*); Zhen *et al.*, 2009a: 139–140, fig. 3A–W; Zhen *et al.*, 2009b: 31–33, fig. 4H–W (*cum syn.*); Viira, 2011: fig. 7O, Q.

Material. 443 specimens from 27 samples (see Tables 1–2).

Remarks. Specimens of this species recovered from the Dawangou section are identical with those recently described from the Yenwashan Formation of the JCY area of South China (Zhen *et al*., 2009a) and from the Thompson Creek area in New Zealand (Zhen *et al*. 2009b). Based on a large collection from Dawangou, *C. ethingtoni* is interpreted as a septimembrate apparatus including a non-geniculate short-based M element (Fig. 6A–D), multicostate long-based S (Sa, Sb, Sc and Sd) elements (Fig. 7A–T) that show a wide variation in respect to the number of costae, and non-costate Pa (Figs 6J–L, 7U) and Pb (Fig. 6E–I) elements. The four types of the S elements were described in detail by Zhen *et al*. (2009a). The M element defined herein was previously referred to as a P element (see Zhang, 1998c, pl. 18, fig. 10; Zhen *et al*., 2009a, fig. 3R–W; Zhen *et al*., 2009b, fig. 4T-W) from which it can be distinguished by having a shorter and more posteriorly flared base. The P elements defined herein were previously referred to as representing the M element (e.g., Zhang, 1998c, pl. 18, fig. 11), and show a rather wide variation from long-based (Fig. 7U) to relatively short-based (Fig. 6G).

Dapsilodus Cooper, 1976

Type species. *Distacodus obliquicostatus* Branson & Mehl, 1933.

Dapsilodus viruensis (Fåhraeus, 1966)

Fig. 9A, ?B–C

Acodus viruensis Fåhraeus, 1966: 12, pl. 2, fig. 2a–b, text-fig. 2A.
Acontiodus sulcatus Fåhraeus, 1966: 17, pl. 2, fig. 6a–b, text-fig. 2F.
Acodus? mutatus (Branson & Mehl).–Löfgren, 1978: 44, pl. 2, figs 9–21 (*cum syn.*); Zeng *et al*., 1983: pl. 12, figs 39–40.
Dapsilodus mutatus (Branson & Mehl).–An, 1987: 142, *partim* only pl. 4, figs 14, 17–18, 22–23, 27; An & Zheng, 1990: 164, pl. 4, figs ?1, 2–5; Stouge & Bagnoli, 1990: 14, pl. 9, figs 19, 26–27; Gao, 1991: 130, pl. 12, figs 10, 17; Ding *et al*. in Wang, 1993: pl. 15, figs ?22, 23–24, 26; Armstrong, 1997: 786, pl. 5–8, ?3–4; Ferretti & Serpagli, 1999: 230, pl. 3, figs 20–23; Wang, 2001: 351, pl. 2, figs 8–9 (*cum syn.*).
Dapsilodus striatus Chen & Zhang, 1984b: 126, 134, pl.1, figs 17–20; Duan, 1990: pl. 3, fig. 1.
Dapsilodus viruensis (Fåhraeus).–Zhang, 1998b: 58–59, pl. 4, figs 1–6 (*cum syn.*); Rasmussen, 2001: 67–68, pl.

4, figs 15–17 (*cum syn.*); Zhen *et al*., 2009a: 142, fig. 4A–O (*cum syn.*).

Material. 74 specimens from 17 samples (see Tables 1–2).

Remarks. Löfgren (1978), An (1987) and Stouge & Bagnoli (1990) regarded *Acodus viruensis* Fåhraeus, 1966 as a junior synonym of *Belodus* (?) *mutatus* Branson & Mehl, 1933, whereas others, including Zhang (1998b), Ferretti & Serpagli (1999) and Rasmussen (2001), considered them as separate species. The taxonomic position of *Belodus* (?) *mutatus* has been discussed for many decades, and it remains as a poorly known species until its species apparatus and constituent elements are revised according to the multielement species concept. In particular, Rasmussen (2001, p. 68) pointed out that the original description of *Belodus* (?) *mutatus* by Branson & Mehl (1933, p. 126) indicated the presence of "one or two minute denticles" on "the posterior end" in some of the specimens from the basal Maquoketa Shale of Missouri. However, this taxonomically important character has not been observed in the type specimens (holotype and other topotype material) and from any of the Swedish and Chinese material previously assigned to *D. mutatus*, and more likely the Chinese specimens belong to *D. viruensis* (see Zhang, 1998b).

Drepanodus Pander, 1856

Type species. *Drepanodus arcuatus* Pander, 1856.

Drepanodus arcuatus Pander, 1856

Fig. 10A–N

Drepanodus arcuatus Pander, 1856: 20, pl. 1, figs 2, 4–5, 17, 30, ?31; An, 1981: pl. 3, fig. 22; An *et al*., 1985: pl. 4, figs 6–11, pl. 12, 10–13, 15; An, 1987: 143–144, pl. 8, figs 7–9, 11–12, 15–18, 24; Ni & Li, 1987: 403, pl. 59, figs 6–7; Bergström, 1988: pl. 1, figs 4–5; Duan, 1990: pl. 2, figs 25–26; Ding *et al*. in Wang, 1993: 171, pl. 10, figs 1–4, 8–11, 17, ?20; Chen & Bergström, 1995: pl. 8, figs 10, 16; Zhang, 1998c: 59–60, pl. 4, figs 7–11, 15–16 (*cum syn.*); Wang & Bergström, 1999a: 334, pl. 2, figs 4–5; Wang, 2001: 352, pl. 1, figs 2, 6; Löfgren & Tolmacheva, 2003b: 211–215, figs 2, 3A–C, E–H, 5K–V, 6M–U, 7H–N, 8A–G (*cum syn.*); Zhen *et al*., 2004a: 52–53, pl. 3, figs 1–12; Agematsu *et al*., 2007: 31, fig. 13.9; Ortega *et al.*, 2008: fig. 6.27–6.28; Zhen *et al*., 2009b: fig. 5A–N (*cum syn.*); Zhen & Nicoll, 2009: 11, fig. 5A–F; Viira, 2011: figs 14A, ?B, C–G, ?H, I, K, S, 15A–E, ?F–G.

Material. 858 specimens from 44 samples (see Tables 1–2).

Remarks. Both species of *Drepanodus*, *D. arcuatus* and *D. reclinatus* are rather common in collections from the Dawangou section, and can be easily recognized by their generally large size in the fauna. They are morphologically similar except that costae are generally absent in all the constituent elements of *D. arcuatus*. Armstrong (2000) included in *D. arcuatus* various forms of costate elements, which were reassigned to *D. reclinatus* by Löfgren & Tolmacheva (2003), who revised both species as having a septimembrate apparatus. Specimens from Dawangou (Fig. 10A–N) are identical with those illustrated by Löfgren & Tolmacheva (2003) from Sweden, except that the Sd element is not distinguished. As indicated by Löfgren & Tolmacheva (2003, p. 215), the Sd element represents the end member of a symmetry transition series and the general morphology is rather similar to the Sb element but with a more compressed base. It is likely that the Sb element documented herein (Fig. 10E–G) incorporates the Sd element as defined by Löfgren & Tolmacheva (2003).

Drepanodus reclinatus (Lindström, 1955a)

Fig. 11A–P

Acontiodus reclinatus Lindström, 1955a: 548, text-fig. 3C, pl. 2, figs 5–6.
Drepanodus reclinatus (Lindström).–Zhang, 1998c: 60–61, pl. 4, figs 12–14, 17–20 (*cum syn.*); Löfgren & Tolmacheva, 2003: 216–217, figs 5A–J, 7A–G (*cum syn.*); Ortega *et al.*, 2007: fig. 6M; Ortega *et al.*, 2008: fig.6.17–6.18.
Drepanodus arcuatus Pander.–Armstrong, 2000: 49, pl. 3, figs 1–18.
Drepanodus sp. A.–Zhen & Percival, 2004b: 159–160, *partim*, only fig. 3D, F–I; non fig. 3E = *Protopanderodus*.
Protopanderodus robustus (Hadding).–An *et al*., 1983: 132, pl. 15, fig. 21; An & Zheng, 1990: pl. 6, figs 15–17; Chen & Bergström, 1995: *partim* only pl. 8, figs 3–4; Wang & Bergström, 1998: 342, *partim* only pl. 2, figs 7, 9.
Cornuodus longibasis (Lindström, 1955).–Wang & Qi, 2001: pl. 1, fig. 11.
Paroistodus sp. An & Zheng, 1990: pl. 6, fig. 11.

Material. 116 specimens from 26 samples (see Tables 1–2).

Remarks. All seven elements (except for the Sd) recovered from Dawangou (Fig. 11A–P) are identical with those illustrated by Löfgren & Tolmacheva (2003). Elements of *D. reclinatus* can be distinguished from *D. arcuatus* and other species of *Drepanodus* by being laterally costate.

Some specimens ascribed to *Drepanodus* sp. A from the Weemalla Formation (Darriwilian) of central New South Wales should be re-assigned to *D. reclinatus* representing the M (Zhen & Percival, 2004b, fig. 3D) and Pa (Zhen & Percival, 2004b, fig. 3F–I) elements. One figured specimen of *D*. sp. A (Zhen & Percival, 2004b, fig. 3E) represents an asymmetrical bicostate element of a *Protopanderodus* species, comparable to those described by Zhen & Percival (2004b, p. 172, fig. 11G–O) as *Protopanderodus robustus* (Hadding, 1913). However, *P. robustus* remains a poorly-known species, and may be more closely related to multicostate species rather than bicostate *Protopanderodus* species (see discussion under remarks of *P. cooperi*). Specimens previously assigned to *P. robustus* by various authors may belong to *D. reclinatus* (see synonymy list; also Löfgren & Tolmacheva, 2003).

Drepanoistodus Lindström, 1971

Type species. *Oistodus forceps* Lindström, 1955a.

Drepanoistodus basiovalis (Sergeeva, 1963)

Fig. 12A–Q

Oistodus basiovalis Sergeeva, 1963: 96, pl. 7, figs 6, 7, text-fig. 3.

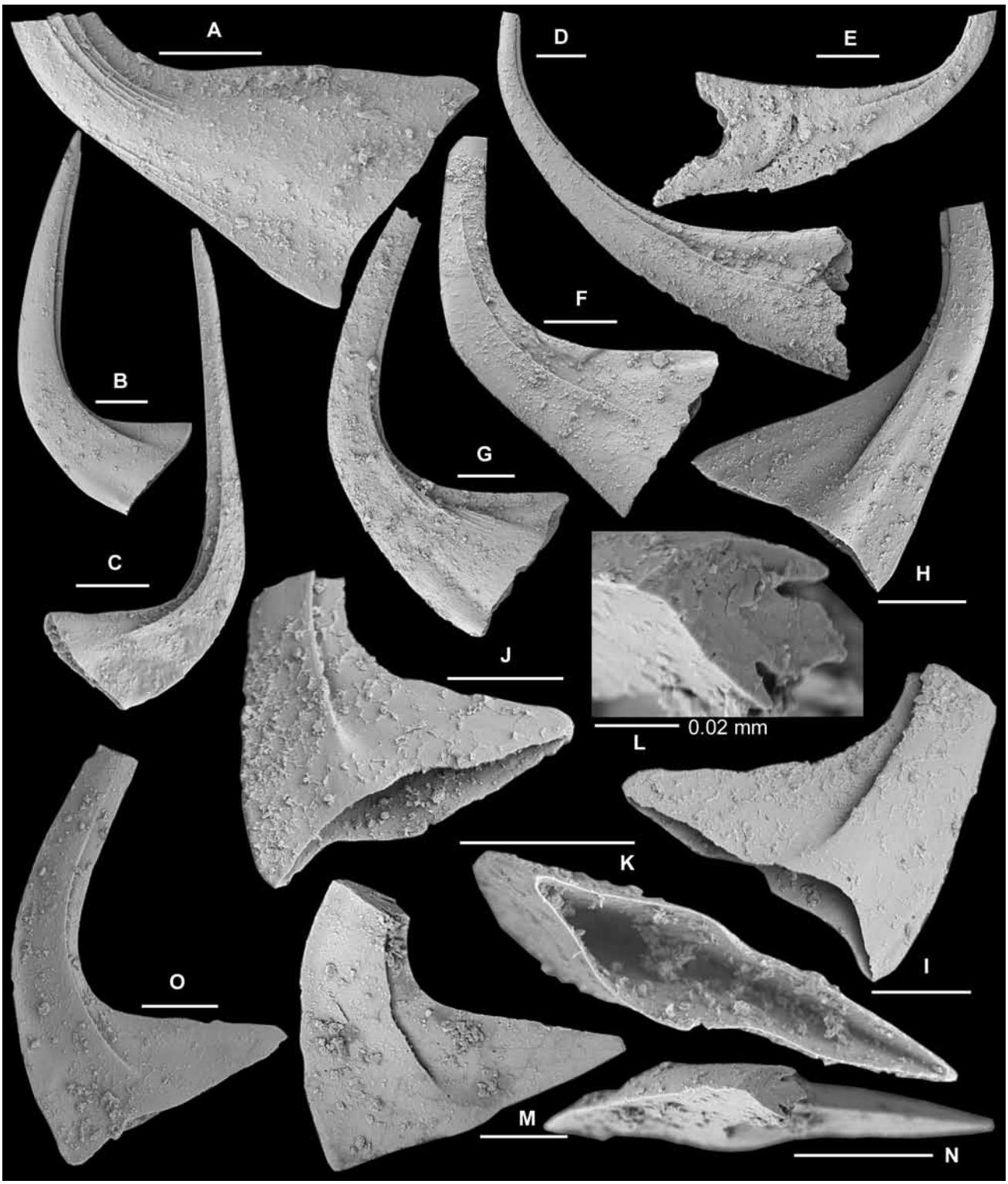

Figure 9. A–C, *Dapsilodus viruensis* (Fåhraeus, 1966). ***A***, Sc element, NIGP 152896, Nj375, outer lateral view (IY159-024). B–C, Sa element; ***B***, NIGP 152897, Nj375, lateral view (IY159-025), tentatively assigned to this species; ***C***, NIGP 152898, Nj375, lateral view (IY159-026). D–O, *Scabbardella altipes* (Henningsmoen, 1948). D–E, long-based acodiform element; ***D***, NIGP 152899, Nj378, outer lateral view (IY153-016); ***E***, NIGP 152900, Nj403, outer lateral view (IY161-021). F–G, medium-based acodiform element; ***F***, NIGP 152901, Nj297, outer lateral view (IY159-012); ***G***, NIGP 152902, AFT-X-K13/13, outer lateral view (IY167-002). H–O, asymmetrical distacodiform element; ***H***, NIGP 152903, Nj376, outer lateral view (IY159-029); ***I–K***, NIGP 152904, Nj378, I, outer lateral view (IY160-017), J, inner lateral view (IY160-017), K, basal view (IY160-020); ***L–N***, NIGP 152905, Nj379, L, upper view, close up of cross section of the cusp (IY160-035), M, inner lateral view (IY160-036), N, upper view (IY160-034); ***O***, NIGP 152906, Nj379, outer lateral view (IY160-033). Scale bars 100 μm, unless otherwise indicated.

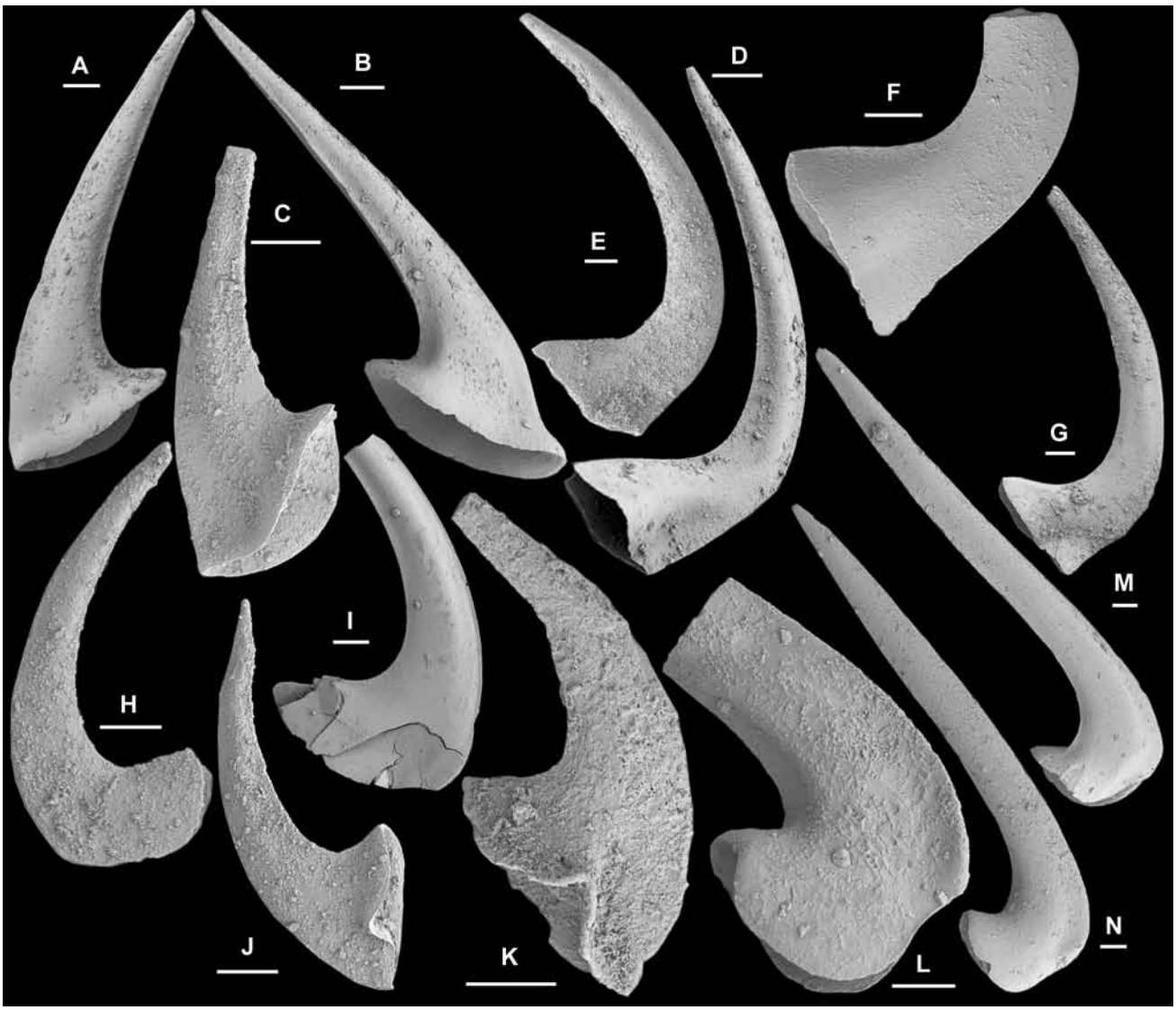

Figure 10. *Drepanodus arcuatus* Pander, 1856. A–C, M element; ***A***, NIGP 152907, AFT-X-K13/13, posterior view (IY166-021); ***B***, NIGP 152908, AFT-X-K13/13, anterior view (IY166-019); ***C***, NIGP 152909, Nj297, posterior view (IY150-034). ***D***, Sa element, NIGP 152910, Nj375, lateral view (IY162-024). E–G, Sb element; ***E***, NIGP 152911, Nj297, inner view (IY150-036); ***F***, NIGP 152912, Nj294, outer lateral view (IY147-035); ***G***, NIGP 152913, Nj297, inner lateral view (IY150-035). H–I, Sc element; ***H***, NIGP 152914, Nj297, inner lateral view (IY150-031); ***I***, NIGP 152915, Nj406, outer lateral view (IY161-004). J–K, Pa element; ***J***, NIGP 152916, Nj297, outer lateral view (IY150-033); ***K***, NIGP 152917, Nj294, outer lateral view (IY147-036). L–N, Pb element; ***L***, NIGP 152918, Nj295, inner lateral view (IY149-010); ***M***, NIGP 152919, AFT-X-K13/13, outer lateral view (IY166-023); ***N***, NIGP 152920, AFT-X-K13/13, inner lateral view (IY166-018). Scale bars 100 μm.

Drepanoistodus basiovalis (Sergeeva).–Lindström, 1971: 43, figs 6, 8; Löfgren, 1978: 55, pl. 1, figs 11–17, text-fig. 26B, C (*cum syn.*); An *et al*., 1985: pl. 13, figs 17–20; An, 1987: 145–146, pl. 9, figs 30–31; An & Zheng, 1990: 164, pl. 8, fig. 9; Ding *et al*. in Wang, 1993: 173, *partim* only pl. 12, figs 1–2, 4; Albanesi in Albanesi *et al*., 1998: 135, pl. 3, figs 15–18; Johnston & Barnes, 2000: 18, pl. 11, figs 10, 11, 15, 16 (*cum syn.*); ?Zhen *et al*., 2003b: 191, fig. 14A–K; Zhen *et al*., 2007: pl. 1, figs 27–37.

Drepanoistodus suberectus (Branson & Mehl).–Cooper, 1981: 164, pl. 26, figs 1, 2, 6.

Material. 110 specimens from 12 samples (Tables 1–2).

Remarks. *Drepanoistodus* is one of the most common genera widely distributed in the Ordovician with nearly 30 species names proposed in the literature. Due to their simple, coniform elements, the majority of these species remain inadequately documented. Recent studies of the group suggest that its species had a seximembrate or septimembrate apparatus (Zhen *et al*., 2007). *Drepanoistodus basiovalis* was originally erected as a form species based on a geniculate coniform element from the Lower Ordovician of the St Petersburg region, Russia (Sergeeva, 1963, pl. 7, figs 6–7, text-fig. 3). Our current understanding of *D. basiovalis* is largely based on the revision of the species by Löfgren (1978) on material from the Middle Ordovician of Jämtland, northern Sweden (also see Zhen *et al*., 2007, pl. 1, figs 27–37). Löfgren (1978) suggested a trimembrate apparatus including homocurvatiform (= P element herein), oistodiform (= M element) and suberectiform (= Sa element). We interpret the homocurvatiform element as P elements having an extended, inwardly flexed antero-basal corner (Löfgren, 1978, pl. 1, fig. 13 and probably also fig. 12), with the S elements forming a

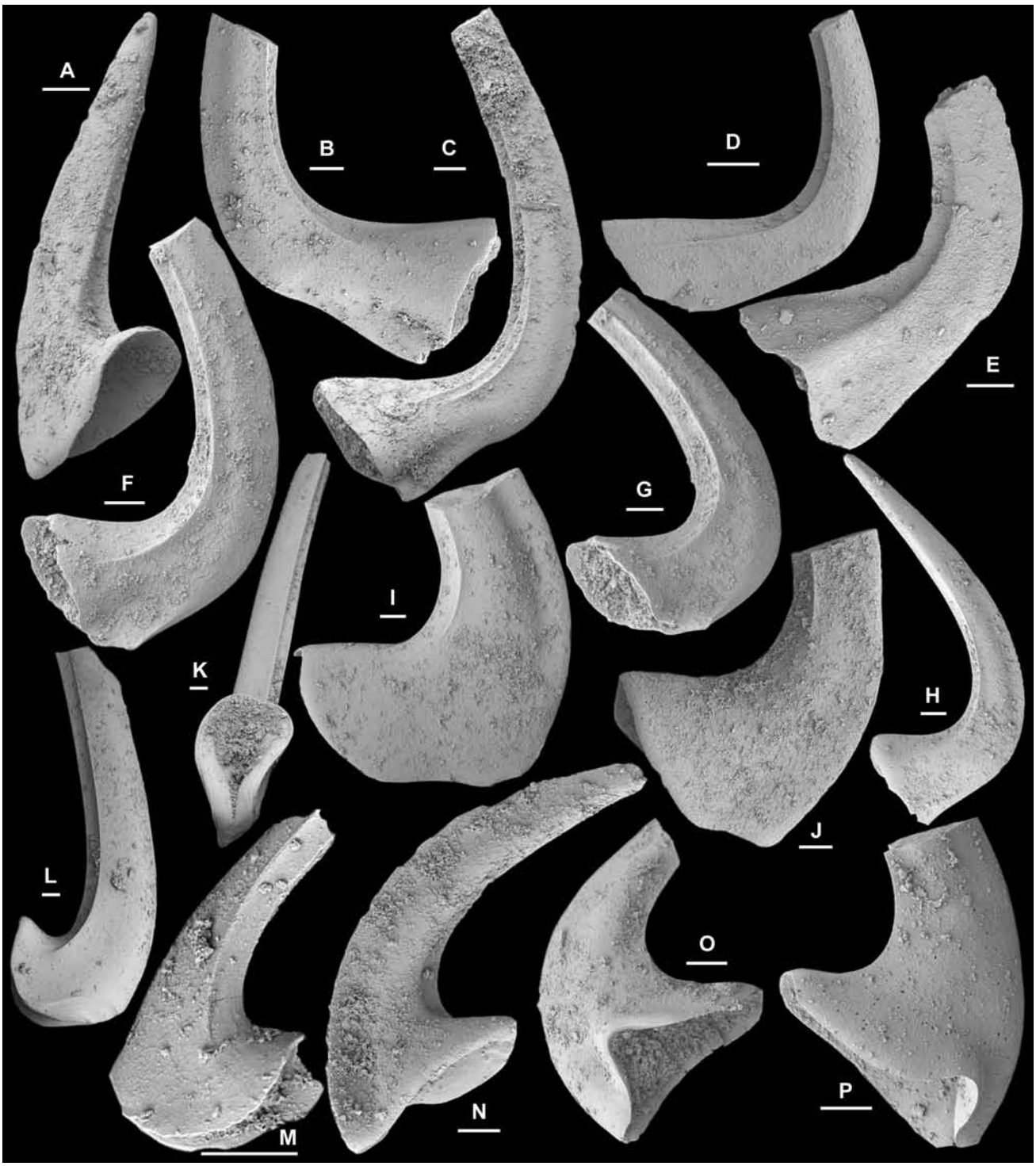

Figure 11. *Drepanodus reclinatus* (Lindström, 1955). ***A***, M element, NIGP 152921, AFT-X-K13/13, posterior view (IY166-005). B–E, Sa element; ***B***, NIGP 152922, AFT-X-K13/13, lateral view (IY166-031); ***C***, NIGP 152923, AFT-X-K13/13, lateral view (IY166-032); ***D***, NIGP 152924, Nj375, lateral view (IY162-025); ***E***, NIGP 152925, Nj295, lateral view (IY149-011). F–H, Sb element; ***F–G***, NIGP 152926, AFT-X-K13/13, F, inner lateral view (IY166-030), G, basal-inner lateral view (IY166-029); ***H***, NIGP 152927, AFT-X-K13/13, outer lateral view (IY166-033). I–J, Sc element; ***I***, NIGP 152928, AFT-X-K13/13, inner lateral view (IY166-026); ***J***, NIGP 152929, AFT-X-K13/13, inner lateral view (IY166-024). K–M, Pb element; ***K–L***, NIGP 152930, Nj375, K basal view (IY152-016), L, antero-inner lateral view (IY152-015); ***M***, NIGP 152931, AFT-X-K13/13, inner lateral view (IY169-010). N–P, Pa element; ***N***, NIGP 152932, AFT-X-K13/13, inner lateral view (IY166-034); ***O***, NIGP 152933, AFT-X-K13/13, outer lateral view (IY166-028); ***P***, NIGP 152934, AFT-X-K13/13, outer lateral view (IY166-036). Scale bars 100 μm.

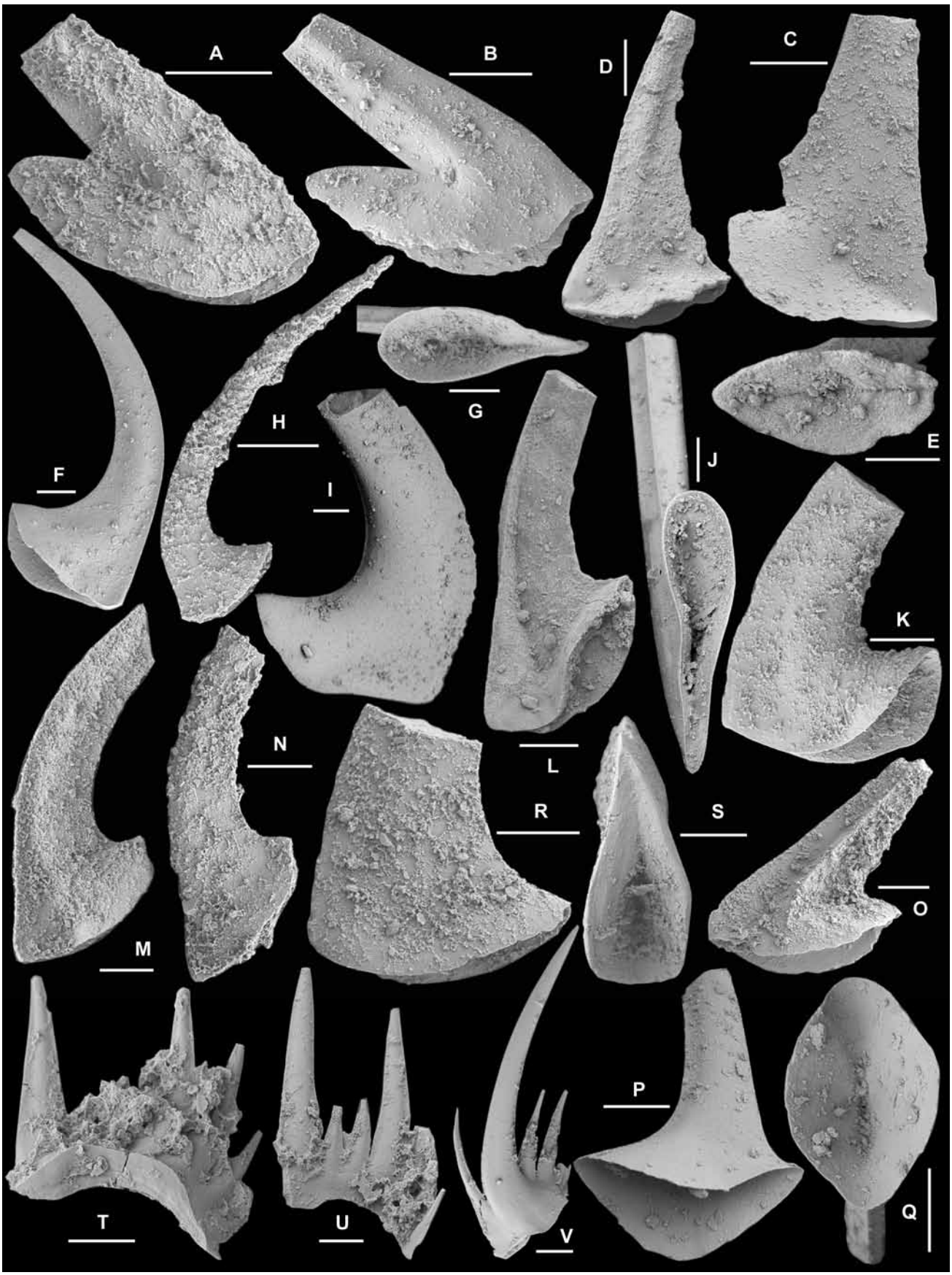

Figure 12. A–Q, *Drepanoistodus basiovalis* (Sergeeva, 1963). A–B, M element; ***A***, NIGP 152935, Nj378, anterior view (IY160-004), ***B***, NIGP 152936, Nj378, posterior view (IY160-005). C–E, Sa element; ***C***, NIGP 152937, Nj379, lateral view (IY160-039); ***D–E***, NIGP 152938, Nj291, D, lateral view (IY158-008), E, basal view (IY158-011). F–H, Sb element; ***F–G***, NIGP 152939, Nj379, F, inner lateral view (IY160-040), G, basal view (IY160-041); ***H***, NIGP 152940, Nj378, outer lateral view (IY160-011)… (continued on facing page)

symmetry transition series (Löfgren, 1978, pl. 1, figs 11, 14). Löfgren also included an element with a prominent costa on the outer lateral face (Löfgren, 1978, pl. 1, fig. 12), which may represent the additional P element. Based on study of the Swedish material, Zhen (in Zhen *et al*. 2007) suggested a septimembrate apparatus for this species, with the Sa element showing a symmetrical outline of the base, which is widest in the middle and tapers anteriorly and posteriorly (Zhen *et al*., 2007, pl. 1, fig. 30).

Lindström (*in* Ziegler, 1974, p. 73) suggested that *D. basiovalis* could be differentiated from the stratigraphically older *D. forceps* in having a rounded outline of the base in the M element, and a more flattened cross-section in the S elements. Zhen *et al.* (2007, pl. 1, fig. 7) noted that the Sa element of *D. forceps* has a oval-shaped outline of the base that is widest anteriorly and only tapers posteriorly.

Drepanoistodus sp. (Fig. 12R–S) shows some resemblance to *Drepanoistodus* sp. cf. *D. nowlani* Ji & Barnes, 1994, a stratigraphically older species described from the Honghuayuan Formation (Early Ordovician) of South China (Zhen *et al*., 2007, pl. 2, figs 4–5) in having the base widest posteriorly, but the Dawangou species has a shorter, laterally less flared base.

The M element of *D. basiovalis* from the Dawangou section typically shows a broad carina or a weakly developed costa on the posterior face (Fig. 12B), but some specimens from sample Nj298 at the top of the Dawangou Formation exhibit a sharp costa on the posterior face (Fig. 12O), and are identical with the M element of *D. basiovalis* recently illustrated from the lower Darriwilian (lowermost *Lenodus antivariabilis* Subzone) of Sweden (Zhen *et al*., 2007, pl. 1, fig. 27). The posterior face of the M element of *Drepanoistodus stougei* Rasmussen, 1991 also has a prominent costa (see Rasmussen, 2001, pl. 6, figs 10, 13), but the holotype of *D. stougei* exhibits a narrower angle between the cusp and the outer-lateral proto-process and a more rounded outline of the basal margin (Rasmussen, 1991, fig. 6J). The M element of *Drepanoistodus costatus* (Abaimova, 1971) also bears a sharp costa on the posterior face, but has a less extended base and is associated with costate S elements (Zhen *et al*., 2003b, fig. 15).

Dzikodus Zhang, 1998

Type species. *Polonodus tablepointensis* Stouge, 1984.

Remarks. Definition of *Dzikodus* and its morphological and phylogenetic relationship with *Polonodus* were reviewed recently by Zhen & Percival (2004b). Zhang's (1998c) original concept is followed herein to define *Dzikodus* as consisting of a septimembrate apparatus including makellate M, ramiform S, stelliscaphate paired Pa, and stelliscaphate but unpaired Pb elements.

Dzikodus ?tablepointensis (Stouge, 1984)

Fig. 13A–K

Polonodus tablepointensis Stouge, 1984: 72, pl. 12, fig. 13, pl. 13, figs 1–5 (*cum syn.*).
Dzikodus tablepointensis (Stouge).–Zhang, 1998c: 65–69, pl. 7, figs 1–12, pl. 8, figs 1–6 (*cum syn.*).

Material. 31 specimens from two samples at the top of the Dawangou Formation (Tables 1–2).

Remarks. This species is rarely represented in the Dawangou samples with stelliscaphate Pb (Fig. 13A–B), alate Sa (Fig. 13C–G), tertiopedate Sb (Fig. 13H–I), and quadriramate Sd (Fig. 13J–K) elements recovered. The Pb element has four processes, an inconspicuous cusp and a wide open basal cavity, and is comparable with those illustrated from the Guniutan Formation of South China (Zhang, 1998c, pl. 7, figs 7–9). However, as the two illustrated specimens assigned to the Pb element are incomplete with one lateral process broken off, they are only tentatively referred to *D. tablepointensis*.

Histiodella Harris, 1962

Type species. *Bryantodina sinuosa* Graves & Ellison, 1941.

Histiodella holodentata Ethington & Clark, 1982

Fig. 14A–B

Histiodella holodentata Ethington & Clark, 1982: 47–48, pl. 4, figs 1, 3, 4, 16 (*cum syn.*); Nowlan & Thurlow, 1984: pl. 1, figs 1, 3, 5; Wang & Zhou, 1998: pl. 4, fig. 12; Zhang, 1998c: 72, pl. 9, figs 14–15; Zhao *et al.*, 2000: 205, pl. 27, figs 12–14; Johnston & Barnes, 2000: pl. 15, fig. 7; Du *et al.*, 2005: 365, pl. 1, figs 22–26, 28 (*cum syn.*); Agematsu *et al*., 2006: fig. 7.18; Chen *et al*., 2006: fig. 10W; Percival & Zhen, 2007: 391, pl. 1, figs 22–23; Agematsu *et al*., 2008b: 189, fig. 7.7; Zhen *et al*., 2009b: 38–39, fig. 2O; Bauer, 2010: pl. 2, fig. 9.
Histiodella tableheadensis Stouge, 1984: 87–88, pl. 18, figs 8, 12–14, text-fig. 17; Zhang, 1998c: 72, pl. 9, figs 14, 15 (*cum syn.*); Albanesi & Ortega, 2003: pl. 1, fig. 4.
Histiodella intertexta An.–An *et al*., 1985: pl. 14, figs 15, 16; An, 1987: 154, pl. 18, figs 15, 16, pl. 30, fig. 10; Gao, 1991: 131–132, pl. 9, fig. 5.
Histiodella infrequensa An in An *et al*., 1983: 105–106, pl. 25, figs 1–2, text-fig. 14–12; An & Zheng, 1990: 166–167, *partim* only pl. 7, fig. 4, non fig. 1 (probably a broken Pa element of Rhipidognathidae).
Histiodella kristinae Stouge.–Zhen *et al.*, 2004a: 97–98, fig. 14A–L.

Material. Three specimens (Pa only) from one sample in the upper Dawangou Formation (see Table 1).

(Figure 12 caption, continued from facing page)… I–K, Sc element; ***I–J***, NIGP 152941, Nj375, I, iner lateral view (IY152-017), J, basal view (IY152-018); ***K***, NIGP 152942, Nj378, inner lateral view (IY160-009). L–N, P element; ***L***, NIGP 152943, Nj291, inner lateral view (IY158-010); ***M***, NIGP 152944, Nj378, inner lateral view (IY160-007); ***N***, NIGP 152945, Nj378, outer lateral view (IY160-006). ***O***, M element, NIGP 152946, Nj298, posterior view showing a sharp costa on the posterior face (IY159-020); ***P–Q***, Sa element, NIGP 152947, AFT-X-K13/43, P, lateral view (IY172-009), Q, basal view (IY172-010). ***R–S***, *Drepanoistodus* sp. Sa element, NIGP 152948, Nj378, R, lateral view (IY160-003), S, basal view (IY160-001). T-V, *Erraticodon* sp. ***T***, Pa element, NIGP 152949, AFT-X-K13/36, posterior view (IY172-005); ***U***, Pa element, NIGP 152950, AFT-X-K13/36, anterior view (IY172-004); ***V***, Sc element, NIGP 152951, AFT-X-K13/36, outer lateral view (IY172-001). Scale bars 100 μm.

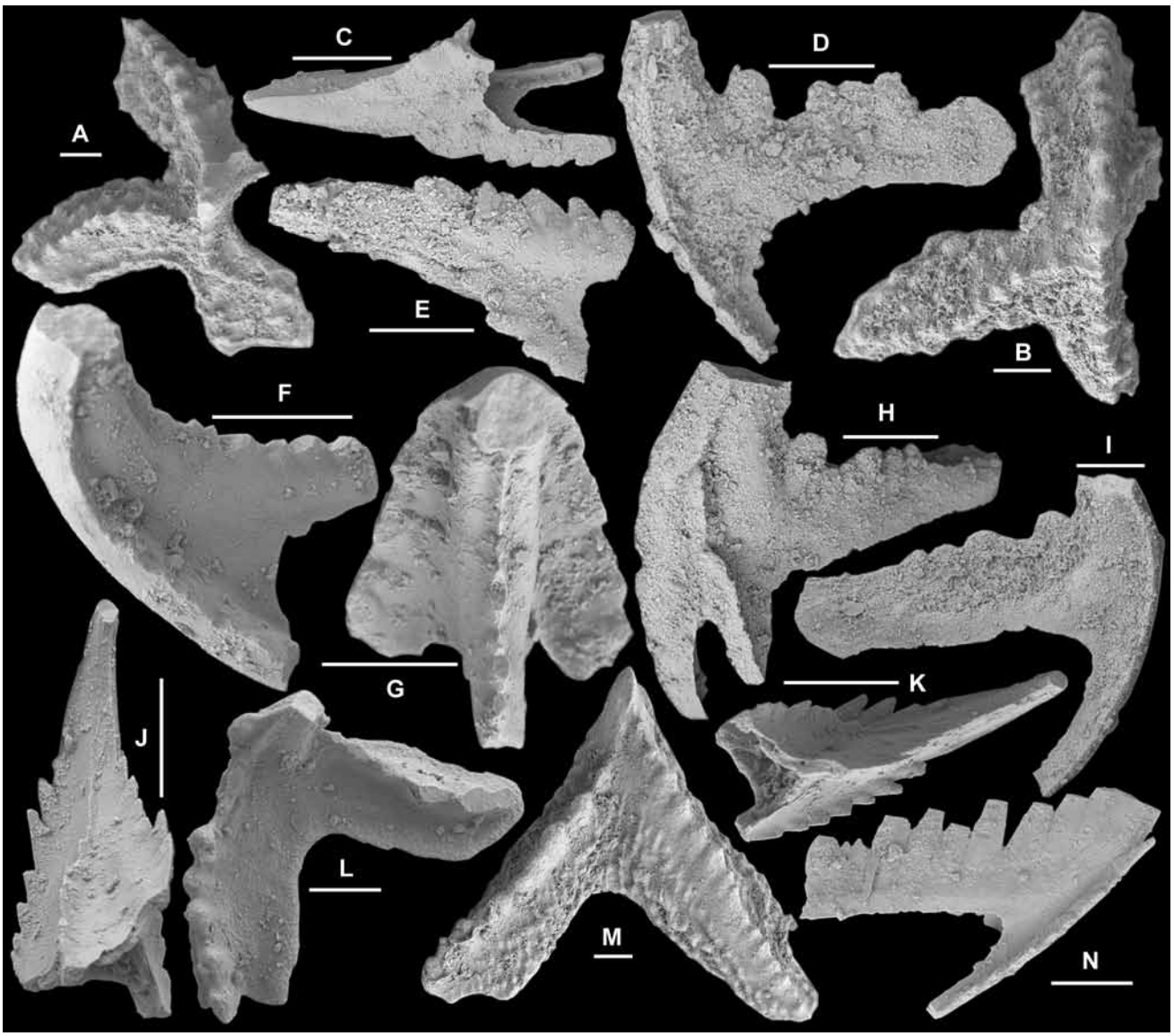

Figure 13. A–K, *Dzikodus* ?*tablepointensis* (Stouge, 1984). A–B, Pb element; ***A***, NIGP 152952, Nj297, upper view (IY150-001); ***B***, NIGP 152953, Nj297, upper view (IY150-002). C–G, Sa element; ***C***, NIGP 152954, Nj297, posterior view (IY150-003); ***D–E***, NIGP 152955, Nj297, D, lateral view (IY150-008), E, anterior view (IY150-010); ***F–G***, NIGP 152956, Nj297, F, lateral view (IY159-006), G, posterior view (IY159-007). ***H–I***, Sb element, NIGP 152957, Nj297, H, outer lateral view (IY150-006), I, inner lateral view (IY150-007). ***J–K***, Sd element, NIGP 152958, Nj297, J, postero-outer lateral view (IY159-005), K, posterior view (IY159-004). L–N, *Polonodus* sp. B. ***L***, P element, NIGP 152959, Nj291, upper view (IY158-002); M, P element, NIGP 152960, Nj291, upper view (IY158-001); ***N***, Sc element, NIGP 152961, Nj291, inner lateral view (IY158-003). Scale bars 100 μm.

Remarks. This species is rare in the Dawangou material and is represented only by the Pa element, which is identical with the holotype of *H. tableheadensis* from the Table Head Formation of western Newfoundland (see Stouge, 1984, pl. 18, fig. 14), and the holotype of *H. holodentata* from the Pogonip Group of the Ibex area of Utah (Ethington & Clark, 1982). Four species of *Histiodella*, including *H. sinuosa* (Graves & Ellison, 1941), *H. holodentata, H. kristinae*, and *H. bellburnensis* Stouge, 1984, were recovered from the Yangjikan Section of Kalpin County, located some 50 km SW of the Dawangou section (Du *et al.*, 2005). These authors recognized four biozones defined by the first appearance of (in ascending order): *H. sinuosa* Zone, *H. holodentata* Zone, *H. kristinae* Zone, and *H. bellburnensis* Zone. The phylogenetic relationship of these species is therefore similar to that reported in Middle Ordovician successions of North America, such as from the Table Head Formation of Newfoundland. Stouge (1984, p. 18, text-fig. 17) demonstrated that the *Histiodella* lineage occurring in the Table Head Formation evolved from older species with a larger cusp and a distally declining upper margin of the anterior process, to younger species with an inconspicuous cusp and a distally raised anterior process. This same evolutionary trend among the *Histiodella* species was also documented by Du *et al.* (2005).

Histiodella infrequensa was erected by An (in An *et al*., 1983) based on Pa elements recovered from the Beianzhuang Formation of Tangshan, Hebei Province. The holotype (An *et al.*, 1983, pl. 25, fig. 1) shows a large cusp (over three times as wide as the adjacent denticles), whereas the paratype

figured (An *et al.*, 1983, pl. 25, fig. 2) exhibits a slightly smaller cusp (about twice as wide as adjacent denticles). An's original definition suggests that *H. infrequensa* is characterized by having an outline more or less quadrilateral with the L/H ratio about 3:2 in lateral view. However, both specimens illustrated by An (in An *et al*., 1983) had the distal part of the cusp broken. Du *et al.* (2005) reassigned to *H. holodentata* the paratype of *H. infrequensa* originally illustrated by An (An *et al.*, 1983, pl. 25, fig. 2). An (in An *et al*., 1983) compared his *H. infrequensa* to *H. sinuosa* (Graves & Ellison, 1941) rather than to *H. holodentata*, implying that when he proposed *H. infrequensa*, An (in An *et al*., 1983) was unaware of the existence of *H. holodentata*. In fact the holotype of *H. infrequensa* is closely comparable with the holotype of *H. holodentata* (Ethington & Clark, 1982, pl. 4, fig. 3) except that the former shows a larger cusp. Therefore, *H. infrequensa* is regarded herein as a junior synonym of *H. holodentata*, with holotype of *H. infrequensa* representing an early form of this species.

Histiodella kristinae Stouge, 1984

Fig. 14C–F

Histiodella kristinae Stouge, 1984: 87, pl. 18, figs 1–7, 9–11, fig. 17 (*cum syn.*); Dzik, 1994: 110, pl. 24, figs 28–30, text-fig. 30; Wang & Zhou, 1998: pl. 3, fig. 5; Zhang, 1998c: 72–73, pl. 9, figs 16–17 (*cum syn.*); Zhao *et al*., 2000: 206, pl. 27, fig. 11; Rasmussen, 2001: 84, pl. 8, figs1–3, 5; Löfgren, 2004: fig. 7u; Du *et al*., 2005: 365, pl. 1, figs 6–21; Chen *et al*., 2006: fig. 10X–Y; Viira, 2011: fig. 9N–O.

Histiodella holodentata Ethington & Clark.–Nowlan & Thurlow, 1984: pl. 1, figs 1, 3, 5; Wang *et al*., 1996: pl. 1, figs 12–13; Rasmussen, 2001: 82, *partim* only pl. 7, fig. 19; Löfgren, 2004: fig. 7t.

Histiodella intertexta An in An *et al*., 1981: pl. 1, fig. 20 (*nomen nudum*); Ding *et al*. in Wang, 1993: 181, pl. 29, fig. 11.

Histiodella serrata Harris.–Landing, 1976: 633–634, pl. 1, fig. 20; Wang & Lou, 1984: 262–263, pl. 10, fig. 1, pl. 11, figs 6–7.

Histiodella sp. nov. 1 Ni, 1981: pl. 1, fig. 26.

Material. 30 specimens from one sample at the top of the Dawangou Formation (Table 2).

Remarks. *Histiodella* species are morphologically distinctive, and several including *H. kristinae*, *H. holodentata* and others have been widely used as index fossils in the Middle Ordovician of the North American Mid-Continent, Argentine Precordillera, South China, Tarim and Australasia. However, definitions of *H. kristinae* and morphologically closely related forms, like *H. holodentata*, have been interpreted rather differently by various authors. In an earlier study of this species from central New South Wales, Zhen & Percival (2004a) attempted to use the H:L ratio to distinguish *H. kristinae* (H:L ratio = 0.50–0.58) from *H. holodentata* (H:L ratio varying from 0.64 to 0.70). Subsequently more material has been made available for examination and comparison, particularly abundant specimens of both species from the Tarim Basin, which has shown that the H:L ratio is rather variable in these two species of *Histiodella*. *H. kristinae* has more recently been interpreted as having a smaller cusp with its tip lower than those of the highest denticles on the anterior process (Zhen *et al*., 2009b, p. 38). Following this definition of *H. kristinae* (more or less as originally given by Stouge, 1984), material from allochthonous limestones in the Oakdale Formation has been re-assigned to *H. holodentata* (Percival & Zhen, 2007; Zhen *et al*., 2009b). Other specimens previously referred to as *H. holodentata* should now also be re-assigned to *H. kristinae*, such as those illustrated by Rasmussen (2001) and Löfgren (2004). The specimen illustrated by Rasmussen (2001, pl. 7, fig. 19, from sample 69668) as *H. holodentata* seems morphologically identical with the specimen assigned to *H. kristinae* (Rasmussen, 2001, pl. 8, fig. 1). This re-assignment is consistent with the information shown in figure 26 of Rasmussen (2001), where *H. kristinae* was recorded as occurring in sample 69668 with *H. holodentata* occurring in the samples immediately below, but not in sample 69668. Löfgren (2004) illustrated both *H. holodentata* (Löfgren, 2004, fig. 7t from sample H6) and *H. kristinae* (Löfgren, 2004, fig. 7u from sample H4) in the Kårgärde section in Sweden, but these two illustrated specimens are nearly identical and can be confidently assigned to *H. kristinae*.

Histiodella intertexta was introduced by An (*in* An *et al*., 1981) as a *nomen nudum* (Zhang, 1998c, p. 73), and the only figured specimen (designated as the holotype: An *et al*., 1981, pl. 1, fig. 20) is rectangular in outline and identical with the type material of *H. kristinae*. However, Zhang (1998c) correctly pointed out that two specimens subsequently identified and illustrated as *H. intertexta* by An *et al.* (1985, pl. 14, figs 15–16) and An (1987, pl. 18, figs 15–16, pl. 30, fig. 10) should be reassigned to *H. holodentata*. They show a much larger cusp which, although distally broken, would extend higher than any of the denticles on the anterior process.

The holotype of *H. sinuosa* (Graves & Ellison, 1941, pl. 2, fig. 13) from the Fort Peña Formation of Texas is a broken Pa element with a large, upward-pointing cusp. Based on the studies of Bradshaw (1969) and Ethington & Clark (1982), the Pa element of *H. sinuosa* (with *H. serrata* Harris, 1962 as a junior synonym) differs from both *H. holodentata* and *H. kristinae* in having a triangular outline in lateral view with the upper margins of the longer anterior and shorter posterior processes gradually declining distally (see Bradshaw, 1969, pl. 137, fig. 24; Sweet *et al*., 1971, pl. 1, fig. 39). Bauer (2010) treated *H. sinuosa* and *H. serrata* as separate species, indicating that small denticles were well-developed in the posterior process of the Pa element in *H. serrata* (pl. 2, fig. 16–17), but they were generally absent in the Pa element of *H. sinuosa* (pl. 2, fig. 19). Although the apparatus configuration of these two species and their ontogeny was well documented by McHargue (1982), specific identifications for some of the specimens previously assigned to either *H. serrata* or *H. sinuosa* by various other authors need to be reassessed (see synonymy list).

Parapanderodus Stouge, 1984

Type species. *Parapanderodus arcuatus* Stouge, 1984 = *Parapanderodus striatus* (Graves & Ellison, 1941) emended by Smith (1991).

Remarks. *Parapanderodus* was erected by Stouge (1984) to accommodate several coniform species characterized by a posterior groove, an unexpanded base, and fine striation

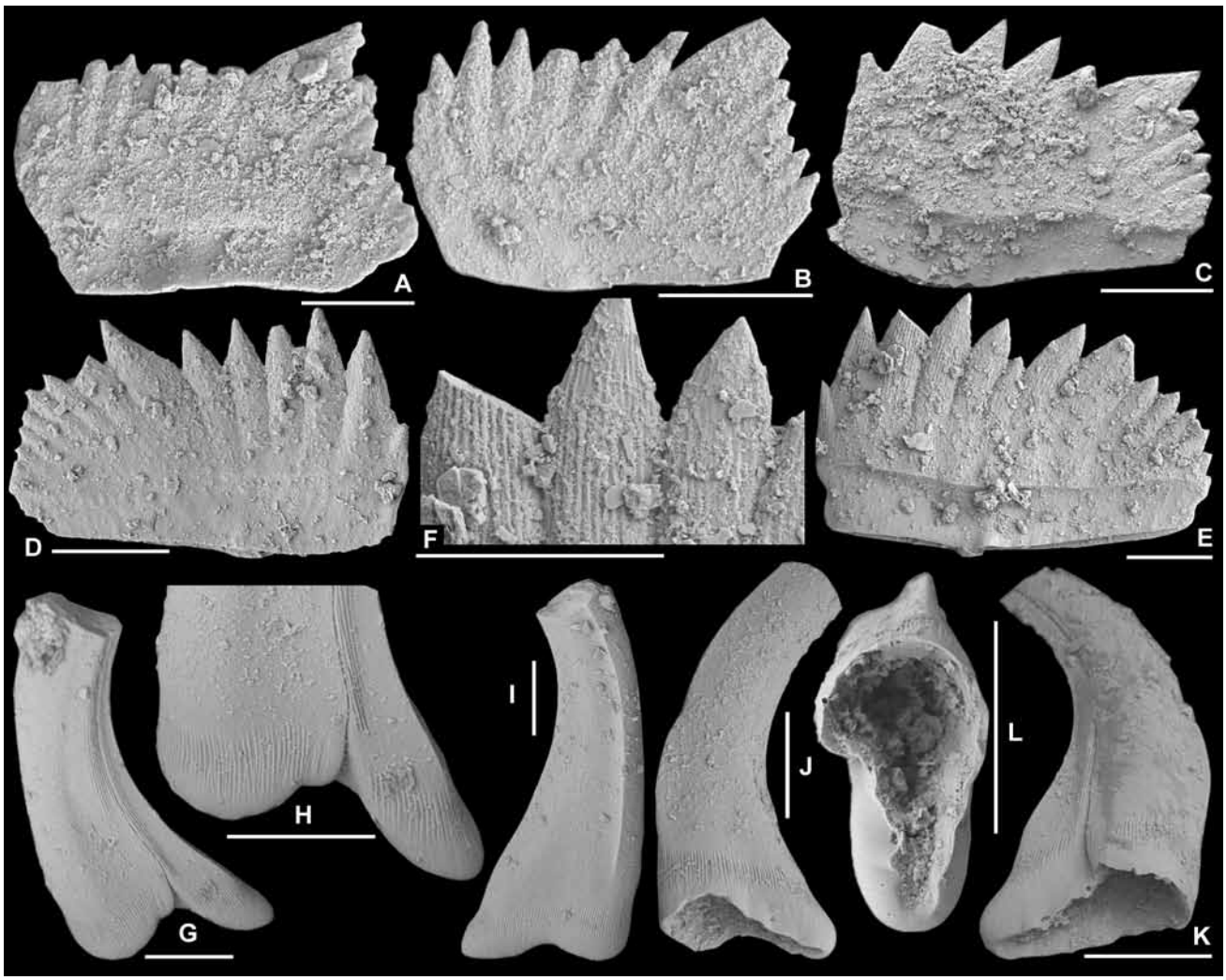

Figure 14. A–B, *Histiodella holodentata* Ethington & Clark, 1982. Pa element, ***A***, NIGP 152962, Nj296, outer lateral view (IY149-023); ***B***, NIGP 152963, Nj296, inner lateral view (IY149-024). C–F, *Histiodella kristinae* Stouge, 1984. Pa element; ***C***, NIGP 152964, AFT-X-K13/13, outer lateral view (IY163-001); ***D***, NIGP 152965, AFT-X-K13/13, inner lateral view (IY163-005); ***E–F***, NIGP 152966, AFT-X-K13/13, E, outer lateral view (IY163-003), F, outer lateral view, close up showing fine surface striation (IY163-004). G–L, *Panderodus gracilis* (Branson & Mehl, 1933). ***G–I***, tortiform element, NIGP 152967, Nj379, G, outer lateral view (IY160-024), H, outer lateral view showing furrow and fine striation on the base (IY160-025), I, inner lateral view (IY160-026). ***J–L***, falciform element, NIGP 152968, Nj379, J, inner lateral view (IY160-027), K, outer lateral view (IY160-028), L, basal view (IY160-029). Scale bars 100 µm.

on the surface. The type species *P. arcuatus* was interpreted as having two element types, but the other four species documented from the Table Head Formation of western Newfoundland—*P.* cf. *consimilis* (Moskalenko, 1973), *P. elegans* Stouge, 1984, *P. striatus* (Graves & Ellison, 1941), and *P.*? aff. *triangularis* (Ethington & Clark, 1964)—were described as form species. Stouge & Bagnoli (1988) revised the genus and considered the two species referred to *Semiacontiodus* by Stouge (1984), *S. asymmetricus* (Barnes & Poplawski, 1973) and *S. preasymmetricus* Stouge, 1984, to form part of the *P. arcuatus* species apparatus, thereby regarding *P. arcuatus* as a junior synonym of *P. asymmetricus* (Barnes & Poplawski, 1973). Subsequently however, Stouge & Bagnoli (1990, p. 21) and Bagnoli & Stouge (1997, p. 151) treated *P. arcuatus* Stouge, 1984 as a valid species.

Based on study of a large collection from Greenland including fused clusters with the occurrence of all the *Parapanderodus* species described by Stouge (1984), Smith (1991) considered all five *Parapanderodus* species, as well as *Semiacontiodus asymmetricus* (Barnes & Poplawski, 1973) and *S. preasymmetricus* Stouge, 1984, described by Stouge (1984) from the Table Head Formation, to represent a single species. Consequently Smith (1991) regarded the originally-designated type species (*P. arcuatus*) and subsequently-redesignated type species (*P. asymmetricus*) as junior synonyms of *P. striatus*, although he acknowledged that the Middle to early Late Ordovician (Whiterockian) representatives described by Barnes & Poplawski (1973) and Stouge (1984) tended to be albid. However, Ji & Barnes (1994) restricted *P. striatus* to the Early Ordovician hyaline elements. As *Parapanderodus* is only represented by a few specimens in the Dawangou material, it is impossible to re-assess the uncertainties and debates arising from the earlier work regarding to the species concept of *P. striatus*, *P. arcuatus* and *P. asymmetricus* and their taxonomic relationships. Therefore Smith's (1991) definition of *P. striatus* is followed herein until a more comprehensive revision of these related species is undertaken.

Smith (1991) erected *Toxotodus* as a coniform genus characterized by having antero-posteriorly compressed symmetrical and asymmetrical elements with a striate cusp and a very shallow or reduced basal cavity. However, the type species of *Toxotodus*, *Scolopodus carlae* Repetski, 1982 was regarded as a species of *Parapanderodus* by Stouge & Bagnoli (1988) and Ji & Barnes (1994). Considering that the species of *Toxotodus* show some rather distinctive characters that readily distinguish them from the type species of *Parapanderodus*, *Toxotodus* is considered herein as a valid genus. Consequently, several species that were assigned to *Parapanderodus* previously by various authors are here regarded as species of *Toxotodus*, such as *Parapanderodus carlae* (Repetski, 1982), and *P. retractus* Ji & Barnes, 1994, from the upper part of the St. George Group of western Newfoundland.

Parapanderodus and *Toxotodus* were sister taxa as evidenced by sharing of several distinctive characters, such as a striate cusp, a conspicuous posterior groove and a shallow basal cavity. It is likely that they are also closely related to Early Ordovician species of *Decoriconus* that, as revised by Löfgren (1998), consist of a seximembrate apparatus.

Parapanderodus striatus (Graves & Ellison, 1941) emended Smith (1991)

Fig. 15A–D

Drepanodus striatus Graves & Ellison, 1941: 11, pl. 1, figs 3, 12.

Scolopodus gracilis Ethington & Clark, 1964: 699, pl. 115, figs 2–4, 8–9; An, 1981: pl. 3, fig. 6; An *et al*., 1985: pl. 6, fig. 6; Pohler, 1994: pl. 4, fig. 11.

Glyptoconus gracilis (Ethington & Clark).–Zhao *et al*., 2000: 204, pl. 7, figs 4–7.

Scolopodus triangularis Ethington & Clark, 1964: 700, pl. 115, figs 6, 11, 13, 17, text-fig. 21.

Protopanderodus asymmetricus Barnes & Poplawski, 1973: 781–782, pl. 1, figs 12, 12a, 14, 16, text-fig. 2A.

Parapanderodus arcuatus Stouge, 1984: 65–66, pl. 9, figs 10–15; Pohler, 1994: pl. 4, fig. 10.

Parapanderodus elegans Stouge, 1984: 66–67, pl. 9, figs 20–27.

Parapanderodus striatus (Graves & Ellison).–Stouge, 1984: 67, pl. 10, figs 1–3; Smith, 1991: 49–52, figs 28a–f, 29a–d, 30 (*cum syn.*); Ji & Barnes, 1994: 49–50, pl. 21, figs 1–10, text-fig. 31A.

Material. Seven specimens from two samples of the Dawangou Formation (see Table 1).

Remarks. Smith (1991) defined *P. striatus* as consisting of a trimembrate apparatus represented by four form species including the s (= form species *Scolopodus gracilis* with a narrow posterior groove and *S. triangularis* with a v-shaped posterior groove), t (= form species *Protopanderodus asymmetricus*), and u (= form species *Scolopodus paracornuformis* Ethington & Clark, 1982) elements. Based on the material from the Lower Catoche Formation of the St. George Group of western Newfoundland, Ji & Barnes (1994) suggested a quadrimembrate apparatus for *P. striatus* (Graves & Ellison, 1941) including a suberect symmetrical element (referred to as the *c* element), subrounded symmetrical element (*a* element), slightly asymmetrical element (*b* element), and laterally compressed element (*e* element), which formed a symmetry transition series.

This species is rarely represented in the Dawangou Formation, and only the slightly asymmetrical element was recovered (Fig. 15A–D). These specimens are identical with those assigned by Zhao *et al*. (2000, pl. 7, figs 4–7) to *Glyptoconus gracilis* (Ethington & Clark, 1964) from the upper part of the Dawangou Formation in the Yangjikan Section of the Tarim Basin. They exhibit a prominent nonstriated rim on the base next to the basal margin, which is the characteristic feature of the form species *P. elegans* Stouge (1984, pl. 9, figs 20–27). Although most of the illustrated type specimens of this form species show a longer base than the Dawangou specimens, Stouge (1984, p. 67) indicated that the length of the base in this form species could be variable.

Periodon Hadding, 1913

Type species. *Periodon aculeatus* Hadding, 1913.

Periodon aculeatus Hadding, 1913

Fig. 16A–P

Periodon aculeatus Hadding, 1913: 33, pl. 1, fig. 14; Lindström, 1955b: 110, pl. 22, figs 10, 11, 14–16, 35; Bergström *et al*., 1974: pl. 1, figs 4–6; Landing, 1976: 636, pl. 3, figs 3–6, 14; Löfgren, 1978: 74, pl. 10, fig. 1; pl. 11, figs 12–26, text-fig. 29 (*cum syn.*); An & Ding, 1982: pl. 4, figs 22–24; An *et al*., 1983: 120–121, pl. 28, figs 7–9; Zeng *et al*., 1983: pl. 12, figs 9–17; An & Xu, 1984: pl. 3, figs 1–6; Chen & Zhang, 1984b: 128, pl. 2, figs 1–7; Zhao *et al*., 1984: 228–229, pl. 92, figs 3, 11, 17; An *et al*., 1985: pl. 13, figs 1–14; An, 1987: 167, pl. 24, figs 7–17; Chen & Zhang, 1989: pl. 3, figs 21–26; Bergström, 1990: *partim* only pl. 1, fig. 15–16, non pl. 2, fig. 15 = *P. grandis*; Duan, 1990: pl. 3, figs 11, 17–20; Pohler & Orchard, 1990: pl. 3, fig. 3; Zhong, 1990: *partim* only pl. 19, figs 3–4, 7–8, 12, 16; Gao, 1991: 134, pl. 7, figs 10, 14–16; Zhang & Chen, 1992: pl. 1, figs 7–12; Ding *et al*. in Wang, 1993: 189–190, pl. 28, figs 1–15; Pohler, 1994: pl. 4, figs 25–27, 30–32; Chen & Bergström, 1995: pl. 6, figs 12, 15–16; Armstrong, 1997: 774–775, pl. 2, figs 13–21, text-fig. 3; Wang & Zhou, 1998: pl. 4, figs 2–4; Zhang, 1998b: 80, 81, pl. 14, figs 1–8 (*cum syn.*); Lehnert *et al*., 1999: pl. 3, fig. 10; Ottone *et al*., 1999: 240, text-fig. 3.8–3.11; Wang & Bergström, 1999a: 340–341, pl. 2, figs 18–19, pl. 3, fig. 11; Wang & Bergström, 1999b: pl. 2, fig. 20; Armstrong, 2000: 52, 56, pl. 6, figs 14–18, pl. 7, figs 1–6; Johnston & Barnes, 2000: 32–35, pl. 13, figs 12–13, 17–18, 20–31, pl. 14, figs 1–7, text-figs 4–5; Rasmussen, 2001: 110, pl. 13, figs 8–11 (*cum syn.*); Wang, 2001: 354, pl. 1, figs 10–11, 13, 16–22; Wang & Qi, 2001: pl. 2, figs 8–11; Norford *et al*., 2002: pl. 2, figs 9–19; Pyle & Barnes, 2002: 107, pl. 21, figs 7–9; Pyle & Barnes, 2003: fig. 15.6–15.8; Xiong *et al*., 2006: pl. 2, fig. 10; Bergström, 2007: 81, fig. 3K–M; Percival & Zhen, 2007: pl. 1, figs 10, 12; Ortega *et al*., 2008: fig. 6.13; Viira, 2008: fig. 6S; Zhen *et al*., 2009a: 145–148, figs 6A–R, 8N, 10L (*cum syn.*).

Material. Over 10406 specimens (see Tables 1–2).

Remarks. *Periodon aculeatus* is a widely distributed species and its apparatus configuration is well established. It is the dominant species in many of the samples from the Dawangou section (Tables 1, 2), and the material is morphologically identical with specimens recently documented from the basal Yenwashan Formation of western Zhejiang (Zhen *et al*., 2009a).

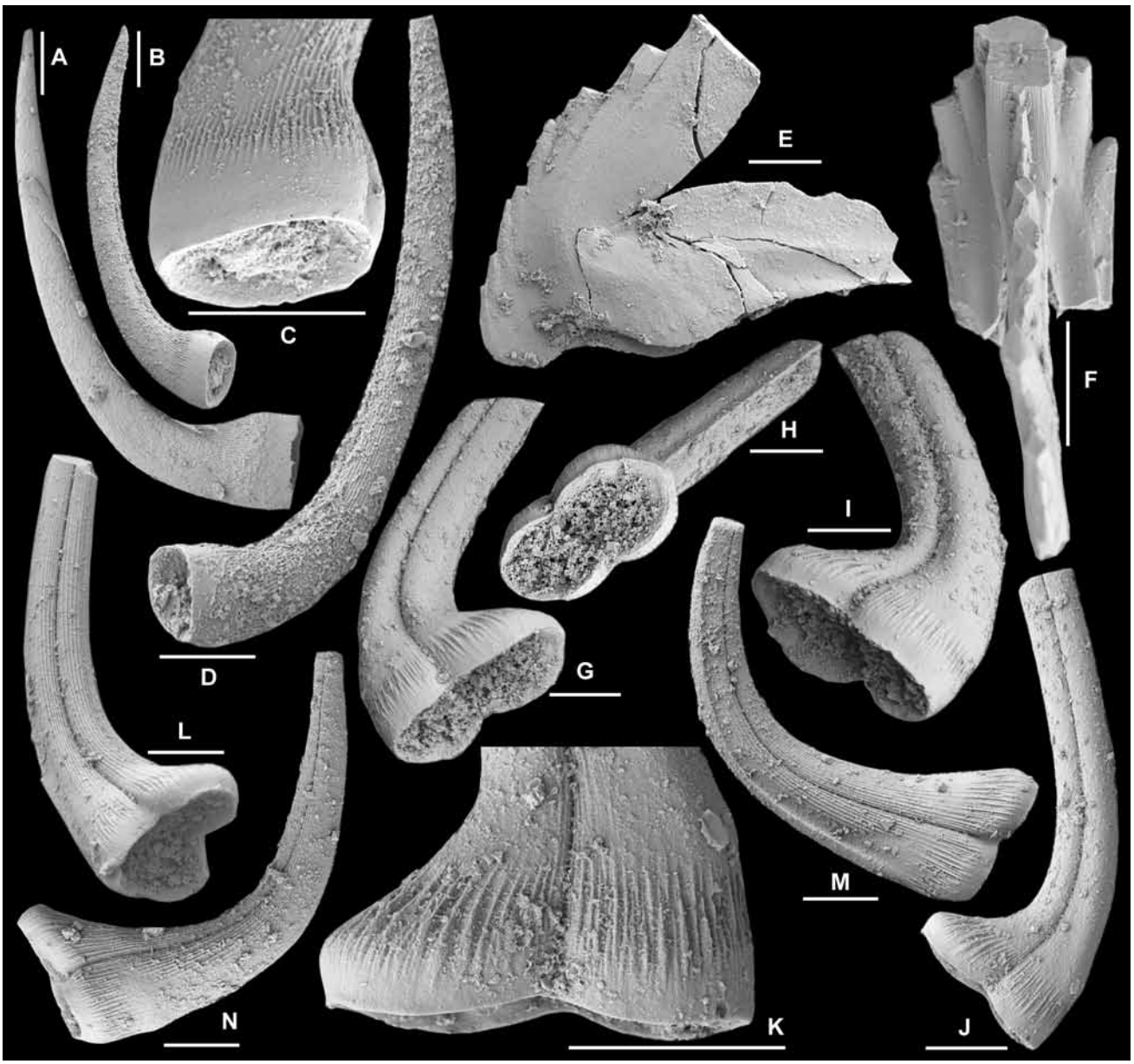

Figure 15. A–D, *Parapanderodus striatus* (Graves & Ellison, 1941). Slightly asymmetrical element; ***A***, NIGP 152969, Nj291, lateral view (IY158-013); ***B–C***, NIGP 152970, Nj297, B, lateral view (IY159-001), C, lateral view, close up showing fine surface striation (IY159-002); ***D***, NIGP 152971, Nj297, lateral view (IY159-003). E–F, *Periodon grandis* (Ethington, 1959). ***E***, M element, NIGP 152972, Nj406, anterior view (IY161-006); ***F***, Sa element, NIGP 152973, Nj406, posterior view (IY161-008). G–N, *Protopanderodus*? *nogamii* (Lee, 1975). G–K, Pa element; ***G–I***, NIGP 152974, AFT-X-K13/13, G, I, lateral views (IY167-009, IY167-011), H, basal view (IY167-010); ***J–K***, NIGP 152975, AFT-X-K13/13, J, lateral view (IY167-014), K, lateral view, close up showing striation, basal wrinkles and longitudinal furrow (IY167-015). ***L***, Sa element, NIGP 152976, AFT-X-K13/13, basal-lateral view (IY167-016). M–N, Sb element; ***M***, NIGP 152977, AFT-X-K13/13, inner lateral view (IY167-019); ***N***, NIGP 152978, AFT-X-K13/13, outer lateral view (IY167-021). Scale bars 100 μm.

The specimens illustrated as *P. aculeatus* from the Kuruktag area of the Tarim Basin by Zhong (1990) included both species, *P. aculeatus* and *P. grandis* (Zhong, 1990, pl. 19, fig. 6). The M element of *P. grandis* typically bears 5–7 denticles on the inner lateral process (Fig. 15E; Wang & Zhou, 1998, pl. 3, fig. 14), whereas only 2–4 denticles characterize the M element of *P. aculeatus* (Fig. 16A–B; also see Zhang & Chen, 1992).

Polonodus Dzik, 1976

Type species. *Ambalodus clivosus* Viira, 1974.

Remarks. Based on the pectiniform elements of the monotypic species, *Ambalodus clivosus* Viira, 1974, Dzik (1976, p. 423) provided a brief diagnosis for *Polonodus* as "conical conodonts with four lobes covered with concentric and radial rows of tubercles" having a "very large basal cavity", and illustrated three specimens showing a wide range of morphology including four-lobed (Dzik, 1976, fig. 29c), three-lobed (Dzik, 1976, pl. 43, fig. 1a–b), and an incomplete specimen with a well-developed anterior

platform (Dzik, 1976, fig. 29d). By applying a form species approach, Löfgren (1978) suggested that the Polish specimens illustrated by Dzik (1976) were not conspecific with the holotype of *P. clivosus*, and in fact they represented two species that were doubtfully included in *Polonodus* as *P.*? sp. A (= Dzik, 1976, pl. 43, fig. 1a–b) and *P.*? sp. B (= Dzik, 1976, fig. 29c–d). Stouge (1984) revised the type species, *P. clivosus*, and also named two new species (*Polonodus tablepointensis* and *P.*? *newfoundlandensis*) from the Table Head Formation of western Newfoundland. In the synonymy list of bimembrate *P. tablepointensis* he included specimens illustrated by Dzik (1976, fig. 28c–d) as *P. clivosus* and those ascribed to *P.*? sp. A and *P.*? sp. B by Löfgren (1978). Stouge (1984) then divided three species occurring in the Table Head Formation into two groups. His first group included *P. clivosus* and *P. newfoundlandensis*, with *P. tablepointensis* comprising the second group. Zhang (1998c) erected *Dzikodus* with *P. tablepointensis* as the type species, and also included M and S elements in the species apparatus of the latter.

Stouge (1984) only doubtfully considered his first group (*P. clivosus* and *P. newfoundlandensis*) as *Polonodus*, preferring to accept a generic definition based on Dzik's (1976) material from Polish erratic boulders rather than the type material of *Ambalodus clivosus* Viira, 1974. However, Löfgren (1990) argued that *P. clivosus* (Viira) might be more closely related to *P. tablepointensis* rather than *P. newfoundlandensis* as Stouge (1984) suggested.

Stouge (1984) recognized two paired pectiniform elements (polyplacognathiform and ambalodiform) in *Polonodus*. Löfgren (1990) recognized geniculate M and ramiform S (including trichnodelliform = Sa, gothodiform = Sb, and tetraprioniodiform = Sd) elements in the species apparatus of *Polonodus*. It is likely that the species apparatus might also include a modified bipennate ramiform element similar to that illustrated by Löfgren (1990, fig. 1e) to take the Sc position.

Polonodus clivosus (Viira, 1974)

Fig. 17L–M

Ambalodus n.sp. Viira, 1967: 323, fig. 3.24a–b.
Polyplacognathus n.sp. A Fåhraeus, 1970: fig. 3F–G.
Ambalodus n.sp. A Fåhraeus, 1970: fig. 3J–K.
Ambalodus clivosus Viira, 1974: 51–52, 134, pl. 8, fig. 1, text-figs 37–38.
Ambalodus? n.sp. Viira, 1974: 52, pl. 8, figs 2–3, text-fig. 39.
Polonodus clivosus (Viira).–Löfgren, 1978: 76, *partim* only pl. 16, figs 12–13; Stouge, 1984: 73, pl. 13, figs 6–13; Ding *et al*. in Wang, 1993: 191, pl. 32, figs 16, ?17.
Polonodus sp. H Ding *et al*. in Wang, 1993: *partim* only pl. 37 fig. 5.

Material. Two specimens from one sample at top of the Dawangou Formation (see Table 2).

Remarks. *Polonodus clivosus* was erected as a form species recovered from subsurface core material of Darriwilian age in the east Baltic (Viira, 1974, pl. 8, fig. 1, text-figs 37–38), and is interpreted herein as representing paired sinistral and dextral Pa (polyplacognathiform) elements. These have a node-like cusp with a row of node-like denticles extending the whole length of the longer anterior process and the short posterior process, and are also present on the inner lateral and secondary inner lateral processes. The anterior and posterior platforms of the holotype (Viira, 1974, pl. 8, fig. 1) form a gently curved outline in upper view without the outer lateral process. Specimens with four processes from the same core sample as the holotype of *P. clivosus* were referred to as *Ambalodus*? sp. n. by Viira (1974, pl. 8, figs 2–3, text-fig. 39), and are considered herein as representing the paired sinistral and dextral Pb (ambalodiform) elements of *P. clivosus*. Although Löfgren (1978) recognized that the Polish specimens from the erratic boulders accommodated in *P. clivosus* by Dzik (1976) belonged to separate species (see discussion above), her definition of *P. clivosus* also doubtfully included Newfoundland material (Table Head Formation) ascribed to *Polyplacognathus* n.sp. A and *Ambalodus* n.sp. A by Fåhraeus (1970). However, the Swedish specimens she illustrated (Löfgren, 1978, pl. 16, figs 12–13) bear a long outer lateral process, implying that the holotype of *P. clivosus* might have the outer lateral process broken off. This view was then accepted by Stouge (1984), who was the first to revise this species as consisting of a bimembrate species apparatus, but his definition of this species was largely based on the material from Newfoundland. *P. clivosus* differs from the corresponding elements of *P. newfoundlandensis* in lacking a prominent notch between the anterior process and the secondary inner lateral process of the Pa element (Stouge, 1984, pl. 13, fig. 13), and in having larger denticles on the anterior process of the Pb element (Stouge, 1984, pl. 13, fig. 11). The definition of *P. clivosus* given by both Löfgren (1978) and Stouge (1984) was also endorsed by Viira (per. comm., 2010), who confirmed that the original holotype of *P. clivosus* (Viira, 1974, specimen Cn 245, text-fig. 37, pl. 8, fig. 1) "has a broken outer lateral process which is seen clearly on the basal view".

One specimen (Fig. 17L–M) recovered from the same sample AFT-X-K13/13 in association with *P. newfoundlandensis* also had the outer lateral process broken off, and is identical with the holotype of *P. clivosus* (Viira, 1974, text-fig. 37, pl. 8, fig. 1). It differs from *P. newfoundlandensis* in lacking a prominent notch between the anterior process and the secondary inner lateral process, and in having a more prominent and laterally more compressed cusp and denticles on the anterior and posterior processes.

Polonodus newfoundlandensis Stouge, 1984

Fig. 17A–K

Polonodus newfoundlandensis Stouge, 1984: 73–74, pl. 13, figs 14–16, text-fig. 28.
Polonodus cf. *newfoundlandensis* Stouge.–Zhao *et al*., 2000: 215, pl. 30, figs 16–17.
Polonodus kunshanensis Ding in Wang, 1993: 191, *partim*, only pl. 33, fig. 17, non figs 15, 18 = ?*Dzikodus tablepointensis*.
?Polonodus sp. Gao, 1991: *partim* only pl. 9, figs 8–9, ?13.

Material. 36 specimens from one sample at the top of the Dawangou Formation (Table 2).

Remarks. Stouge (1984) erected *P. newfoundlandensis* as consisting of a bimembrate apparatus including paired (in mirror image) Pa (polyplacognathiform) and paired Pb (ambalodiform) elements, and suggested that it differed from the type species, *P. clivosus* in having smaller denticles on the anterior process of the Pb element and in having a

Figure 16. *Periodon aculeatus* Hadding 1913. A–B, M element; ***A***, NIGP 152979, posterior view (IY145-001); ***B***, NIGP 152980, anterior view (IY145-002). C–E, Sa element; ***C–D***, NIGP 152981, C, anterior view (IY145-003), D, lateral view (IY145-004); ***E***, NIGP 152982, lateral view (IY145-006). F–I, Sb element; ***F–G***, NIGP 152983, F, inner lateral view (IY145-010), G, outer lateral view (IY145-013); ***H–I***, NIGP 152984, H, upper view (IY145-018), I, inner lateral view (IY145-020). J–K, Sc element; ***J***, NIGP 152985, outer lateral view (IY145-016); ***K***, NIGP 152986, inner lateral view (IY145-017). L–N, Pa element; ***L***, NIGP 152987, inner lateral view (IY145-023); ***M***, NIGP 152988, outer lateral view (IY145-024); ***N***, NIGP 152989, basal view (IY145-025N). O–P, Pb element; ***O***, NIGP 152990, outer lateral view (IY145-027); ***P***, NIGP 152991, inner lateral view (IY145-026). All from sample Nj294; scale bars 100 µm.

deeper inner notch on the anterior process. The holotype is a sinistral Pa element from the lower part of the Table Head Formation (A3, *H. holodentata* Zone) of western Newfoundland (Stouge, 1984).

Only pectiniform P elements have been recovered in our material from the Dawangou Formation. The Pa element (Fig. 17A–D) shows some features intermediate between *P. newfoundlandensis* and *P. clivosus* (Viira, 1974). It is comparable with the holotype of *P. newfoundlandensis* in having a prominent notch on the inner side of the anterior process. However, the denticle row on the anterior process of the Pa element from Dawangou is more strongly curved inner laterally than that of the holotype, a feature that is more comparable with the specimen that Stouge (1984, pl. 13, fig. 13) referred to as *P. clivosus*. The Pb element of the Dawangou material (Fig. 17E–K) is comparable with the type material in having small denticles on a narrower platform of the anterior process, but the angle between the denticle rows on the outer lateral process and the anterior process is more acute (around 50°) and the denticle row on the inner lateral process forms an acute angle with that on the posterior process (Fig. 17F) rather than a right angle as

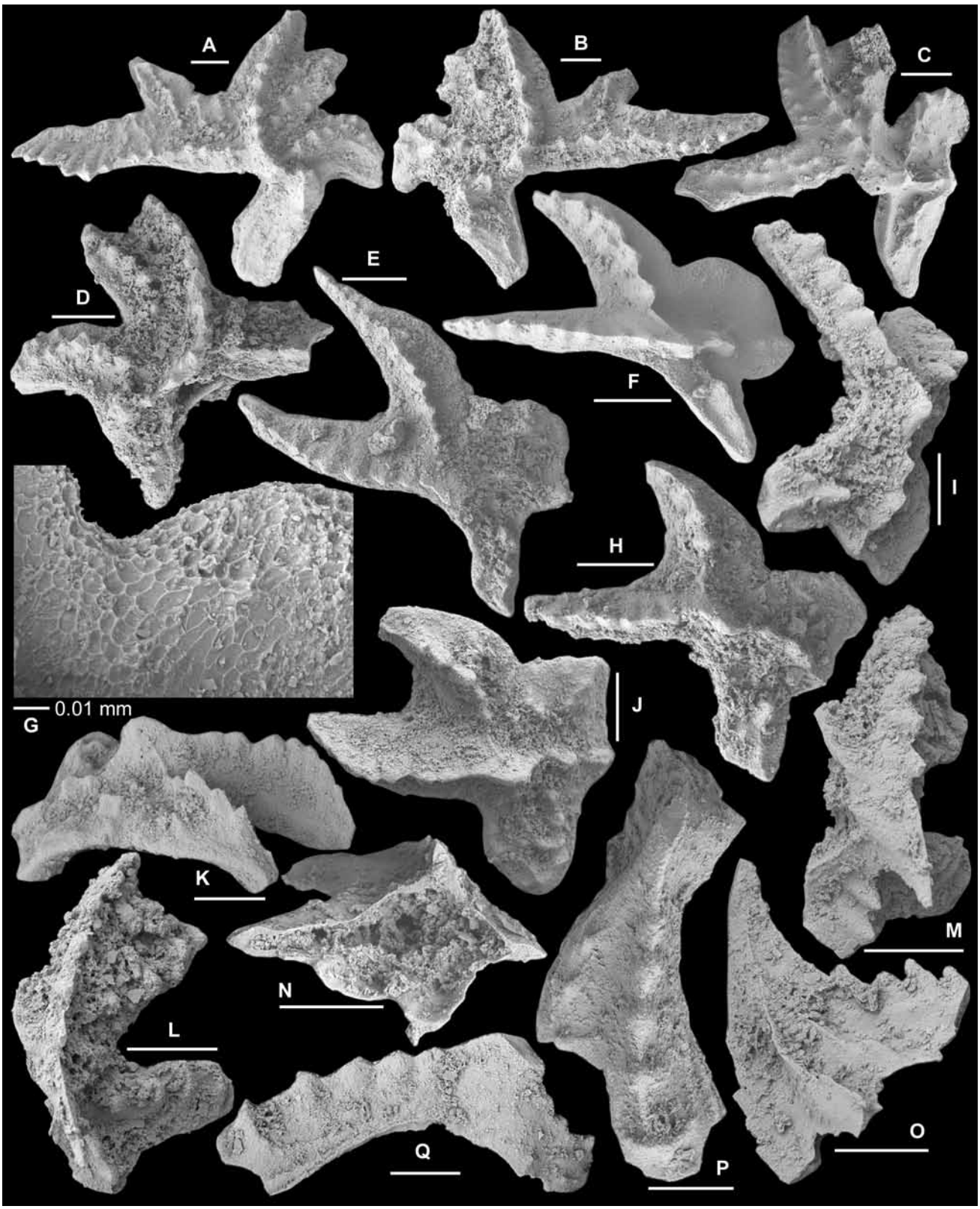

Figure 17. A–K, *Polonodus newfoundlandensis* Stouge, 1984. A–D, Pa (polyplacognathiform) element; ***A***, NIGP 152992, AFT-X-K13/13, sinistral, upper view (IY165-026); ***B***, NIGP 152993, AFT-X-K13/13, dextral, upper view (IY165-027); ***C***, NIGP 152994, AFT-X-K13/13, sinistral, upper view (IY165-031); ***D***, NIGP 152995, AFT-X-K13/13, dextral, upper view (IY165-025). E–K, dextral Pb (ambalodiform) element; ***E***, NIGP 152996, AFT-X-K13/13, upper view (IY165-032); ***F–G***, NIGP 152997, AFT-X-K13/13, F, upper view (IY165-029), G, upper view, close up showing reticulate surface structure (IY165-030); ***H–I***, NIGP 152998, AFT-X-K13/13, H, upper view (IY165-020), I, lateral view (IY165-022); ***J–K***, NIGP 152999, AFT-X-K13/13, J, upper view (IY165-021), K, lateral view (IY165-023). ***L–M***, *Polonodus clivosus* (Viira, 1974). Pa (polyplacognathiform) element, NIGP 153000, AFT-X-K13/13, L, upper view (IY163-018), M, outer lateral view (IY163-017). ***N–O***, Gen. et sp. indet. Sd element, NIGP 153001, AFT-X-K13/13, N, basal view (IY163-014), O, inner lateral view (IY163-014). ***P–Q***, *Polonodus* sp. A. ?Pb element, NIGP 153002, AFT-X-K13/13, P, upper view (IY163-008), Q, inner lateral view (IY163-009). Scale bars 100 μm, unless otherwise indicated.

in the type material (Stouge, 1984, pl. 13, fig. 15). In some of the Dawangou specimens, a weak secondary row with several low nodes may also be developed on the posterior lobe (Fig. 17J).

No ramiform S and geniculate M elements have been recognized for *P. newfoundlandensis* in the literature. However, one specimen of a quadriramate element from the same sample (AFT-X-K13/13) is nearly symmetrical, with denticulate anterior and posterior processes, and an adenticulate, blade-like costa on each lateral side. This specimen, assigned herein as gen. et sp. indet. (Fig. 17N–O), possibly represents the Sd element of *P. newfoundlandensis*.

An incomplete pectiniform specimen recovered from the same sample (AFT-X-K13/13) has a robust, laterally compressed cusp, a long anterior process with a row of node-like denticles, a short (possibly broken) posterior process, and an outer lateral process with a denticle row forming an angle of about 30° with that on the anterior process (Fig. 17P–Q). Likely a Pb element, it is morphologically different from the Pb element of *P. newfoundlandensis* associated in this sample from the top of the Dawangou Formation, and is therefore referred to herein as *Polonodus* sp. A.

The three illustrated specimens of *Polonodus kunshanensis* Ding in Wang, 1993 represent poorly preserved Pa (polyplacognathiform) elements recovered from the Guniutan Formation of Kunshan, Jiangsu Province. Zhang (1998c) considered this species to be a junior synonym of *Dzikodus tablepointensis* (Stouge, 1984). However, the holotype (Wang, 1993, pl. 33, fig. 18) is badly preserved with distal parts of the processes broken off, making its identification at the species level almost impossible. The illustrated paratype (Wang, 1993, pl. 33, fig. 15) seems comparable with the dextral Pa element of *D. tablepointensis* illustrated by Zhang (1998c, pl. 7, fig. 6) from the Guniutan Formation of Hunan Province, South China, but the other figured specimen (Wang, 1993, pl. 33, fig. 17) with the posterior process broken off can be well compared with both the material from the Dawangou Formation and the holotype of *P. newfoundlandensis* from the Table Head Formation of western Newfoundland (Stouge, 1984, pl. 13, fig. 16), in having a prominent notch between the anterior process and the secondary inner lateral process, and in having the inner lateral process posteriorly curved.

Tarim specimens illustrated as *P.* cf. *newfoundlandensis* by Zhao *et al*. (2000, pl. 30, figs 16–17) exhibit a more prominent cusp in comparison with the Dawangou material and the types from western Newfoundland.

Protopanderodus Lindström, 1971

Type species. *Acontiodus rectus* Lindström, 1955a.

Remarks. McCracken (1989) and Mellgren & Eriksson (2006) presented a comprehensive study of this genus, particularly reconstruction of the species apparatuses, and the latter revision was based on a large, well-preserved, collection of several species of *Protopanderodus* from the Swedish Middle Ordovician. Three species, *P. cooperi*, *P. graeai* and *P. calceatus*, dominate many of the Dawangou samples. Our study of the Tarim material supports, in general, the apparatus reconstruction and notation system proposed by Mellgren & Eriksson (2006), namely, the antero-posteriorly compressed M elements with a non-costate anterior face and costate or carinate posterior face, the short-based and costate P elements, and generally long-based and costate S elements that form a symmetry transition series. However, as Zhen *et al*. (2009a) suggested, material that Mellgren & Eriksson (2006) described as *Protopanderodus robustus* (Hadding, 1913) should in fact be referred to *P. cooperi*. Our current study also indicates that *Protopanderodus parvibasis* Löfgren, 1978 may be a junior synonym of *P. graeai* (see further discussion under remarks of the relevant species).

Protopanderodus calceatus Bagnoli & Stouge, 1997

Fig. 18A–Y

?Acontiodus robustus (Hadding).–Sweet & Bergström, 1962: 1222, pl. 169, fig. 11, text-fig. 11.

Protopanderodus robustus (Hadding).–Gao, 1991: 135, pl. 12, fig. 7 = Pb element.

Protopanderodus sp. cf. *varicostatus* (Sweet & Bergström).–Löfgren, 1978: 91, pl. 3, figs 26–31; McCracken, 1989: 22, 23, pl. 3, figs 1–8, fig. 3F; Stouge & Bagnoli, 1990: 23, pl. 8, figs 9–12; Rasmussen, 1991: 283, fig. 8D–E; Löfgren, 1994: fig. 7:3; Lehnert, 1995: 118, pl. 13, fig. 17, pl. 17, figs 5–6, 8–9; Norford *et al*., 2002: pl. 3, figs 2–3; Zhen *et al*., 2009b: 47–48, fig. 10A–O.

Protopanderodus calceatus Bagnoli & Stouge, 1997: 154–156, pl. 8, figs 13–19 (*cum syn.*); Zhang, 1998c: 82, 83, pl. 15, figs 6–13 (*cum syn.*); Wang & Bergström, 1999a: 341, pl. 1, figs 12–13; Wang & Bergström, 1999b: pl. 2, figs 3, 5; Rasmussen, 2001: 122, 124, pl. 15, figs 20–21; Mellgren & Eriksson, 2006: 108–110, figs 14, 15 (*cum syn.*).

Protopanderodus graeai (Hamar).–Ding *et al*. in Wang, 1993: *partim* only pl. 16, figs 10–11.

Protopanderodus varicostatus (Sweet & Bergström).–Wang & Lou, 1984: 278, pl. 5, figs 2–3, 7, 9–11; An *et al*., 1985: pl. 6, fig. 5, pl. 12, figs 1–4; An, 1987: 173–174, pl. 11, figs 2–3; Duan, 1990: pl. 3, figs 27–29; Gao, 1991: 135–136, pl. 12, figs 9, 15; Ding *et al*. in Wang, 1993: 196, *partim* only pl. 16, figs 1, 5–6; Wang *et al*., 1996: pl. 1, fig. 17; Wang, 2001: 356, pl. 1, figs 5, 7, 24, 28; Wang & Qi, 2001: pl. 1, fig. 6; Zhen *et al*., 2004b: 157, fig. 8N–X.

Material. 247 specimens from 20 samples (see Tables 1–2).

Remarks. Bagnoli & Stouge (1997) originally defined *Protopanderodus calceatus* as consisting of a trimembrate apparatus including scandodiform, bicostate symmetrical and multicostate asymmetrical elements. Zhang (1998c) assigned the scandodiform element to the M position and differentiated the P, Sa, Sb and Sc elements. She (1998c, p. 83) suggested that *P. calceatus* could be distinguished from *P. varicostatus* by having only a weakly developed indentation of the basal margin. Mellgren & Eriksson (2006) suggested a septimembrate apparatus for *P. calceatus* including scandodiform M (differentiated as M1 and M2), bicostate (one costa each side) Sa, multicostate Sb, Sc and Sd, and short-based P (differentiated as Pa, Pb1 and Pb2) elements. Swedish material documented by Mellgren & Eriksson (2006) showed the occurrence of a bifurcated "twin" costa in the Sa, Sb, Sd and Pa elements of *P. calceatus*, but this feature is not recognized in the Dawangou material.

Specimens referred to *P. calceatus* from Dawangou are comparable with those from Sweden (Löfgren, 1978;

Bagnoli & Stouge, 1997; Mellgren & Eriksson, 2006), South China (Zhang, 1998c) and New Zealand (Zhen *et al.*, 2009b). *P. calceatus* is interpreted as consisting of a septimembrate apparatus with Sa (Fig. 18G–J) and Sb (Fig. 18K–L) elements represented by bicostate (one lateral costa on each side) symmetrical and slightly asymmetrical forms respectively (Fig. 18G–J, K–L), with Sc (Fig. 18M–P), Pa (Fig. 18T-V) and Pb (Fig. 18X–Y) elements represented by multicostate strongly asymmetrical forms (one costa on the outer lateral face and two costae separated by a groove on the inner lateral face), and with the Sd element represented by the multicostate weakly asymmetrical form (two costae separated by a groove on each lateral face, Fig. 18Q–S). The Pa element with a rounded antero-basal corner and the Pb element with a more or less quadrate outline in lateral view differ from the S elements in having a shorter base. The M elements have a gently curved basal margin and a prominent shallow groove on the posterior face located more towards the inner-lateral margin (Fig. 18A–F), and can be further differentiated into M1 without additional costa (Fig. 18 A–E) and M2 with a broad mid costa (or several costae) on the posterior face (Fig. 18F). These two morphotypes of the M element were also represented in the type material of early Darriwilian age from Sweden with the holotype comparable with the M2 morphotype (Bagnoli & Stouge, 1997; pl. 8, fig. 18), and also are present in the Guniutan Formation of South China (Zhang, 1998c, pl. 15, fig. 12 =M1, fig. 13 =M2).

Before *P. calceatus* was formally established, Stouge & Bagnoli (1990) and other authors followed Löfgren (1978) who referred to specimens informally as *Protopanderodus* cf. *varicostatus* (see synonym list). This assignment conveyed the fact that these species were closely similar to each other. In fact, Löfgren (1978) did a detailed study on this form and noted the highly variable nature of *P.* cf. *varicostatus*. She suggested that the elements were very similar to those of *P. varicostatus*, except that the symmetrical elements were not represented in her material from Jämtland of northern Sweden. This is also true in the specimens from the Dawangou section in that the element with two costae on each side is weakly asymmetrical and is assigned herein to the Sd position (Fig. 18Q–S).

Protopanderodus calceatus resembles *P. varicostatus* in having two costae separated by a groove on one or both sides of some constituent elements. The symmetrical element (=Sa herein) represented by a paratype (Bagnoli & Stouge, 1997; pl. 8, fig. 15) is clearly a bicostate element with a postero-laterally located costa on each lateral face. The symmetrical element (=Sa herein) of *P. varicostatus* as represented by the holotype (Sweet & Bergström, 1962; pl. 168, fig. 8) is apparently multicostate with two costae separated by a groove on each lateral face. Re-examination of topotype material of *P. varicostatus* from the Pratt Ferry Formation of Alabama has convinced us that this and *P. calceatus* represent separate species. *P. varicostatus* has multicostate S and P elements characterized by having a strongly curved basal margin with a distinctive indentation near the antero-basal corner and often with an anticusp-like extension similar to that of *P. cooperi*. Differing from those of *P. varicostatus*, the Sa and Sb elements of *P. calceatus* have the costa bordering the posterior side of the groove varying from weakly developed (Mellgren & Eriksson, 2006; fig. 14C, N) to nearly absent (Fig. 18I), and the costa bordering the anterior side of the groove being more posteriorly directed. These bicostate forms were often assigned to *P. robustus* by some authors (see synonymy list). Moreover, the basal margin of the M element of *P. calceatus* is generally less strongly curved (Fig. 18A–F), and the P elements of *P. calceatus* are strongly asymmetrical with two costae separated by a groove only on the inner lateral face (Fig. 18V, X), and the outer lateral face is ornamented with a postero-lateral costa (Fig. 18T, U, Y).

Protopanderodus cooperi (Sweet & Bergström, 1962)

Figs 19A–R, 20A–E

Acontiodus cooperi Sweet & Bergström, 1962: 1221–1222, pl. 168, figs 2, 3, text-fig. 1G; Burrett *et al.*, 1983: 180, fig. 9E; Wang & Lou, 1984: 249, pl. 5, figs 12–13, 16, 18, pl. 11, fig. 1; Bergström, 1990: pl. 2, fig. 9.

Scandodus sp. Sweet & Bergström, 1962: 1246, pl. 168, figs 13, 16.

Protopanderodus cooperi (Sweet & Bergström).–Chen & Zhang, 1989: pl. 4, figs 23–25; An & Zheng, 1990: *partim* only pl. 6, fig. 13, not fig. 14 = *P. varicostatus*; Gao, 1991: 135, pl. 12, fig. 6; Ding *et al.*, in Wang, 1993: 194–195, pl. 16, figs 7–9; Wang *et al.*, 1996: pl. 1, figs 22–23; Zhang, 1998c: 81, 82, pl. 14, figs 13–17 (*cum syn.*); Wang, 2001: 354–355, pl. 1, fig. 14; Wang & Qi, 2001: pl. 8, fig. 8; Pyle & Barnes, 2003: fig. 15.33; Zhen & Percival, 2004b: 170, fig. 11C–F; Zhen *et al.*, 2004b: 155, fig. 8A–E; Zhen *et al.*, 2009a: 148–150, fig. 7A–S (*cum syn.*); Zhen *et al.*, 2009b: 47, fig. 10S.

Protopanderodus gradates Serpagli.–Ortega *et al.*, 2008: fig. 6.32.

Protopanderodus rectus (Lindström).–Zhao *et al.*, 2000: 217–218, pl. 21, figs 1–17; Wang, 2001: 355–356, pl. 1, fig. 23.

Protopanderodus robustus (Hadding).–Löfgren, 1978: 94–95, *partim*, only pl. 3, figs 32–33; Pohler & Orchard, 1990: pl. 1, fig. 17; Rasmussen, 2001: 125, pl. 16, figs 5–8; Mellgren & Eriksson, 2006: 106–108, figs 9H–N, 13A–K.

Protopanderodus parvibasis Löfgren.–Mellgren & Eriksson, 2006: 104–105, *partim* only fig. 11A, H.

Material. 1076 specimens from 39 samples (see Tables 1–2).

Remarks. *Acontiodus cooperi* was erected as a form species based on the symmetrical acontiodiform element. The holotype (Sweet & Bergström, 1962, pl. 168, figs 2–3) has a suberect cusp with a postero-lateral costa on each side, a moderately extended base with a sinuous basal margin, and a prominent anticusp-like antero-basal extension. Specimens originally assigned to *Scandodus* sp. by Sweet & Bergström (1962, p. 1246, pl. 168, figs 13, 16) are likely to represent the M position of *P. cooperi*, which was recently revised as a multielement taxon consisting of a septimembrate apparatus including scandodiform M element, bicostate short-based P element, and bicostate longer-based S elements forming a symmetry transition series (Mellgren & Eriksson, 2006; Zhen *et al.*, 2009a). However, the development of the anticusp-like extension varies amongst the constituent elements of *P. cooperi* from the same fauna and also amongst various faunas reported. For instance, this feature is strongly developed in the holotype and in some specimens reported from the Yenwashan Formation of South China (Zhen *et al.*, 2009a, fig. 7M) and from the Tarim Basin (Zhao *et al.*, 2000, pl. 21, figs 2, 6), but is less strongly developed in the material from the Dawangou section (Fig. 19). Generally it is more strongly developed in the S elements (Fig. 19D, H, K), and

Figure 18. *Protopanderodus calceatus* Bagnoli & Stouge, 1997. A–E, M1 element; ***A***, NIGP 153003, Nj297, posterior view (IY150-016); ***B***, NIGP 153004, Nj295, posterior view (IY149-012); ***C***, NIGP 153005, AFT-X-K13/13, posterior view (IY168-007); ***D***, NIGP 153006, Nj296, posterior view (IY149-029); ***E***, NIGP 153007, AFT-X-K13/13, anterior view (IY168-008). ***F***, M2 element, NIGP 153008, AFT-X-K13/13, posterior view (IY168-006). G–J, Sa element; ***G–I***, NIGP 153009, Nj297, G, H, lateral views (IY162-022, IY162-018), I, upper view showing cross section of cusp (IY162-021); ***J***, NIGP 153010, AFT-X-K13/13, lateral view (IY168-013). ***K–L***, Sb element, NIGP 153011, Nj294, K, inner lateral view (IY147-020), L, outer lateral view (IY147-021). M–P, Sc element; ***M–N***, NIGP 153012, Nj294, M, inner lateral view (IY147-022), N, upper view showing cross section of cusp (IY147-023)… (caption continued on facing page)

less so in the P (Fig. 19N, R) and M (Fig. 19A–B) elements. Two topotypes of *P. cooperi* from the Pratt Ferry Formation of Alabama are illustrated herein (Fig. 20A–E) for detailed comparison. They represent the M (Fig. 20A–C) and weakly asymmetrical Sb (Fig. 20D–E) elements, and are identical with specimens from the Dawangou section (Fig. 19), and material from the Yenwashan Formation of South China (Zhen *et al*., 2009a, fig. 7). The types and topotypes of *P. cooperi* mostly have a basal funnel attached (see Sweet & Bergström, 1962; pl. 168, figs 2, 3), and the base often shows a recessive basal margin (Fig. 20B), which is also preserved in some specimens from the Dawangou section (Fig. 19F–I).

Protopanderodus cooperi is widely distributed in North America (Sweet & Bergström, 1962), Australia (Burrett *et al*., 1983; Zhen *et al*., 2004), New Zealand (Zhen *et al*., 2009b), South China (Chen & Zhang, 1989; Wang *et al*., 1996; Zhang, 1998c; Zhen *et al*., 2009a), North China (Wang & Lou, 1984), Tarim (Zhao *et al*., 2000; Wang & Qi, 2001; this study), and Europe (Löfgren, 1978; Rasmussen, 2001; Mellgren & Eriksson, 2006). Although *P. cooperi* is readily distinguished from other species of *Protopanderodus* by having an anticusp-like extension at the antero-basal corner and an undulating basal margin of the bicostate P and S elements, it was considered by various authors as a junior synonym of a number of *Protopanderodus* species that are less well documented. Zhao *et al.* (2000) regarded P. *cooperi* as a junior synonym of *P. rectus* Lindström, 1955a. The type material of the latter from the Lower Ordovician (Floian) of Sweden shows a curved basal margin with development of a weak extension at the antero-basal corner (Lindström, 1955a, pl. 2, figs 7–11). This character was also well-documented by material included in *P. rectus* from Sweden, such as Löfgren (1978, pl. 3, figs 1–2), Rasmussen (2001, pl. 16, figs 1–4), and Mellgren & Eriksson (2006, fig. 8E, H, fig. 9D–G). As evidenced by this and other shared characters of these two species, it is likely that *P. cooperi* evolved from its direct ancestor (and also stratigraphically older species) *P. rectus* (Rasmussen, 2001, p. 125). Stouge (1984, p. 52) considered *Acontiodus cooperi* Sweet & Bergström, 1962 as the senior synonym of *Scolopodus varicostatus* Sweet & Bergström, 1962, representing the symmetrical acontiodiform element of a single species apparatus, and suggested that *A. cooperi* could only be differentiated from the latter by "having one pair of lateral costae". However, Landing (1976) regarded *P. varicostatus* as a junior synonym of *P. cooperi*. The specimens that he illustrated as *P. cooperi* should be excluded from this species. In fact one of the specimens is multicostate (Landing, 1976, pl. 4, fig. 6) and the other is likely a drepanodiform element (Landing, 1976, pl. 4, fig. 7).

Löfgren (1978, p. 94–95) indicated that many of her specimens assigned to *P. robustus* (Hadding, 1913) developed "an antero-basal 'hook' as in the acondiodiform elements described as *Acontiodus cooperi* by Sweet & Bergström (1962)". One of her illustrated specimens (Löfgren, 1978, pl. 3, fig. 33) is comparable with the holotype of *P. cooperi* (Sweet & Bergström, 1962, pl. 168, figs 2–3). Rasmussen (2001) and Mellgren & Eriksson (2006) followed the concept of *P. robustus* given by Löfgren (1978), and the Swedish material that they described and illustrated as *P. robustus* are identical both with the types of *P. cooperi* and with material from the Dawangou section (this study, Fig. 19) and from South China (Zhang, 1998c; Zhen *et al*., 2009a).

The holotype of *P. robustus* was re-illustrated and described in detail by Lindström (1955b, pl. 22, fig. 1). It is a symmetrical element with a suberect cusp and a short, non-expanded base, and has a sharp anterior and posterior margins and more than one lateral costa (one major postero-lateral costa and two shorter minor costae) on each side. Bergström (2007, p. 81) also indicated that the holotype of *P. robustus* "possesses several small but distinct lateral costae". It is certain that *P. robustus* is a species of *Protopanderodus* (Bergström, 2007) rather than a species of *Drepanodus* (Dzik, 1994; Armstrong, 2000), but it seems more closely related to multicostate species like *Protopanderodus calceatus* rather than to bicostate *P. cooperi*. However, as Hadding's (1913) type material is preserved in shale, and the published illustrations are drawings only, *P. robustus* remains as a poorly known species until detailed taxonomic revision of the type material can be undertaken.

Protopanderodus graeai (Hamar, 1966)

Fig. 21A–V

Acontiodus rectus Lindström.–Hamar, 1964: 258, pl. 1, figs 10, 12, 13, 17, text-fig. 4a–b.
Acodus graeai Hamar, 1966: 47, pl. 3, figs 11–14, text-fig. 3.5.
Protopanderodus graeai (Hamar).–Löfgren, 1978: 93–94, pl. 3, figs 19–25, text-fig. 31K–M (*cum syn.*); Mellgren & Eriksson, 2006: 105–106, figs 9V–BB, 12 (*cum syn.*).
Protopanderodus parvibasis Löfgren, 1978: 93, pl. 3, figs 11–18, text-fig. 31D–F (*cum syn.*); Mellgren & Eriksson, 2006: 104–105, figs 9O–U, 11 (*cum syn.*).
Protopanderodus robustus (Hadding).–Wang, 2001: 356, pl. 1, figs 3–4.

Material. 1249 specimens from 18 samples (see Tables 1–2).

Diagnosis. A species of *Protopanderodus* with a septimembrate apparatus; all the elements having an erect or suberect cusp and a short, non-expanded base, except for the Sb element bearing a longer base; M element with acostate anterior and posterior faces; S and P elements bearing a sharp posterior margin and a postero-lateral costa on each side, except for the strongly asymmetrical Sc element only having a sharp postero-lateral costa on the inner lateral side; basal margin straight or gently arched except for the Pb element.

Description. M element scandodiform, antero-posteriorly strongly compressed; cusp suberect in posterior or anterior view and curved posteriorly, with sharp inner and outer lateral margins; anterior face smooth and gently convex; posterior face less convex, varying from smooth to bearing a broad carina; basal margin straight (Fig. 21A–C).

(Figure 18 caption, continued from facing page)… ***O***, NIGP 153013, Nj296, inner lateral view (IY149-025); ***P***, NIGP 153014, Nj296, outer lateral view (IY149-026). Q–S, Sd element; ***Q–R***, NIGP 153015, AFT-X-K13/13, Q, lateral view (IY168-016), R, basal view (IY168-017); ***S***, NIGP 153016, Nj378, upper view showing cross section of cusp (IY160-012). T–V, W, Pa element; ***T***, NIGP 153017, AFT-X-K13/13, outer lateral view (IY168-012); ***U–V***, NIGP 153018, Nj295, U, outer lateral view (IY149-022); V, inner lateral view (IY149-021); ***W***, NIGP 153019, Nj384, outer lateral view (IY162-014), tentatively assigned to this species. X–Y, Pb element; ***X***, NIGP 153020, AFT-X-K13/13, inner lateral view (IY168-009); ***Y***, NIGP 153021, AFT-X-K13/13, outer lateral view (IY168-010). Scale bars 100 μm, unless otherwise indicated.

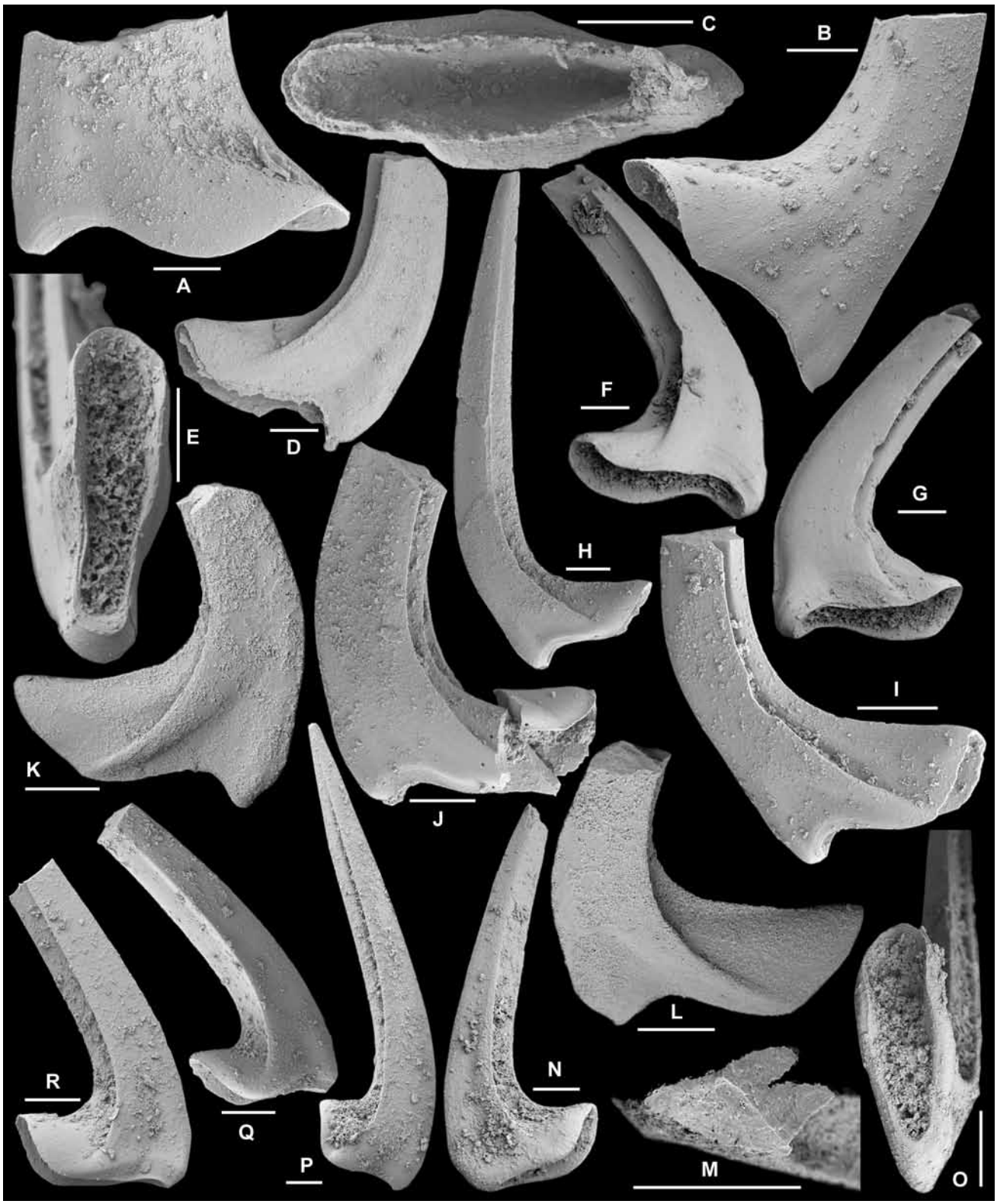

Figure 19. *Protopanderodus cooperi* (Sweet & Bergström, 1962). A–B, M element; ***A***, NIGP 153022, Nj376, posterior view (IY159-030); ***B***, NIGP 153023, Nj376, posterior view (IY159-033). C–G, Sa element; ***C–D***, NIGP 153024, Nj297, C, basal view (IY147-014), D, lateral view (IY147-015); ***E–G***, NIGP 153025, AFT-X-K13/13, E, basal view (IY168-020), F–G, lateral views (IY168-021, IY168-022). H–I, Sb element; ***H***, NIGP 153026, AFT-X-K13/13, outer lateral view (IY168-032); ***I***, NIGP 153027, AFT-X-K13/13, inner lateral view (IY168-029). J–M, Sc element; ***J***, NIGP 153028, AFT-X-K13/13, outer lateral view (IY168-034); ***K–M***, NIGP 153029, Nj294, K, inner lateral view (IY147-017), L, outer lateral view (IY147-019), M, upper view, close up showing cross section of the cusp (IY147-018). ***N–O***, Pa element, NIGP 153030, AFT-X-K13/13, N, inner lateral view (IY169-023), O, basal view (IY169-024). P–R, Pb element; ***P***, NIGP 153031, AFT-X-K13/13, antero-outer lateral view (IY168-018); ***Q***, NIGP 153032, AFT-X-K13/13, inner lateral view (IY168-030); ***R***, NIGP 153033, AFT-X-K13/13, inner lateral view (IY169-029). Scale bars 100 μm.

Figure 20. A–E, *Protopanderodus cooperi* (Sweet & Bergström, 1962), from the Pratt Ferry Formation of Alabama. ***A–C***, M element, OSU 52802, from the topotype locality, A–B, posterior views (IY170-024, IY170-025), C, anterior view (IY171-011). ***D–E***, Sb element, OSU 52803, from the topotype locality, D, outer lateral view (IY171-012), E, inner lateral view (IY170-023). F–L, *Protopanderodus varicostatus* (Sweet & Bergström, 1962); from the Pratt Ferry Formation of Alabama. ***F–H***, M2 element, OSU 52804, topotype, sample 64B2-12 from the top bed of the formation, F–G, posterior views (IY170-002, Iy170-001), F, anterior view (IY171-015); ***I–J***, M2 element, OSU 52805 from the topotype locality, I, posterior view (IY170-007), J, anterior view (IY171-018). K–L, M1 element, OSU 52806, topotype, sample 64B2-12 from the top bed of the formation, K, posterior view (170-026), L, anterior view (IY171-013). Scale bars 100 μm.

Sa element symmetrical; cusp suberect with a sharp posterior margin and a posterolateral costa on each side (Fig. 21D–G). Sb element like Sa, but asymmetrical, and often with a longer base, and with costa on the outer lateral face more strongly developed and located more towards posterior margin (Fig. 21H–J). Sc element strongly asymmetrical with a convex, smooth outer lateral face and a less convex inner lateral face; cusp suberect with a sharp posterior margin and a sharp posterolateral costa on the inner lateral face (Fig. 21K–P). Sd element nearly symmetrical, with a sharp posterior margin and a sharp posterolateral costa on each side; similar to Pa element, but less asymmetrical (Fig. 21Q–R).

Pa element asymmetrical, with a convex outer lateral face and a less convex (or even concave) inner lateral face to form sharp anterior and posterior margins, and with a gently arched basal margin; cusp suberect with a strongly developed sharp postero-lateral costa on the outer lateral face and a only weakly developed costa on the inner lateral face, costa on the outer lateral face more towards posterior margin (Fig. 21S–T). Pb element slightly asymmetrical; cusp erect with a sharp posterior margin and a sharp postero-lateral costa on each side; basal margin strongly curved with anterior portion and the posterior portion nearly normal to each other, forming a rectangular outline of the base (Fig. 21U–V).

Remarks. In their recent revision of this species, Mellgren & Eriksson (2006) referred the strongly asymmetrical element (herein designated as Sc) to the M position, and split the Sb element defined herein into Sb1, Sb2, and Sc elements. They also assigned the M element (as defined herein) to the M element of *P. cooperi* (referring to it as *P. robustus*; see Mellgren & Eriksson, 2006, fig. 13E), and to the M element of *P. parvibasis*.

The Sc element of *P. graeai* is morphologically more closely related to the other S and the P elements of this species (by its size and location of the postero-lateral process on the

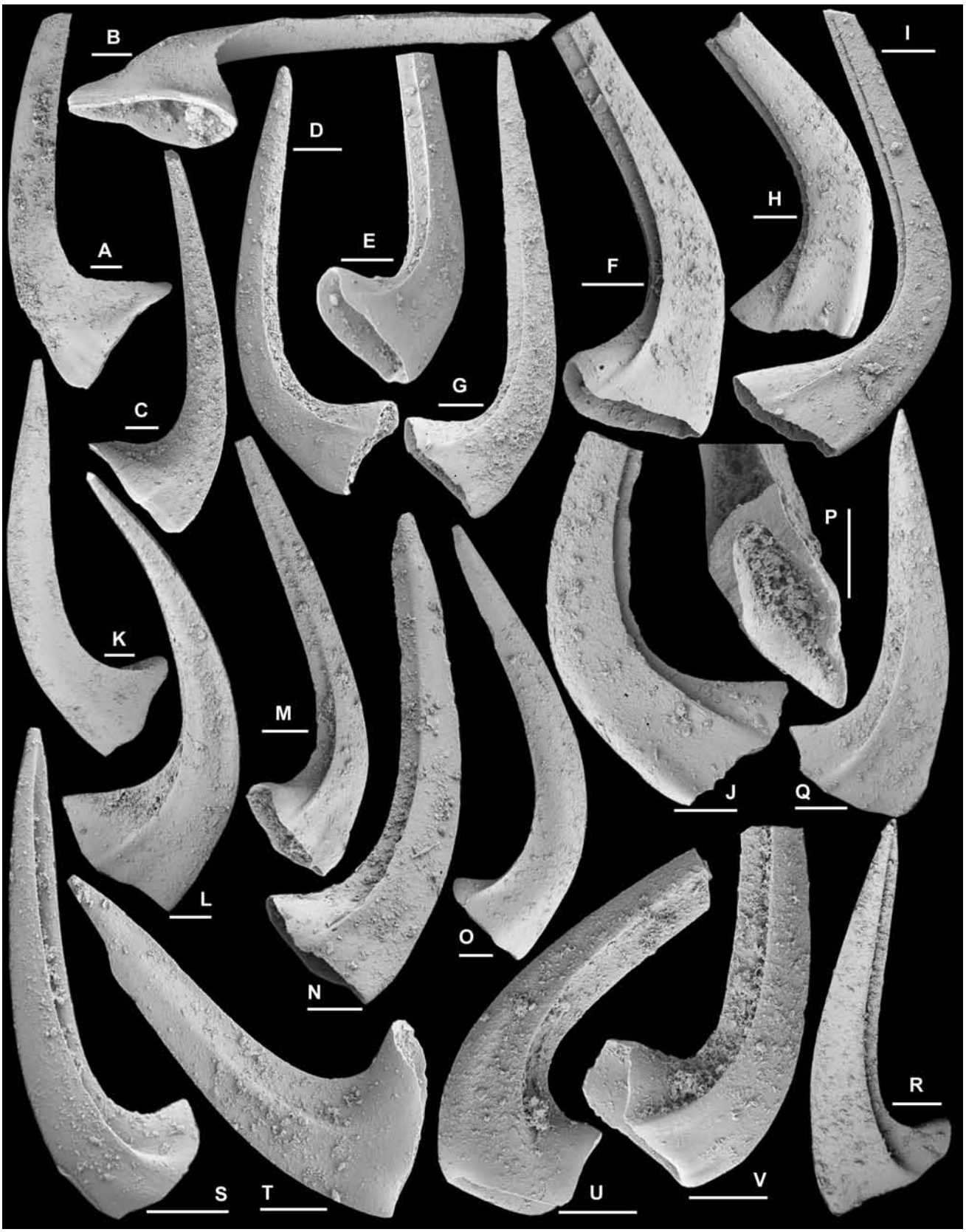

Figure 21. *Protopanderodus graeai* (Hamar, 1966). A–C, M element; ***A–B***, NIGP 153034, A, anterior view (IY167-045), B, basal-posterior view (IY167-044); ***C***, NIGP 153035, posterior view (IY169-006). D–G, Sa element; ***D***, NIGP 153036, lateral view (IY168-001); ***E–F***, NIGP 153037, E, basal-lateral view (IY168-003), F, lateral view (IY168-002); ***G***, NIGP 153038, lateral view (IY167-030). H–J, Sb element; ***H***, NIGP 153039, outer lateral view (IY167-036); ***I***, NIGP 153040, outer lateral view (IY167-029); ***J***, NIGP 153041, inner lateral view (IY167-037). K–P, Sc element; ***K–L***, NIGP 153042, K, outer lateral view (IY167-038), L, inner lateral view (IY167-039); ***M***, NIGP 153043, inner lateral view (IY167-032); ***N***, NIGP 153044, inner lateral view (IY167-033); ***O***, NIGP 153045, outer lateral view (IY167-035); ***P***, NIGP 153046, basal view (IY169-002). ***Q–R***, Sd element, NIGP 153047… (continued on facing page)

inner surface), and is also rather different from the M elements recognized in other species of *Protopanderodus,* which are generally larger than the P and S elements and strongly compressed antero-laterally. The M element of *P. graeai* defined herein is comparable with the M element of *P. cooperi*, but the latter characteristically has a sinuous basal margin and a prominent anticusp-like basal extension (Fig. 19; also see Zhang, 1998c, pl. 14, figs 13–17; Mellgren & Eriksson, 2006, fig. 13A–D, F–K). *P. graeai* differs from *P. cooperi* in having a straight basal margin and in lacking the anticusp-like antero-basal corner; it is distinguished from the bicostate elements of *P. calceatus* in having a less expanded base.

The long-based element assigned to the Sb1 and Sb2 position by Mellgren & Eriksson (2006) is only rarely represented in our collection from the Dawangou section (Fig. 21I).

Löfgren (1978) originally defined *P. parvibasis* as having a trimembrate apparatus including symmetrical and asymmetrical bicostate elements, and an acostate scandodiform element. The holotype of this species is a scandodiform element (Löfgren, 1978, pl. 3, fig. 18) bearing a suberect cusp with a faintly developed groove near the inner lateral margin on the posterior face and a short base with straight basal margin. It is morphologically closely related to M elements of the associated species *P. cooperi* and *P. calceatus*. Löfgren (1978, p. 93) suggested that the asymmetrical bicostate element of *P. parvibasis* was difficult to distinguish from the corresponding elements of other *Protopanderodus* species, and could only be differentiated by its shallower basal cavity, and differed from the corresponding element of *P. graeai* by having "the apex of the basal cavity placed more centrally". These minor differences between *P. graeai* and *P. parvibasis* may be recognizable in the well-preserved Swedish material, but are of little use when dealing with less well preserved specimens with a higher CAI.

Detailed comparison between *P. parvibasis* and *P. graeai* using the recently revised and illustrated Swedish material (Mellgren & Eriksson, 2006) and our collections indicates that most likely these represent only one species. Elements referable to both species are well represented among our material from Tarim, but we had extreme difficulty in distinguishing one from the other. Close examination of the *P. parvibasis* specimens illustrated by Mellgren & Eriksson (2006, fig. 11A, 11H) suggests that their Sb1 and Sb2 elements should be reassigned to *P. cooperi*, and all the other figured specimens except the M element (Mellgren & Eriksson, 2006, fig. 11D, 11I) are identical with those illustrated by them as *P. graeai*. However, if we consider the M element of *P. graeai* defined by Mellgren & Eriksson (2006) to represent the Sc position of this species, and the M element of *P. parvibasis* as defined by Mellgren & Eriksson (2006) to represent the M position in the *P. graeai* apparatus, and further combining the Sb1, Sb2 and Sc elements of Mellgren & Eriksson (2006) as the Sb element of *P. graeai*, then *P. parvibasis* becomes a junior synonym of *P. graeai*. These two species also have similar stratigraphical ranges (Mellgren & Eriksson, 2006, fig. 10).

Protopanderodus liripipus Kennedy, Barnes & Uyeno, 1979

Fig. 23C–E

Protopanderodus liripipus Kennedy, Barnes & Uyeno, 1979: 546–550, pl. 1, figs 9–19; An, 1981: pl. 3, fig. 29; An *et al*., 1981: pl. 1, figs 16–17; An & Ding, 1982: pl. 2, figs 4, 13; Zeng *et al*., 1983: pl. 12, fig. 34; An & Xu, 1984: pl. 1, fig. 21; Chen & Zhang, 1984b: 129, pl. 2, figs 22–24; Wang & Lou, 1984: 278, pl. 8, figs 6–10; An *et al*., 1985: pl. 12, figs 5–9; An, 1987: 173, pl. 11, figs 4, 11–14; Ding, 1987: pl. 5, fig. 28; Chen & Zhang, 1989: pl. 4, figs 26, ?27; McCracken, 1989: 18–20, pl. 3, figs 15–16, 18, 20–25, text-fig. 3G–J (*cum syn.*); An & Zheng, 1990: pl. 6, figs ?5, 9–10; Bergström, 1990: pl. 2, figs 7–8, pl. 4, figs 1–4; Duan, 1990: pl. 3, figs 2, 4; Gao, 1991: 135, pl. 12, fig. 8; Ding *et al*. in Wang, 1993: 195, pl. 38, fig. 17; Trotter & Webby, 1994: 485, pl. 4, figs 2–6; Zhen *et al*., 1999: 92, fig. 9.10–9.13 (*cum syn.*); Leslie, 2000: 1125, fig. 6.19–6.24; Zhao *et al*., 2000: 217, pl. 20, figs 1–2, 5, 7, 10–13; Pyle & Barnes, 2001: pl. 2, figs 6–7; Wang, 2001: pl. 1, fig. 12; Wang & Qi, 2001: pl. 1, figs 5, 22; Agematsu *et al*., 2007: 29, fig. 13.4, 13.5, 13.8, 13.10 (*cum syn.*); Agematsu *et al*., 2008a: 969, fig. 12.23–12.28.

Material. 12 specimens from two samples of the upper Kanling Formation (see Table 1).

Remarks. *P. liripipus* was originally interpreted as a quadrimembrate apparatus including the scandodiform element (= M element herein) and a transition series of protopanderodiform (symmetrical = Sa, slightly asymmetrical = Sb, and strongly asymmetrical = Sc) elements, with the holotype representing the Sa element (Kennedy *et al*., 1979, pl. 1, fig. 14), from the Tetagouche Group (upper Sandbian) at Camel Back Mountain in New Brunswick, Canada. This species was defined as having an extended and distally tapering base with the scandodiform element bearing a narrow groove near the inner lateral margin on the posterior face, the symmetrical and slightly asymmetrical elements bearing two costae separated by a groove on each side, and the strongly asymmetrical element bearing two costae on one side and one costa on the other. Some specimens among the illustrated types which have a shorter and lower base (Kennedy *et al*., 1979, pl. 1, figs 16–17) are defined herein as representing the P positions. Amongst the type material the short-based P elements showed symmetry variations. The short-based P elements have also been reported from Australia (Trotter & Webby, 1994, pl. 4, fig. 4), North China (An & Zheng, 1990, pl. 6, fig. 10) and from the Tarim Basin (Gao, 1991, pl. 12, fig. 8; Zhao *et al*., 2000, pl. 20 figs 10, 13; this study, Fig. 23C–D). Therefore, *P. liripipus* is considered herein as consisting of a seximembrate or septimembrate apparatus. Zhen *et al*. (1999, fig. 9.10–9.11) illustrated a Sc element that was strongly asymmetrical with a smooth outer lateral face and a costa-bounded deep groove on the inner lateral face.

Wide variations of the S elements in respect of the number of costae and their positions on the lateral faces were observed by Kennedy *et al*. (1979) among the type material,

(Figure 21 continued from facing page)… Q, inner lateral view (IY167-040), R, outer lateral view (IY167-041). S–T, Pa element; ***S***, NIGP 153048, outer lateral view (IY167-023); ***T***, NIGP 153049, inner lateral view (IY167-024). U-V, Pb element; ***U***, NIGP 153050, inner lateral view (IY167-028); ***V***, NIGP 153051, outer lateral view (IY167-026). All from sample AFT-X-K13/13; scale bars 100 μm.

Figure 22. *Protopanderodus varicostatus* (Sweet & Bergström, 1962); from the Pratt Ferry Formation of Alabama. ***A–C***, Sa element, OSU 52807, from the topotype locality, A–B, lateral views (IYIY170-010, IY171-019), C, upper view showing cross section of cusp (IY170-012). ***D–E***, Sb element, OSU 52808, from the topotype locality, D, inner lateral view (IY171-021), E, outer lateral view (IY170-017). ***F–G***, Pa element, OSU 52809, topotype, sample 64B2-12 from the top bed of the formation, F, inner lateral view (IY170-029), G, outer lateral view (IY171-016). H–M, Sc element; ***H–I***, OSU 52810, from the topotype locality, H, outer lateral view (IY170-018), I, inner lateral view (IY171-022); ***J–K***, OSU 52811, from the topotype locality, J, inner lateral view (IY170-020), K, outer lateral view (IY171-023); ***L–M***, OSU 52812, from the topotype locality, L, inner lateral view (IY170-021)… (continued on facing page)

but none of the illustrated S elements in the type collection showed the development of an anticusp-like extension on the antero-basal corner, as do those specimens documented from Australia (Trotter & Webby, 1994, pl. 4, fig4 1, 5), Tarim (Gao, 1991, pl. 12, fig. 8), South China (e.g., Chen & Zhang, 1984b, pl. 2, fig. 22; An *et al*., 1985, pl. 12, figs 5–7; Ding *et al*. in Wang, 1993, pl. 38, fig. 17), and Malaysia (Agematsu *et al*., 2008a). Further study of these forms with a prominent anticusp-like extension may lead to the conclusion that they represent a separate species, which was more closely related to *P. cooperi-P. rectus*, while *P. liripipus* might be derived from the multi-costate *P. calceatus-P. varicostatus* group, which formed a separate lineage more closely related to *P. gradatus* Serpagli, 1974 (see McCracken, 1989, fig. 2).

Protopanderodus varicostatus (Sweet & Bergström, 1962)

Figs 20F–L, 22A–R

Scolopodus varicostatus Sweet & Bergström, 1962: 1247–1248, pl. 168, figs 4–9, text-fig. 1A, C, K.

Scandodus unistriatus Sweet & Bergström, 1962: 1245, pl. 168, fig. 12, text-fig. 1E.

Protopanderodus varicostatus (Sweet & Bergström).–Bergström *et al*., 1974: pl. 1, figs 9–10; An *et al*., 1983: 132, pl. 16, figs 9–12; Burrett *et al*., 1983: 184, fig. 9C, D; Fåhraeus & Hunter, 1985: 183, text-fig. 2; Dzik, 1994: 74, pl. 14, figs 1–5, text-fig. 11b; Zhang, 1998b: 83, 84, pl. 15, figs 14–19 (*cum syn*.); Lehnert *et al*., 1999: pl. 2, fig. 16, pl. 3, fig. 14; Zhen & Percival, 2004b: 172–175, fig. 12A–M (*cum syn.*); Xiong *et al*., 2006: pl. 2, fig. 22; Ortega *et al.*, 2008: fig. 6.20–6.21; Zhen *et al*., 2009a: 151, fig. 8B–I.

Protopanderodus sp. cf. *calceatus* Bagnoli & Stouge.–Zhen & Percival, 2004a: 102–104, partim only figs 17A–J, M–S, not K–L.

Protopanderodus gradates Serpagli.–Ding *et al*. in Wang, 1993: 196, *partim* only pl. 16, figs 14, 16.

Material. 18 topotype specimens recovered from two samples (sample at topotype locality and sample 64B2–12 at the top bed) of the Pratt Ferry Formation of Alabama (see Sweet & Bergström, 1962).

Diagnosis. A multicostate species of *Protopanderodus* consisting of a septimembrate apparatus including scandodiform M, longer-based S (Sa, Sb, Sc, and Sd) and short-based P (Pa and Pb) elements; all elements bearing a suberect and distally reclined cusp, and a slightly expanded base with a shallow basal cavity and a strongly curved basal margin, which shows a characteristic indentation near the antero-basal corner and often an anticusp extension at the antero-basal corner in the S and P elements.

Description. M element scandodiform, antero-posteriorly compressed, asymmetrical with a suberect to reclined cusp and a rather extended base with a strongly curved basal margin (Fig. 20F–L); cusp with a smooth and convex anterior face (Fig. 20H, J, L) and costate posterior face (Fig. 20F–G, I, K). Two morphological variants are recognized based on development of costae on the posterior face: M1 element bearing a shallow groove on the posterior face more towards inner-lateral margin (Fig. 20K) with least development of the costae; M2 element bearing one or more costae to the outer-lateral side of the groove on the posterior face (Fig. 20 F–G, I).

Sa element symmetrical and multicostate (Fig. 22 A–C) with a suberect cusp and a long, non-expanded base; cusp laterally compressed with costate anterior and posterior margins, and two sharp costae separated by a narrow groove on each lateral face; basal margin sharply curved with posterior portion nearly normal to the anterior portion, and with a well-developed indentation near the antero-basal corner (Fig. 22A–B).

Sb element like Sa but asymmetrical, with more convex outer lateral face (Fig. 22E) and with sharp anterior margin slightly curved inner laterally (Fig. 22D).

Sc element strongly asymmetrical and multicostate (Fig. 22H–M) with a suberect cusp and a long, non-expanded base; cusp laterally compressed with sharply costate anterior and posterior margins, a sharp costa on the inner lateral face (Fig. 22 I, J, L), and two costae separated by a groove on the more convex outer lateral face (Fig. 22H, K, M); anterior margin slightly curved inner laterally.

Sd element weakly asymmetrical and multicostate (Fig. 22N–O) with a suberect cusp and a long, posteriorly curved base; cusp laterally compressed with sharply costate anterior and posterior margins; each lateral face ornamented with a prominent groove with a strong, sharp costa forming its anterior border and two less well-developed costa forming its posterior border; outer lateral face slightly more convex; anterior margin thin and slightly inner laterally curved, and forming a long blade-like anticusp projecting downward.

Pa element weakly asymmetrical and multicostate (Fig. 22F–G) with a suberect cusp and a short base; cusp laterally compressed with thin and sharply costate anterior and posterior margins; each lateral face ornamented with a prominent groove bordered by a strong costa on each side; anterior margin slightly curved inner laterally and forming a rounded antero-basal corner; basal margin strongly curved posteriorly, with the indentation near the antero-basal corner only weakly developed or even absent.

Pb element like Pa, but with a more or less quadrate outline of the base in lateral view (Fig. 22P–R) with well-developed indentation of the basal margin near the antero-basal corner to form a small, but prominent anticusp; anterior margin straight or only slightly curved and more or less perpendicular to the anterior portion of the basal margin (Fig. 22P, R).

Remarks. Sweet & Bergström (1962) proposed the species as consisting of a trimembrate apparatus including the bilaterally symmetrical (= Sa herein) element represented by the holotype (Sweet & Bergström, 1962; pl. 168, fig. 8), the slightly asymmetrical element represented by two illustrated paratypes that are interpreted herein as the Pb element (Sweet & Bergström, 1962; pl. 168, fig. 6) and the Sb element

(Figure 22 continued from facing page)… M, outer lateral view (IY171-007). ***N–O***, Sd element, OSU 528013, from the topotype locality, N, inner lateral view (IY170-016), O, outer lateral view (IY171-020). P–R, Pb element; ***P–Q***, OSU 528014, topotype, sample 64B2-12 from top bed of the formation, P, outer lateral view (IY171-014), Q, inner lateral view (IY170-027); ***R***, OSU 528015, topotype, sample 64B2-12 from the top bed of the formation, outer lateral view (IY171-017). Scale bars 100 μm, unless otherwise indicated.

Figure 23. A–B, *Venoistodus balticus* Löfgren, 2006. M element; ***A***, NIGP 153052, Nj296, posterior view (IY158-034); ***B***, NIGP 153053, Nj296, posterior view (IY158-032). C–E, *Protopanderodus liripipus* Kennedy, Barnes & Uyeno, 1979. C–D, P element (low based); ***C***, NIGP 153054, Nj406, inner lateral view (IY161-013); ***D***, NIGP 153055, Nj406, outer lateral view (IY161-014). ***E***, Sa element, NIGP 153056, Nj406, lateral view (IY155-010). F–L, *Protopanderodus* sp. ***F–G***, Sa element, NIGP 153057, Nj297, lateral views (IY150-027, IY150-026). H–I, Sc element; ***H***, NIGP 153058, Nj297, inner lateral view (IY150-028); ***I***, NIGP 153059, Nj297, inner lateral view (IY150-029). ***J–L***, Sb element, NIGP 153060, Nj296, J, outer lateral view (IY149-032), K, inner lateral view (IY149-031), L, basal view (IY149-030). M–N, *Pseudooneotodus mitratus* (Moskalenko, 1973). Pa element; ***M***, NIGP 153061, Nj375, upper view (IY159-022); ***N***, NIGP 153062, AFT-X-K13/44, upper view (IY164-029). O–P, *Spinodus spinatus* (Hadding, 1913). Sc element; ***O***, NIGP 153063, Nj406, outer lateral view (IY161-001); ***P***, NIGP 153064, Nj406, inner lateral view (IY161-002). Scale bars 100 μm.

(Sweet & Bergström, 1962; pl. 168, fig. 7), and the markedly asymmetrical (= Sc herein) element. As indicated by their choice of species name, Sweet & Bergström (1962) noted a wide variation in respect of the number and disposition of the lateral costae.

Protopanderodus varicostatus, characterized by strongly multicostate elements, was widely distributed and many variants or closely related forms have been described as *P*. sp. cf. *varicostatus* or *P*. sp. cf. *calceatus* (e.g., Zhen & Percival, 2004a). However, in the most of the material we studied previously, multicostate species of *Protopanderodus* comprised only a minor component of the faunas, which hindered a better understanding of variations, thereby sometimes leading to inconsistencies in interpretation of the species apparatus. Therefore, a close comparison of *P. varicostatus* and *P. calceatus* is essential to resolve this taxonomic uncertainty. For this purpose, the topotype material of *P. varicostatus* was re-examined and documented herein (see discussion under *P. calceatus*). We now suspect that material described as *P.* cf. *varicostatus* from a limestone lens exposed on Kirkup Station of central New South Wales may represent a separate species (Zhen & Pickett, 2008). These resemble specimens described as *P.* cf. *calceatus* from allochthonous limestones in the Oakdale Formation of central New South Wales (Zhen & Percival, 2004a) in having a broad anterior margin of the Sa element. The Oakdale specimens with multicostate S and P elements showing an indentation on the base are comparable with *P. varicostatus*, but some of

the figured specimens have a relatively shorter base without indentation (Zhen & Percival, 2004a, fig. 17K–L), suggesting they may not belong to this species. The Kirkup species is similar to both *P. varicostatus* and *P. calceatus* in having multicostate elements in the apparatus, but these elements have a less extended base (Zhen & Pickett, 2008, fig. 10J) and its bicostate Sa element has a broad anterior face (Zhen & Pickett, 2008, fig. 10 A–E), whereas the bicostate Sa element of *P. calceatus* (Fig. 18G–J) and multicostate Sa element of *P. varicostatus* (Fig. 22A–C) have a sharp anterior margin.

Pseudooneotodus Drygant, 1974a

Type species. *Oneotodus*? *beckmanni* Bischoff & Sannemann, 1958.

Pseudooneotodus mitratus (Moskalenko, 1973)

Fig. 23M–N

Ambalodus mitratus mitratus Moskalenko, 1973: 86, pl. 17, figs 9–11.

Ambalodus mitratus nostras Moskalenko, 1973: 87, pl. 17, figs 12–14, ?15.

Pseudooneotodus mitratus (Moskalenko).–Orchard, 1980: 25, pl. 3, figs 35, 42; Nowlan & Barnes, 1981: 23, pl. 2, figs 17–19; Nowlan, 1983: 667, pl. 3, figs 17, 21; Chen & Zhang, 1989: pl. 4, fig. 29; Pohler & Orchard, 1990: pl. 6, fig. 12; Dzik, 1994: 55, pl. 11, fig. 7; Zhen & Webby, 1995: 285, pl. 4, figs 16–17 (*cum syn.*); Zhang, 1998c: 85, pl. 14, fig. 12; Zhen *et al.*, 1999: fig. 9.14–9.15; Leslie, 2000: 1139, fig. 5.37 (*cum syn.*); Sweet, 2000: fig. 9.7; Pyle & Barnes, 2001: 1396, 1398, pl. 2, fig. 13; Zhen *et al.*, 2003a: fig. 6Q; Zhen *et al.*, 2004b: fig. 9A; Zhen & Pickett, 2008: 79, fig. 9A–B (*cum syn.*).

Pseudooneotodus mitratus mitratus (Moskalenko).–Zhao *et al.*, 2000: 219, pl. 43, figs 19, 23.

Pseudooneotodus mitratus nostras (Moskalenko).–Zhao *et al.*, 2000: 219, pl. 43, figs 20–22, 24–25.

Material. Nine specimens from five samples (see Tables 1–2).

Remarks. This species, characterized by a trilobate basal outline, is a very minor component of the Dawangou fauna, comparable to its rarity in various faunas from New South Wales (Zhen & Webby, 1995; Zhen *et al.*, 1999; Zhen *et al.*, 2003a; Zhen *et al.*, 2004b; Zhen & Pickett, 2008). Nowlan & Barnes (1981) and Nowlan (1983) regarded the two subspecies originally erected by Moskalenko (1973), *A. mitratus mitratus* and *A. mitratus nostras*, as constituent elements of a single species apparatus, and recognized a symmetry transition series among its elements. Although *P. mitratus* was a widely distributed species, its relative rarity in many faunas has hindered a formal reconstruction of its species apparatus in the literature. From our experience, the two morphotypes represented by Moskalenko's (1973) two subspecies are often found co-occurring, but forms with nodes on the upper surface are much rarer and have not been recovered in the Dawangou samples.

The broad-conical morphotype of *Pseudooneotodus triangulus* Chen & Zhang, 1984b is similar to *P. mitratus* in having a triangular outline in upper view, but the former species has the three processes more extended with a tendency to form a secondary ridge splitting from the posterior process (Chen & Zhang, 1984b, pl. 2, figs 25–26).

Pygodus Lamont & Lindström, 1957

Type species. *Pygodus anserinus* Lamont & Lindström, 1957.

Remarks. Most Ordovician conodont workers accept that species of *Pygodus* consisted of a seximembrate or septimembrate apparatus including pygodiform Pa, pastinate Pb, ramiform S (alate Sa, tertiopedate Sb, bipennate Sc and quadriramate Sd), and possibly geniculate M elements (Zhang, 1998a; Rasmussen, 2001; Zhen *et al.*, 2009a, table 2). The M elements of the two *Pygodus* species (*P. anserinus* and *P. serra*) occurring in the Dawangou section have not been recovered, although the Pa, Pb and S elements of both species were represented by a large collection (Tables 1–2). Very rare reports of a geniculate M element occurring in association with other elements of *Pygodus* have cast doubts on the inclusion of the M element in the *Pygodus* species apparatus (Dzik, 1994; Zhen *et al.*, 2009a). Armstrong (1997, 2000) provided an alternative reconstruction for *P. anserinus* and *P. serra*, interpreting the *P. anserinus* species apparatus to include a pygodiform Pa with four rows of denticles and a pygodiform Pb element with three rows of denticles, the latter generally considered by other workers as representing the Pa element of P. *serra* (Zhang, 1998a).

Pygodus anserinus Lamont & Lindström, 1957

Fig. 24A–P

Pygodus anserinus Lamont & Lindström, 1957: 67, pl. 5, figs 12–13, Fig. 1a–c (non d); Bergström, 1971: 149, pl. 2, figs 20, 21; Bergström *et al.*, 1974: pl. 1, figs 16–17; Harris *et al.*, 1979: pl. 3, figs 16–17, pl. 4, fig. 17; An & Ding, 1982: pl. 5, figs 15, 17, 18; Chen *et al.*, 1983: pl. 1, figs 5, 6; Zeng *et al.*, 1983: pl. 12, figs 4, 22; Chen & Zhang, 1984b: 130, pl. 2, figs 18–21; Wang & Luo, 1984: 279, pl. 11, figs 10, 19, pl. 12, figs 14; An *et al.*, 1985: pl. 17, figs 7–9; An, 1987: 176–177, pl. 26, figs 9–12, 14; Ding, 1987: pl. 5, fig. 8; Ni & Li, 1987: 435, pl. 59, fig. 26; Chen & Zhang, 1989: 222–223, pl. 5, figs 3–5; An & Zheng, 1990: pl. 14, figs 1, 2, 5, 6; Pohler & Orchard, 1990: pl. 2, fig. 20; Zhong, 1990: 152, pl. 16, figs 17, 18, pl. 20, 13, 15; Bergström, 1990: pl. 1, figs 19–22; Gao, 1991: 136, pl. 10, figs 6–12; Ding *et al.*, in Wang, 1993: 198, pl. 35, figs 22, 23, 25; Dzik, 1994: 105, 106, pl. 17, figs 7, 8, text-figs 26, 27; Armstrong, 1997: 777–778, *partim* only pl. 4, figs 1–3, 5–7, non fig. 4 = *P. serra*; Bednarczyk, 1998: pl. 2, figs 4, 16; Wang & Zhou, 1998: pl. 2, figs 5–8, 13; Zhang, 1998a: pl. 3, figs 1–8, text-fig. 2E; Zhang, 1998b: 87–88, pl. 16, figs 1–5 (*cum syn.*); Lehnert *et al.*, 1999: pl. 3, fig. 6; Zhao *et al.*, 2000: 220, pl. 30, figs 1–4, 19–21; Rasmussen, 2001: 127–127, pl. 16, figs 13–17 (*cum syn.*); Wang, 2001: pl. 2, figs 5–6, 10, 13–15, 17–18, 20–26 (*cum syn.*); Wang & Qi, 2001: pl. 2, figs 19, 21, 25, 26; Pyle & Barnes, 2003: fig. 13.8–13.10; Xiong *et al.*, 2006: pl.1, figs 17, 19; Agematsu *et al.*, 2007: 25, fig. 9.1–9.4; Bergström, 2007: fig. 3A; Ortega *et al.*, 2008: fig. 6.11; Viira, 2008: fig. 6O; Zhen *et al.*, 2009a: 152–157, figs 8N, 9A–I, 10A–L (*cum syn.*); Bergström, 2007: fig. 3A–B.

Pygodus serrus-anserinus transition.–An & Zheng, 1990: pl. 14, figs 3, 4; Zhao *et al.*, 2000: 221, *partim*, only pl. 30, fig. 6; Xiong *et al.*, 2006: pl. 1, fig. 14.

Pygodus serrus (Hadding).–Zhong, 1990: 152, pl. 20, *partim* only, fig. 17.

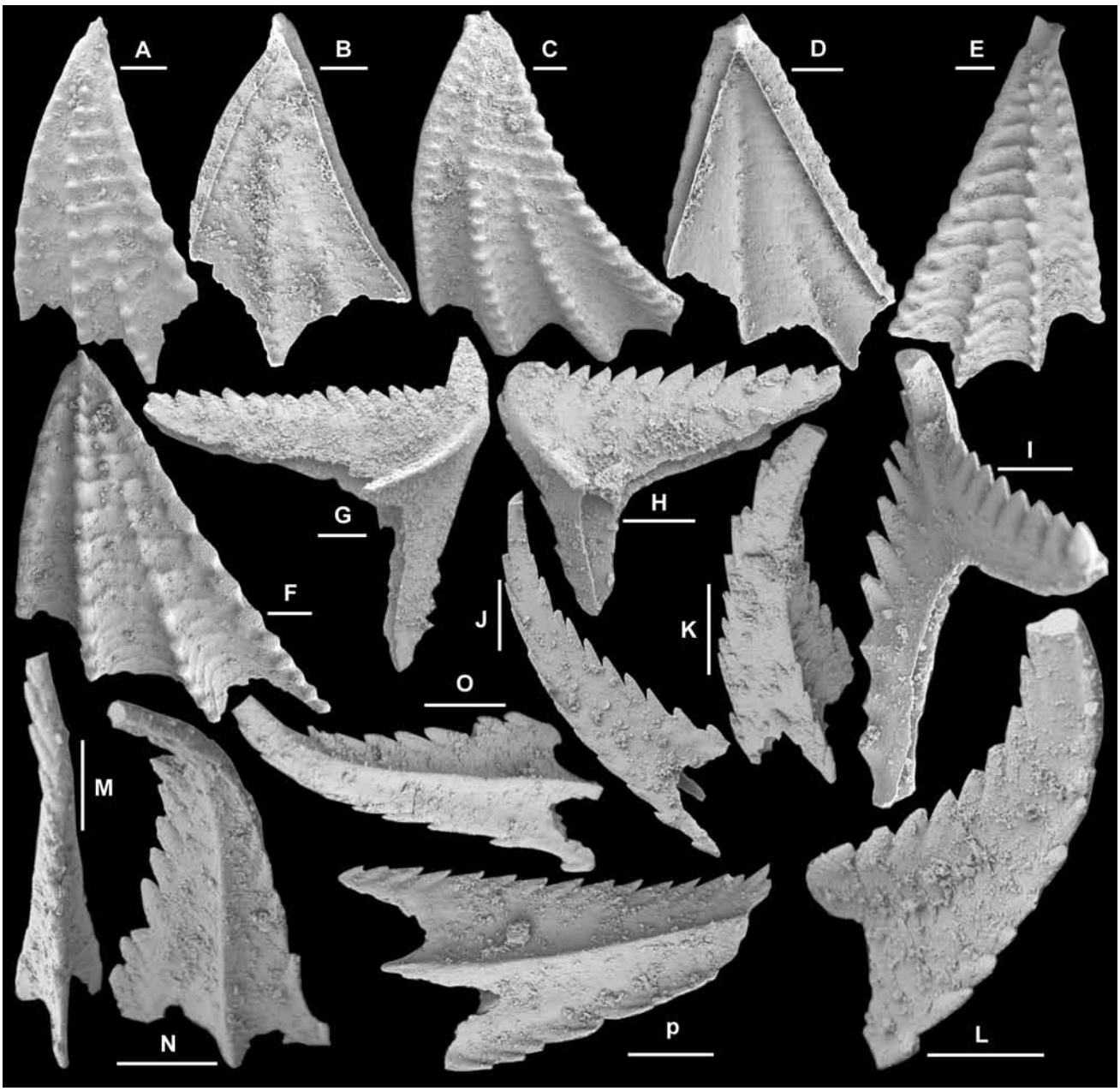

Figure 24. *Pygodus anserinus* Lamont & Lindström, 1957. A–F, Pa element; ***A***, NIGP 153065, Nj276, upper view (IY152-022); ***B***, NIGP 153066, Nj276, basal view (IY152-023); ***C***, NIGP 153067, Nj388, upper view (IY155-002); ***D***, NIGP 153068, Nj388, basal view (IY155-003); ***E***, NIGP 153069, Nj379, upper view (IY154-004); ***F***, NIGP 153070, Nj389, upper view (IY155-004). G–I, Pb element; ***G***, NIGP 153071, Nj378, outer lateral view (IY153-015); ***H***, NIGP 153072, Nj376, basal-outer lateral view (Iy153-001); ***I***, NIGP 153073, Nj376, inner lateral view (IY153-002). ***J***, Sa element, NIGP 153074, Nj376, lateral view (IY153-003). ***K–L***, Sb element, NIGP 153075, Nj377, K, outer lateral view (IY153-012), L, inner lateral view (IY153-013). M–P, Sd element; ***M–O***, NIGP 153076, Nj376, M, posterior view (IY153-006), N, inner lateral view (IY153-007), O, outer lateral view (IY153-008); ***P***, NIGP 153077, Nj379, outer lateral view (IY154-008). Scale bars 100 μm.

Material. 1816 specimens plus 1518 specimens of undifferentiated Pb and S elements of both *P. anserinus* and *P. serra* (see Tables 1–2).

Remarks. *P. anserinus* differs from the slightly older or contemporaneous *P. serra* in having four rows of denticles on the platform of the Pa element (Bergström, 2007; Zhen *et al*., 2009a). The fourth row of denticles inserted between the middle row and the inner row of the Pa element in *P. anserinus* is variably developed in transitional forms from *P. serra* to *P. anserinus*. The lowest occurrence of *Pygodus* in the Dawangou section was recorded in sample Nj375 near the top of the Saergan Formation, where the early form of *P. anserinus* (with the fourth row of denticles represented by a few weakly developed nodes near the distal margin of the platform) is associated with *P. serra*.

Morphologically, *P. anserinus* and *P. serra* can only be differentiated from each other by their Pa elements. When the two species are co-occurring as in the upper part of the Saergan Formation and in the lower part of the Kanling Formation, it is difficult or nearly impossible to tell the differences between Pb and S elements of these two species

Figure 25. *Pygodus serra* (Hadding, 1913). A–E, Pa element; ***A***, NIGP 153078, 13/40, upper view (IY155-018); ***B***, NIGP 153079, Nj375, upper view (IY151-016); ***C***, NIGP 153080, Nj375, basal view (IY151-010); ***D***, NIGP 153081, Nj375, upper view (IY151-014); ***E***, NIGP 153082, 13/40, upper view (IY155-019). F–H, Pb element; ***F***, NIGP 153083, 13/40, outer lateral view (IY155-020); ***G***, NIGP 153084, Nj375, outer lateral view (IY151-017); ***H***, NIGP 153085, Nj375, inner lateral view (IY151-018). I–L, Sa element; ***I–K***, NIGP 153086, Nj375, I, posterior view (IY151-015), J, lateral view (IY151-020), K, antero-lateral view (IY151-22); ***L***, NIGP 153087, Nj375, posterior view (IY152-001). ***M–N***, Sb element, NIGP 153088, Nj375, M, lateral view (IY152-005), N, posterior view (IY152-006). ***O–P***, Sc element, NIGP 153089, Nj375, O, posterior view (IY152-009), P, inner lateral view (IY152-010). Q–R, Sd element; ***Q***, NIGP 153090, Nj375, outer lateral view (IY152-004); ***R***, NIGP 153091, Nj375, outer lateral view (IY152-011). Scale bars 100 μm.

(Tables 1–2). The ancestor-descendent relationship from *P. serra* to *P. anserinus* was well documented by their closely comparable morphological similarities and transformation of the Pa elements from a three-ridged platform of *P. serra* to a four-ridged platform of *P. anserinus* (Zhang, 1998a). Based on detailed studies of the distribution and palaeoecology of these two species in the Cobbs Arm Formation of north-central Newfoundland (Fåhraeus & Hunter, 1981), Fåhraeus (1982b, p. 5) favoured an allopatric speciation for *P. anserinus*, suggesting that *P. serra* was generally restricted to near shore setting, whereas *P. anserinus* "preferred the more open, probably deeper and cooler environment".

However, co-occurrence of these two species found in the lower part of the *P. anserinus* Zone in the Tarim Basin (this study) and other regions (Zhang, 1998a) points towards a sympatric speciation for *P. anserinus*, and co-occurrence of both *P. serra* and *P. anserinus* in the basinal shales does not support the ecological differentiation of these two species as suggested by Fåhraeus.

Pygodus serra (Hadding, 1913)

Fig. 25A–R

Arabellites serra Hadding, 1913, p. 13, pl. 1, figs 12, 13.
Pygodus aff. *anserinus* Lamont & Lindström.–Viira, 1967: fig. 4.6.
Haddingodus serra (Hadding).–Viira, 1967: fig. 4.7.
Pygodus serrus (Hadding).–Bergström, 1971: 149, pl. 2, figs 22, 23; Bergström *et al*., 1974: pl. 1, fig. 18; Nicoll, 1980: fig. 3H–L; An, 1981: pl. 4, figs 1–3; Ni, 1981: pl. 1, figs 28–29; An & Ding, 1982: pl. 5, figs 4, 13, 14, 16, 19, 22; Chen *et al*., 1983: pl. 1, figs 11, 12; Zeng *et al*., 1983: pl. 12, figs 3, 5; Chen & Zhang, 1984b: 130–131, pl. 2, figs 16–17; Wang & Luo, 1984: 279, pl. 11, fig. 18; An *et al*., 1985: pl. 17, figs 2–6; An, 1987: 177, pl. 24, fig. 25, pl. 26, figs 1–8, 13, 15, pl. 29, figs 2–3; Ding, 1987: pl. 5, figs 6–7; Chen & Zhang, 1989: 223, pl. 5, figs 1–2; An & Zheng, 1990: pl. 13, figs 11–14, 17–21; Zhong, 1990: 152, pl. 16, figs 10–11, 13–15, pl. 20, *partim* only, figs 14, 16, 18 (not fig. 17 = *P. anserinus*); Gao, 1991: 136, pl. 10, fig. 5; Ding *et al*., in Wang, 1993: 198, pl. 30, figs 10, 13, 15–18, 20–22, 24, pl. 35, 24, 26; Wang *et al*., 1996: pl. 1, fig. 14; Wang & Zhou, 1998: pl. 3, figs 1–2; Lehnert *et al*., 1999: pl. 2, fig. 12; Zhao *et al*., 2000: 220–221, *partim* only, pl. 30, figs 7–10, 18; Wang, 2001: 357, pl. 2, figs 4, 11, 16, 19; Wang & Qi, 2001: pl. 2, fig. 24; Xiong *et al*., 2006: pl. 1, figs 15–16, 18.
Pygodus serra (Hadding).–Harris *et al*., 1979: pl. 2, fig. 18; Zeng *et al*., 1983: pl. 12, figs 3, 5; Ni & Li, 1987: 435, pl. 59, fig. 25; Bergström, 1990: pl. 1, figs 23–24; Pohler & Orchard, 1990: pl. 1, fig. 18; McCracken, 1991: p. 51, pl. 2, figs 4, 6 7, 9, 11, 12, 14–18, 20–23, 28–30; Dzik, 1994: 103–105, pl. 17, figs 9–12, text-fig. 26; Wang *et al*., 1996: pl. 1, fig. 14; Wang & Zhou, 1998: pl. 3, figs 1–2; Zhang, 1998a: 96, pl. 2, figs 3–5, 8–14, text-figs 2C1, C3, 4B (doubtful pl. 2, figs 1, 2, 6, 7, text-fig. 2C2 = *P. xinjiangensis*) (*cum syn.*); Lehnert *et al*., 1999: pl. 2, fig. 12; Ottone *et al*., 1999: 242, pl. 6, figs 2–3; Percival *et al*., 1999: fig. 8.18; Stouge & Bagnoli, 1999: 154, text-fig. 5; Pickett & Percival, 2001: fig. 4C; Wang, 2001: p. 357, pl. 2, figs 4, 11, 16, 19 (*cum syn.*); Wang & Qi, 2001: pl. 2, fig. 24; Norford *et al*., 2002: pl. 3, figs 7–10; Bergström, 2007: fig. 4; Percival & Zhen, 2007: pl. 1, figs 1–3, 19.
Pygodus protoanserinus Zhang, 1998a: 96, text-fig. 2D, pl. 3, figs 9–18 (*cum syn.*); Zhang, 1998b: 86–87, pl. 16, figs 6–8 (*cum syn.*); Zhen *et al*., 2004b: 158, fig. 9B–J (*cum syn.*); Percival & Zhen, 2007: pl. 1, figs 17–18.
Pygodus serrus-anserinus transition.–Zhao *et al.*, 2000: 221, *partim*, only pl. 30, fig. 5.
Pygodus anserinus Lamont & Lindström, 1957: 68, *partim*, only fig. 1d; Armstrong, 1997: 777–778, *partim* only pl. 4, fig. 4.
Pygodus cf. *anserinus* Lamont & Lindström.–Dong & Wang, 2006: pl. 7, fig. 17.
?Pygodus serra (Hadding).–Zhen *et al*., 2004b: 158, fig. K–L = *Pygodus xinjiangensis*.
?Pygodus xinjiangensis Wang & Qi, 2001: 144, pl. 2, figs 18, 20.

Material. 839 specimens plus 1518 specimens of undifferentiated Pb and S elements of both *P. anserinus* and *P. serra* (see Tables 1–2).

Remarks. Zhang (1998a) proposed *Pygodus protoanserinus* to accommodate intermediate forms between *P. serra* and *P. anserinus*, and defined it as having three rows of denticles on the Pa element with the middle row situated more towards the outer lateral row rather than in a mid position or towards the inner row as in *P. serra*. However, based on examination of topotypes of *P. serra*, Bergström (2007) considered *P. protoanserinus* to be a junior synonym of *P. serra*, and indicated that Zhang's definition of *P. serra* also include forms ascribed to *Pygodus xinjiangensis* by Wang and Qi (2001). The latter has a Pa element bearing a narrower platform with outer and inner margins parallelling each other distally and with the middle row of the denticles located more closely to the inner lateral margin (Wang & Qi, 2001, pl. 2, fig. 18) rather than closer to the outer margin as in *P. serra*.

The abundant material of *Pygodus* species (both *P. serra* and *P. anserinus*) from the Dawangou section shows a distally expanding triangular outline of the platform, and the Pa element of *P. serra* exhibits the middle row of denticles varying from nearly centrally-positioned (Fig. 25E) to closer to the outer lateral margin (Fig. 25D). Zhang (1998a) also illustrated some specimens of *P. serra* bearing a narrow platform with parallel distal margins and a centrally positioned middle row of denticles from the Hällekis section of Sweden (Zhang, 1998a, text-fig. 2C2, pl. 2, fig. 7). Similar forms were also reported from the Guniutan Formation of South China (An, 1987, pl. 26, figs 1, 2, 5). These intermediate forms between typical *P. serra* and those referred to as *P. xinjiangensis* by Wang and Qi (2001) made it difficult to distinguish between these species on the characters originally employed. Moreover, forms referable to *P. xinjiangensis* occurred in association with *P. serra* (An, 1987; Zhang, 1998a, fig. 2). Therefore, we follow Bergström's (2007) opinion that *P. xinjiangensis* is a possible junior synonym of *P. serra* pending further study. Forms typical of *P. xinjiangensis* have not been recognized in the Dawangou material.

Scabbardella Orchard, 1980

Type species. *Drepanodus altipes* Henningsmoen, 1948.

Remarks. Orchard (1980) originally defined *Scabbardella* as a multielement genus consisting of three morphotypes (drepanodiform, acodiform and distacodiform), and suggested that it could be distinguished from *Dapsilodus* mainly by including the drepanodiform elements in the apparatus and in absence of striations on the lateral faces of elements, particularly near the anterior margin. The type species, *S. altipes* (Henningsmoen) was revised by Orchard (1980) as having a seximembrate apparatus, including two drepanodiform, two acodiform and two distacodiform elements differentiated mainly by the curvature of the cusp. Orchard (1980) regarded *Scabbardella similaris* (Rhodes, 1953) as a junior synonym of *S. altipes*. However, An (1987, p. 179–180) considered them as separate species (based on curvature of the cusp and length of the base), and re-assigned to *S. similaris* the material from England and Wales that Orchard (1980) referred to as *S. altipes*. Our interpretation concurs with that of Orchard (1980).

Figure 26. *Scolopodus striatus* Pander, 1856. ***A–B***, P element (acontiodiform), NIGP 153092, Nj294, A, anterior view (IY148-14), B, posterior view (IY148-015). ***C–D***, Sa element (subrounded), NIGP 153093, Nj294, C, posterior view (IY148-012), D, postero-lateral view (IY148-011). E–I, Sb element (short-based variant of compressed paltodiform); ***E–G***, NIGP 153094, Nj294, E, inner lateral view (IY148-007), F, posterior view (IY148-008), G, antero-outer lateral view (IY148-006); ***H–I***, NIGP 153095, Nj294, H, outer lateral view (IY148-029), I, upper view showing cross section of cusp (IY148-028). J–O, Sc element (medium-based variant of paltodiform); ***J***, NIGP 153096, Nj292, inner lateral view (IY158-025); ***K–L***, NIGP 153097, Nj292, K, inner lateral view (IY158-022), L, outer lateral view (IY158-020); ***M–O***, NIGP 153098, Nj294, M, basal view of basal cavity (IY148-017), N, outer lateral view (IY148-016), O, inner lateral view (IY148-018). ***P–Q***, Sd element (long-based variant of compressed paltodiform), NIGP 153099, Nj294, P, inner lateral view (IY148-009), Q, basal view of cusp (IY148-010). R–W, M element (short-based variant of paltodiform); ***R–S***, NIGP 153100, Nj294, R, inner lateral view (IY148-004), S, outer lateral view (IY148-005); ***T–U***, NIGP 153101, Nj292, T, inner lateral view (IY158-023), U, outer lateral view (IY158-024); ***V***, NIGP 153102, Nj295, inner lateral view (IY149-009); ***W***, NIGP 153103, Nj294, inner lateral view (IY158-031). Scale bars 100 μm.

Scabbardella altipes (Henningsmoen, 1948)

Fig. 9D–O

Drepanodus altipes Henningsmoen, 1948: 420, pl. 25, fig. 14; Wang & Lou, 1984: 257, pl. 2, figs 3–4, 15, 17.

Scabbardella altipes (Henningsmoen).–Orchard, 1980: 25–26, pl. 5, figs 2–5, 7–8, 12, 14, 18, 20, 23–24, 28, 30, 33, 35, text-fig. 4C (*cum syn.*); Nowlan, 1983: 668, pl. 1, figs 6–7, 11–14; Chen & Zhang, 1984b: 131, pl. 2, figs 29–30; Ni & Li, 1987: 437, pl. 55, figs 19–20, pl. 59, figs 21–22, 31–32; Chen & Zhang, 1989: pl. 5, figs 8–9; Gao, 1991: 137, pl. 12, fig. 18; Ding *et al*. in Wang, 1993:199, pl. 12, figs 26–27; Trotter & Webby, 1994: 487, pl. 3, figs 1–6, 8–11; Wang *et al.*, 1996: pl. 1, fig. 18; Wang & Zhou, 1998: pl. 2, fig. 3; Ferretti & Serpagli, 1999: pl. 2, figs 17–23; Leslie, 2000: 1125, fig. 3.36–3.37; Sweet, 2000: fig. 9.14–9.15; Zhao *et al*., 2000: 221–222, pl. 23, figs 10–12; Rasmussen, 2001: 130, pl. 17, figs 4–5; Agematsu *et al*., 2007: 29–30, fig. 11.4, 11.8–11.10, 11.12–11.17 (*cum syn.*); Agematsu *et al*., 2008a: 969, fig. 10.25–10.34.

Dapsilodus similaris (Rhodes).–An, 1981: pl. 3, figs 4–5; An & Ding, 1982: pl. 1, figs 17–18; An *et al*., 1983: 91, pl. 15, fig. 22; An & Xu, 1984: pl. 1, figs 8, 15; An *et al*., 1985: pl. 11, figs 9–10, 13–14; Ding, 1987: pl. 5, fig. 23; Duan, 1990: pl. 3, figs 13–15.

Scabbardella similaris (Rhodes).–An, 1987: 179–180, pl. 5, figs 14–17, 19–24, 26–27; Ding *et al*. in Wang, 1993: 199, pl. 17, figs 22–28.

Material. 232 specimens from 17 samples (see Tables 1–2).

Remarks. The revised multielement concept given by Orchard (1980) is followed herein. Amongst the specimens of *S. altipes* illustrated by Orchard (1980) from the Upper Ordovician of England and Wales, seven morphotypes can be differentiated. They are short-based drepanodiform (Orchard, 1980, pl. 5, figs 23, 33), long-based drepanodiform (pl. 5, fig. 24), acodiform with short base and erect or reclined cusp (pl. 5, figs 18, 20), acodiform with medium base (Fig. 9F–G herein; Orchard, 1980, pl. 5, figs 14, 30), long-based acodiform (Fig. 9D–E; pl. 5, figs 3–4, 7–8, 12), long-based symmetrical distacodiform (pl. 5, figs 2, 35), and asymmetrical distacodiform (Fig. 9H–O; pl. 5, fig. 28).

Scolopodus Pander, 1856

Type species. *Scolopodus sublaevis* Pander, 1856.

Remarks. *Scolopodus* is well-defined and widely understood as a dominantly hyaline, robust, thick-walled coniform genus with a non-expanded base and sharp costae. However, as Pander's (1856) original material was lost, there has long been confusion and misinterpretations concerning various species erected by Pander (1856) and several subsequent authors (e.g., Lindström, 1955a). Pander (1856) recognized six form species of *Scolopodus*, including *S. sublaevis, S. striatus, S. costatus, S. semicostatus, S. aequilateralis*, and *S. quadratus*. Fåhraeus (1982a) considered that only two species were valid, namely the type species, *S. sublaevis* (= *S. aequilateralis*), and *S. quadratus* (= *S. costatus* and *S. striatus*); furthermore he regarded *S. rex* Lindström, 1955a as a junior synonym of *S. quadratus*. Based on material recovered from the Mining Institute in St. Petersburg that is believed to be part of Pander's type collection, and additional new material collected from one of Pander's original localities on the Popowka River of St. Petersburg, Tolmacheva (2006) provided a comprehensive revision of Pander's species of *Scolopodus*. She concluded that all Pander's form species belonged to a single species, except for the type species, *S. sublaevis*, which was not recognized in her material. Tolmacheva (2006) suggested that *S. striatus* was the valid name for this multielement species, with the widely-used *S. rex* forming a junior synonym. Her conclusion is supported by a large collection of *Scolopodus* collected by one (SB) of the authors from the type locality (Popowka River).

Scolopodus rex Lindström, 1955a was erected as a form species of a multicostate symmetrical element with rounded cross section (Lindström, 1955a, pl. 3, fig. 32), and *S. rex* var. *paltodiformis* Lindström, 1955a was proposed originally as a form species represented by a short-based, strongly compressed element with multicostate inner lateral face and only faintly costate outer lateral face (Lindström, 1955a, pl. 3, figs 33–34). Tolmacheva (2006, fig. 2) considered them to represent the Sa (subrounded) and M (scandodiform) positions respectively of her revised multielement species, *S. striatus*.

Our current understanding of *Scolopodus* is largely based on the now well-established multielement species *S. striatus*, as the type species originally designated by Pander remains as a poorly known species, whose validity may also be questionable (Tolmacheva, 2006). In the revision by Tolmacheva, *S. striatus* was defined as having five or more nongeniculate elements representing the M, S and P positions. However, some species of *Scolopodus*, such as *S.*? *oistodiformis* An & Ding, 1985 from China, and *S. subrex* Ji & Barnes, 1994 and *S. cornutiformis* (Branson and Mehl, 1933) from North America, have a distinctive geniculate M element in their species apparatus, rather a nongeniculate scandodiform M element as in *S. striatus*. *S.*? *oistodiformis* is widely reported in the Darriwilian of South China and Tarim. Its M element from the Dawangou Formation (Fig. 27A–C) is geniculate with a recurved, robust and antero-laterally strongly compressed cusp, which has a smooth, non-costate anterior face and a costate less convex posterior face. It remains uncertain whether this distinctive species group with a geniculate M element should be included in *Scolopodus*.

Scolopodus? oistodiformis An & Ding, 1985

Fig. 27A–I

Scolopodus rex oistodiform An & Ding, 1982: pl. 1, fig. 9 (*nomen nudum*); An & Ding, 1985: 8, pl. 1, figs 16–18; An *et al.*, 1985: pl. 8, fig. 5, pl. 10, figs 2–4; An, 1987: 187, pl. 7, figs 12, 24, 30; Gao, 1991: 140–141, pl. 6, fig. 20; Ding *et al.* in Wang, 1993: 205–206, pl. 14, figs 13–15; Zhao *et al.*, 2000: 224, pl. 14, figs 1, 9.

Scolopodus rex Lindström.–Zhang, 1998c: 90–91, pl. 17, figs 5–8.

Scolopodus longibasis Ni *in* Ni & Li, 1987: 439, pl. 57, figs 47–50.

Material. Six specimens from three samples (see Tables 1–2).

Remarks. *Scolopodus rex oistodiformis* was first introduced into the literature as a *nomen nudum* by illustration only (An & Ding, 1982). Subsequently, An & Ding (1985) formally defined this subspecies as consisting of a bimembrate apparatus including an asymmetrical geniculate element and a symmetrical, short-based multicostate scolopodiform element. They indicated that the geniculate element was

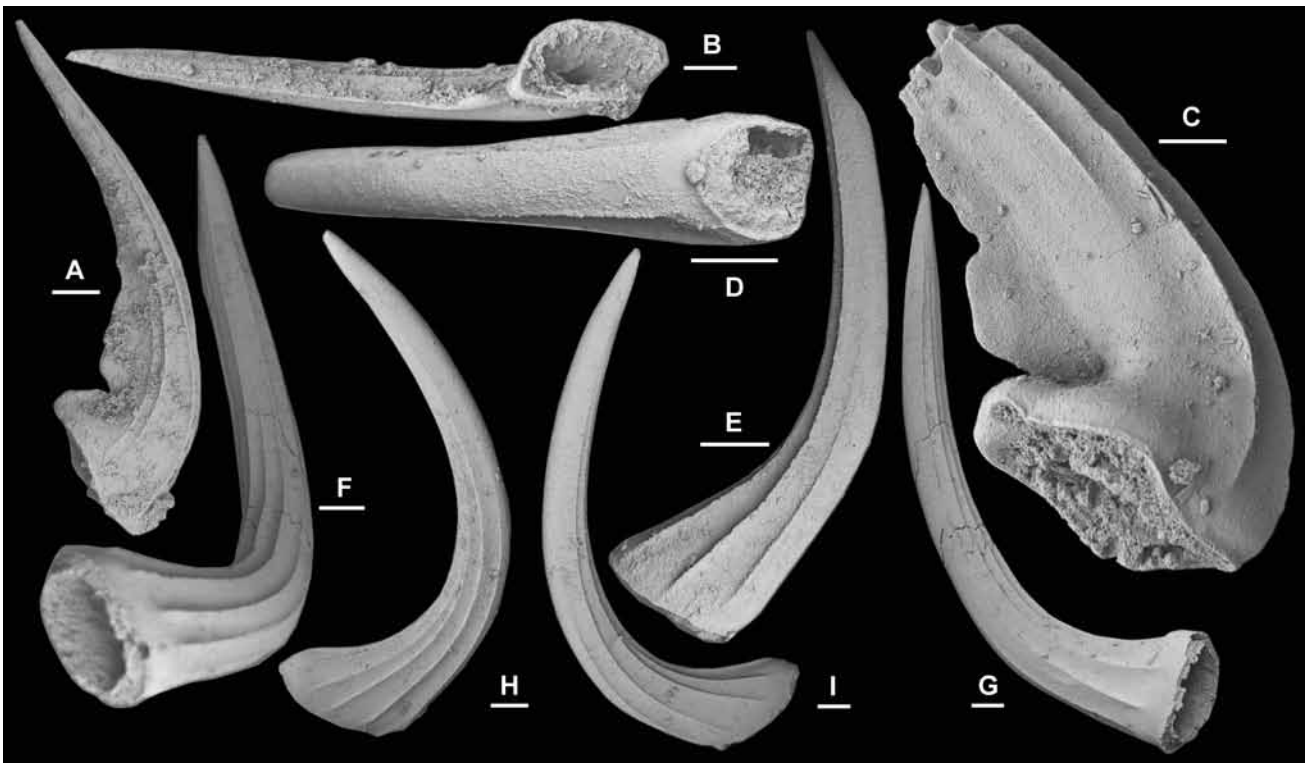

Figure 27. *Scolopodus*? *oistodiformis* An & Ding, 1985. A–C, M element; ***A–B***, NIGP 153104, Nj294, posterior view (IY148-020), B, basal view (IY148-019); ***C***, NIGP 153105, Nj295, posterior view (IY149-008). ***D–E***, Sa element, NIGP 153106, Nj294, D, anterior view (IY148-023), E, lateral view (IY148-031); ***F–G***, Sb element, NIGP 153107, Nj294, F, basal-inner lateral view (IY148-022), G, outer lateral view (IY148-021). ***H–I***, Sc element, NIGP 153108, Nj294, inner lateral view (IY148-030), I, outer lateral view (IY148-031). Scale bars 100 μm.

closely comparable with the form species *S. rex* var. *paltodiformis* Lindström, 1955a. Zhang (1998c) considered *S. rex oistodiformis* as a junior synonym of *S. rex* and included geniculate M, short-based scolopodiform P and long-based scolopodiform S elements with the S elements forming a symmetry transition series. In the recent revision of *S. striatus*, Tolmacheva (2006) regarded *S. rex* as a junior synonym of *S. striatus*, but rejected the specimens figured as *S. rex* by Zhang (1998c) from her revised multielement species, *S. striatus*. Therefore *S.*? *oistodiformis* is considered herein as representing a separate species as defined by Zhang (1998c). *S. longibasis* Ni in Ni & Li, 1987 is identical with the long-based S elements of this species from the Guniutan Formation of South China (Zhang, 1998c) and from the Dawangou Formation of the Tarim Basin (Fig. 27D–I). Therefore it is considered to be a junior synonym of *S.*? *oistodiformis*. In the Dawangou samples, *S.*? *oistodiformis* and *S. striatus* co-occur, and the short-based P and long-based S elements of *S.*? *oistodiformis* are difficult to differentiate from those of *S. striatus*. In particular, some of the long-based specimens referred to as the Sd element of *S. striatus* might likely belong to the S elements of *S.*? *oistodiformis*, which typically have a lesser number of costae, a longer base and a cusp varying from proclined to suberect (Fig. 27D–I).

Scolopodus? oistodiformis shows close resemblance to *S. subrex* Ji & Barnes, 1994, particularly the M elements which are nearly identical (see Ji & Barnes, 1994, pl. 19, figs 9–14), but *S. subrex* has S elements with a relatively shorter base (Ji & Barnes, 1994, pl. 19, figs 1–8), and the Pa element is rather distinctive with a very short base and a prominent notch on the basal margin (Ji & Barnes, 1994, pl. 19, fig. 15).

Scolopodus striatus Pander, 1856

Fig. 26A–W

?Scolopodus costatus Pander, 1856: 26, pl. 2, fig. 7a–d, pl. A, fig. 5e.

Scolopodus semicostatus Pander, 1856: 26, pl. 2, fig. 4a–b.

Scolopodus aequilateralis Pander, 1856: 26, pl. 2, fig. 5a–c, pl. A, fig. 5c.

Scolopodus quadratus Pander, 1856: 26, pl. 2, fig. 6a–d, pl. A, fig. 5d; Fåhraeus, 1982a: 21, pl. 2, figs 1–14, pl. 3, figs 1–8, 15 (*cum syn.*); Rasmussen, 2001: 131, pl. 17, fig. 12; Zhen *et al*., 2003b: 212, fig. 27A–O (*cum syn.*); Zhen *et al*., 2004a: 58–59, pl. 5, figs 15–21 (*cum syn.*).

Scolopodus striatus Pander, 1856: 26, pl. 2, figs 8a–d, pl. A, fig. 5f; Tolmacheva, 2006: 255–259, figs 5A–B, D, ?E, F, 6–8 (*cum syn.*); Viira, 2011: fig. 11E.

Scolopodus rex Lindström, 1955a: 595–596, pl. 3, fig. 32; van Wamel, 1974: 94, pl. 5, fig. 18; Landing, 1976: 640, pl. 4, fig. 14; Löfgren, 1978: 109–110, pl. 1, 38–39; An, 1981: pl. 3, fig. 10; An & Ding, 1982: pl. 1, fig. 22; Zeng *et al*., 1983: pl. 12, fig. 35; An *et al*., 1985: pl. 10, figs 8, 13; An, 1987: 187, pl. 7, figs 1–4, 6–8, pl. 9, fig. 6; Ding, 1987: pl. 5, fig. 20; Ni & Li, 1987: 440, pl. 57, figs 23, 32–34; Stouge & Bagnoli, 1990: 25, pl. 9, figs 1–6; Duan, 1990: pl. 2, fig. 6; Gao, 1991: 140, pl. 7, fig. 1; Ding *et al*. in Wang, 1993: 205, pl. 14, figs 21–26; Löfgren, 1994: fig. 7.1; Chen & Bergström, 1995: pl. 7, fig. 7; Wang *et al*., 1996: pl. 2, figs 18–19; Wang & Bergström, 1999a: 342, pl. 2, fig. 14; Zhao *et al*., 2000: 224, pl. 14, figs 2–8.

Scolopodus rex var. *paltodiformis* Lindström, 1955a: 596, pl. 3, figs 33–34.

Paltodus scolopodiformis Sergeeva, 1974: pl. 1, figs 10–11.

Scolopodus multicostatus Ni *in* Ni & Li, 1987: 439, pl. 58, fig. 6.
?Scolopodus praerex Ni *in* Ni & Li, 1987: 440, pl. 57, figs 51–54.

Material. 37 specimens from five samples of the Dawangou Formation (see Table 1).

Remarks. As revised by Tolmacheva (2006), *Scolopodus striatus* consists of a quinquimembrate apparatus including scandodiform M (Fig. 26R–W), acontiodiform P (Fig. 26A–B), subrounded Sa (Fig. 26C–D), and paltodiform and compressed paltodiform S (undifferentiated) elements. Tolmacheva (2006, fig. 2) further differentiated the compressed paltodiform element into short-based and long-based variants, and the paltodiform element into short-based and medium-based variants. Her short-based paltodiform element (Tolmacheva, 2006, fig. 7A) exhibits a multicostate inner lateral face and smooth outer lateral face; such features are identical with those exhibited by what she defined as the M element, although that is more strongly compressed with a shorter, but more expanded base. We regard the scandodiform element and short-based variant of the paltodiform element as representing the M element, whereas the medium-based variant of the paltodiform element is interpreted as occupying the Sc position (Fig. 26J–O). The long-based variant of the compressed paltodiform element is assigned to the Sd position (Fig. 26P–Q), and the short-based variant of the compressed paltodiform element is regarded as the Sb element (Fig. 26E–I).

The M element from the Dawangou section (Fig. 26R–W) is identical with the short-based variant of Tolmacheva's paltodiform element (2006, fig. 7A). Both have an antero-posteriorly compressed cusp and a short base. The convex anterior face is smooth (Fig. 26U) or only faintly costate basally (fig. 24S), and the posterior face is less convex but strongly costate (Fig. 26R, T, V–W). The typical scandodiform element defined by Tolmacheva (2006, fig. 6F–G, fig. 8D–F) has not been recognized in our Tarim material.

Yangtzeplacognathus Zhang, 1998b

Type species. *Polyplacognathus jianyeensis* An & Ding, 1982.

Remarks. Species of *Yangtzeplacognathus* were previously assigned to *Eoplacognathus*, which has a bimembrate apparatus including stelliplanate Pa and pastiniplanate Pb elements. Both elements of *Eoplacognathus* are paired, but not in mirror images. Zhang (1998b) proposed *Yangtzeplacognathus* to accommodate a group of species with unpaired, markedly dissimilar sinistral and dextral Pa (stelliplanate) and Pb (pastiniplanate) elements. She suggested that species of *Yangtzeplacognathus* formed a separate evolutionary lineage that originated in central China, and was the sister group sharing a common ancestor with the *Baltoplacognathus* lineage centred in the Baltoscandic area. Both lineages are postulated to have formed sister groups with the *Eoplacognathus-Polyplacognathus* lineage (Zhang, 1998b, fig. 11).

Löfgren & Zhang (2003) recognized geniculate M, and ramiform S elements (referred to as alate Sa, quadriramate Sb, bipennate ScA, and tertiopedate ScB) for *Yangtzeplacognathus crassus* (Chen & Zhang). However, considering analogies to the other related genera with ramiform-pectiniform apparatus structures, the quadriramate and tertiopedate elements defined by Löfgren & Zhang (2003) are better assigned to the Sd and Sb positions respectively.

The following four species have been included in *Yangtzeplacognathus*: (1) *Y. foliaceus* (Fåhraeus, 1966): holotype representing a sinistral Pb (pastiniplanate) element, recorded from the Vikarby Limestone of south-central Sweden; (2) *Y. protoramosus* (Chen, Chen & Zhang, 1983): recorded from lower part of the Miaopo and Datianba formations in South China (Zhang, 1998c), Tarim (this study), Baltoscandia (Bergström, 1971), and Poland (Dzik, 1978, 1994); 3) *Y. crassus* (Chen & Zhang in Wang, 1993), recorded from South China (Chen & Zhang in Wang, 1993; Zhang, 1997; Bergström & Wang, 1998; Wang & Bergström, 1999a; Zhang, 1998c), Tarim Basin (Wang & Zhou, 1998; this study), Baltoscandia (Stouge & Bagnoli, 1990; Löfgren, 2000; Löfgren & Zhang, 2003), and Poland (Dzik, 1994); and 4) *Y. jianyeensis* (An & Ding, 1982): reported from the Miaopo and Datianba formations in South China (An *et al.*, 1981, 1985; An & Ding, 1982; Chen *et al.*, 1983; Chen & Zhang, 1984a, 1984b; An, 1987; Zhang, 1998b, 1998c), basal Sandbian of Yunnan Province (Dong & Wang, 2006), and from the top Saergan Formation and lower part of the Kanling Formation (lower Sandbian) of the Tarim Basin (this study).

Yangtzeplacognathus crassus (Chen & Zhang in Wang, 1993)

Figs 28A–O, 29A–O

Ambalodus pseudoplanus Viira.–Ni & Li, 1987: pl. 55, fig. 16.
Eoplacognathus pseudoplanus (Viira).–Viira *et al*., 2001: fig. 8a–l, 8q-t; Wang *et al*., 1996: pl. 4, fig. 6.
Amorphognathus variabilis (Sergeeva).–Wang *et al*., 1996: pl. 4, fig. 17.
Eoplacognathus crassus Chen & Zhang in Wang, 1993: 174, pl. 37, figs 12–17; Zhang, 1997: 61–65, figs 2A–B, 3A–L, 4A–L (*cum syn.*); Bergström & Wang, 1998: 91–93; Wang & Zhou, 1998: pl. 1, fig. 2, ?pl. 4, fig. 8; Wang & Bergström, 1999a: 335, pl. 3, fig. 16; Wang & Bergström, 1999b: pl. 2, fig. 14; non Xiong *et al*., 2006: 368, pl. 1a–b = element of *Dzikodus*.
Yangtzeplacognathus crassus (Chen & Zhang).–Zhang, 1998c: 96–97, pl. 20, figs 5–8 (*cum syn.*); Löfgren, 2003: fig. 8A–D; Löfgren & Zhang, 2003: 731–735, figs 6, 12 (*cum syn.*); Viira, 2011: fig. 9B.

Material. 63 specimens from two samples of the Dawangou Formation (see Table 1).

Remarks. Specimens from the Dawangou Formation are identical with those previously documented from the Guniutan Formation in South China (Chen & Zhang in Wang, 1993; Zhang, 1998c) and from Sweden (Löfgren, 2003; Löfgren & Zhang, 2003). Chen & Zhang (in Wang, 1993) recognized two types of pectiniform (Pa = stelliplanate = polyplacognathiform, and Pb = pastiniplanate = ambalodiform) elements, each of which also has morphologically distinctive and consistent sinistral and dextral variants, based on study of the type material of this species from the Guniutan Formation in Tangshan, near Nanjing. Detailed study of the pectiniform elements of this species from China and Baltoscandia led Zhang (1997) to suggest that *Y. crassus* had a restricted age range that was important for international stratigraphic correlation.

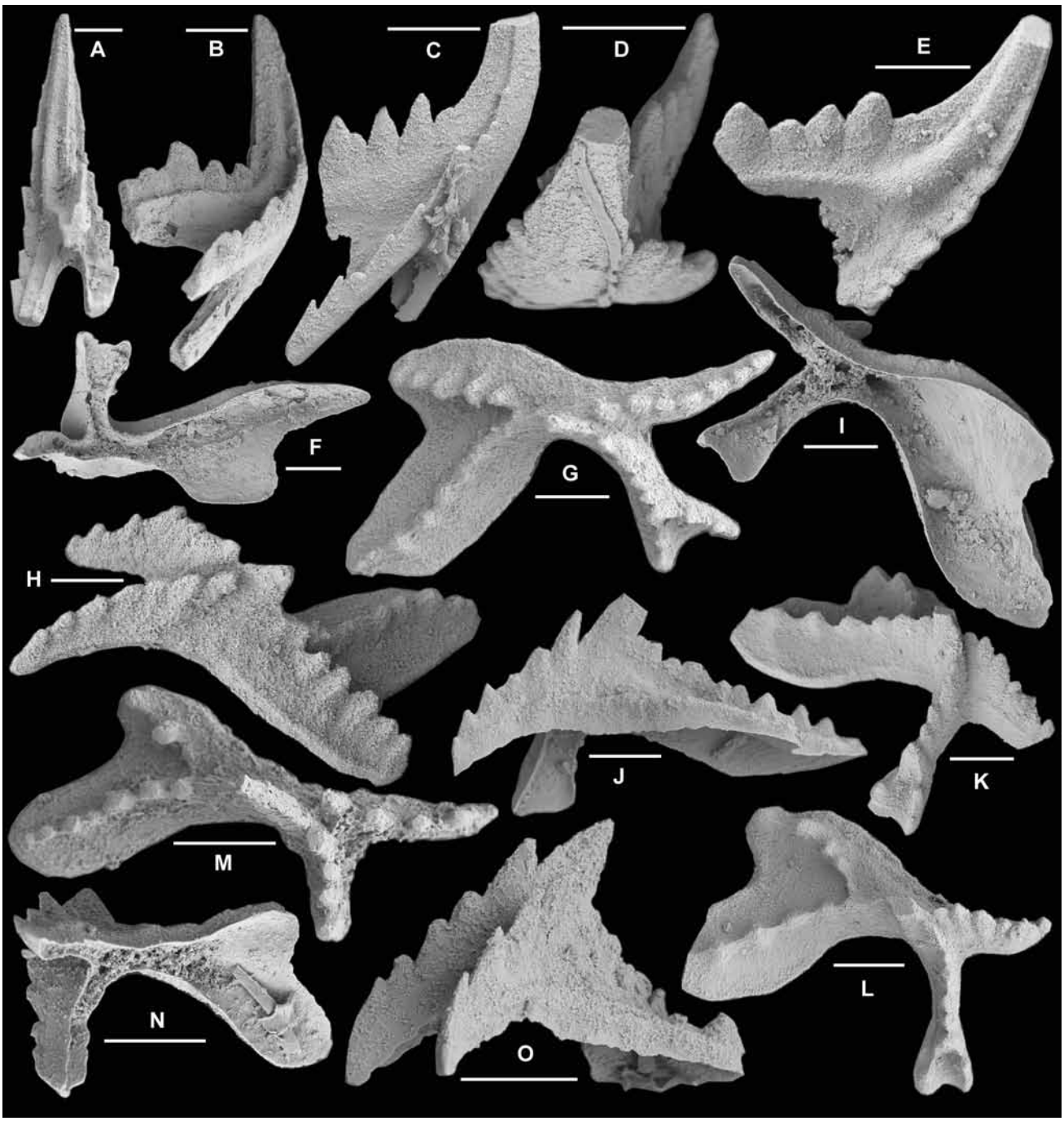

Figure 28. *Yangtzeplacognathus crassus* (Chen & Zhang, 1993). ***A–B***, Sa element, NIGP 153109, A, posterior view (IY146-036), B, lateral view (IY146-038); ***C***, Sa element, NIGP 153110, lateral view (IY146-033). ***D–E***, Sb element, NIGP 153111, D, antero-upper view (IY146-034), E, inner lateral view (IY146-035). ***F***, sinistral Pa element, NIGP 153112, basal view (IY146-003). G–O, dextral Pa element; ***G–H***, NIGP 153113, G, upper view (IY146-001), H, upper lateral view (IY146-002); ***I–J***, NIGP 153114, I, basal view (IY146-016), J, postero-lateral view (IY146-017); ***K–L***, NIGP 153115, K, antero-upper view (IY146-004), L, upper view (IY146-005); ***M***, NIGP 153116, upper view (IY146-020); ***N–O***, NIGP 153117, N, basal view (IY146-021), O, lateral view (IY146-022). All from sample Nj294; scale bars 100 μm.

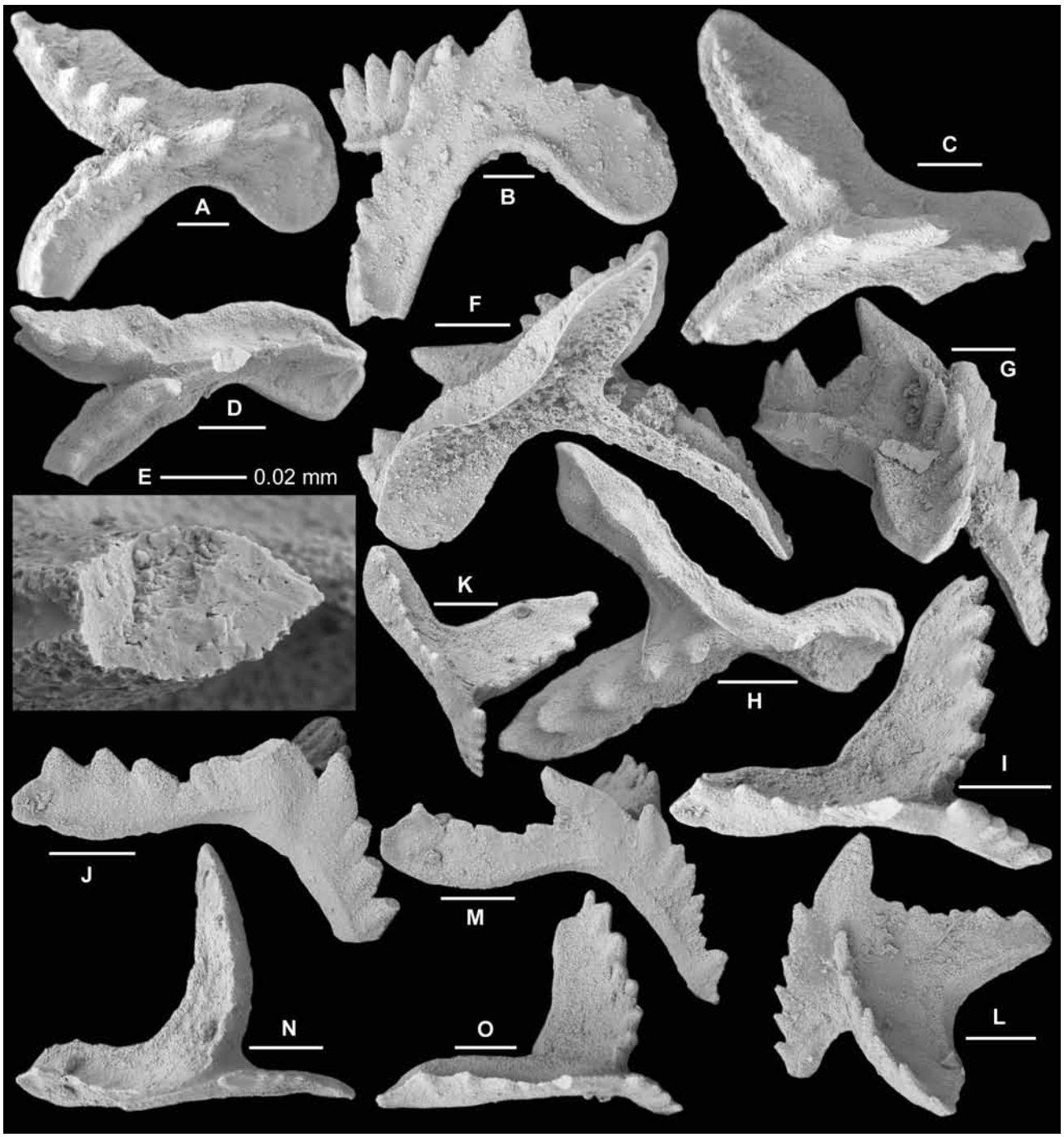

Figure 29. *Yangtzeplacognathus crassus* (Chen & Zhang, 1993). A–H, sinistral Pb element; ***A–B***, NIGP 153118, Nj295, A, upper view (IY149-001), B, lateral view (IY149-002); ***C***, NIGP 153119, Nj295, upper view (IY149-004); ***D–E***, NIGP 153120, Nj294, D, upper view (IY146-013), E, upper view, close up showing cross section of the cusp (IY146-015); ***F–G***, NIGP 153121, Nj294, F, basal view (IY146-010), G, lateral view (IY146-011); ***H***, NIGP 153122, Nj294, upper view (IY146-009). I–O, dextral Pb element; ***I–J***, NIGP 153123, Nj294, I, upper view (IY146-024), J, lateral view (IY146-023); ***K–L***, NIGP 153124, Nj294, K, upper view (IY146-032), L, lateral view (IY146-030); ***M–N***, NIGP 153125, Nj294, M, lateral view (IY146-029), N, upper view (IY146-031); ***O***, NIGP 153126, Nj294, upper view (IY146-025). Scale bars 100 μm, unless otherwise indicated.

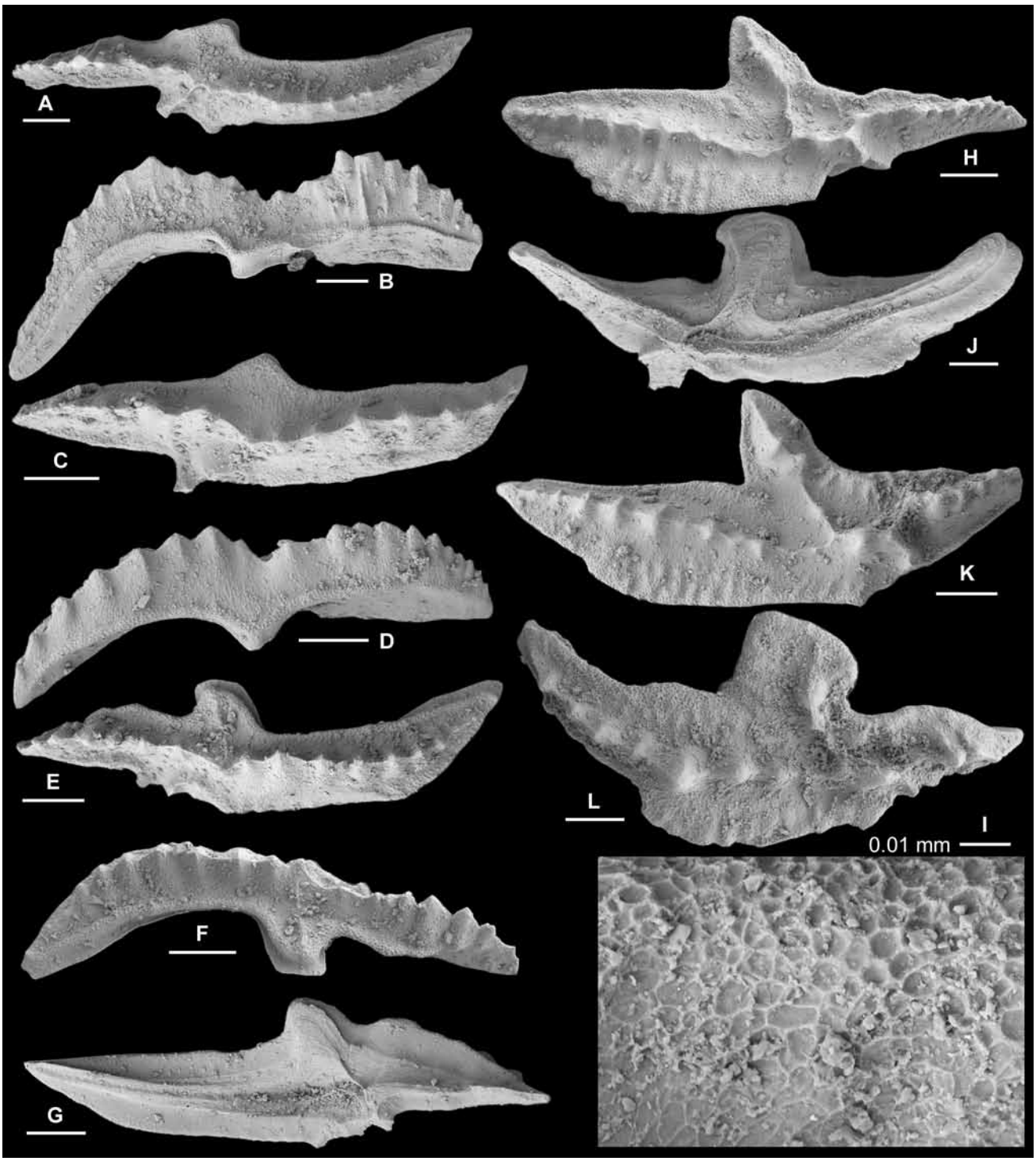

Figure 30. *Yangtzeplacognathus jianyeensis* (An & Ding, 1982). A–G, sinistral Pa element; ***A–B***, NIGP 153127, AFT-X-K13/44, A, upper view (IY165-011), B, lateral view (IY165-010); ***C–D***, NIGP 153128, AFT-X-K13/43, C, upper view (IY164-018), D, lateral view (IY164-016). ***E–F***, NIGP 153129, AFT-X-K13/41, E, upper view (IY164-008), F, upper-lateral view (IY164-007); ***G***, NIGP 153130, AFT-X-K13/44, basal view (IY165-012). H–L, dextral Pa element; ***H–I***, NIGP 153131, AFT-X-K13/44, H, upper view (IY165-003), I, upper view, close up showing fine reticular surface structure (IY166-005); ***J***, NIGP 153132, AFT-X-K13/44, basal view (IY165-006); ***K***, NIGP 153133, AFT-X-K13/43, upper view (IY164-014); ***L***, NIGP 153134, AFT-X-K13/40, upper view (IY164-001). Scale bars 100 µm, unless otherwise indicated.

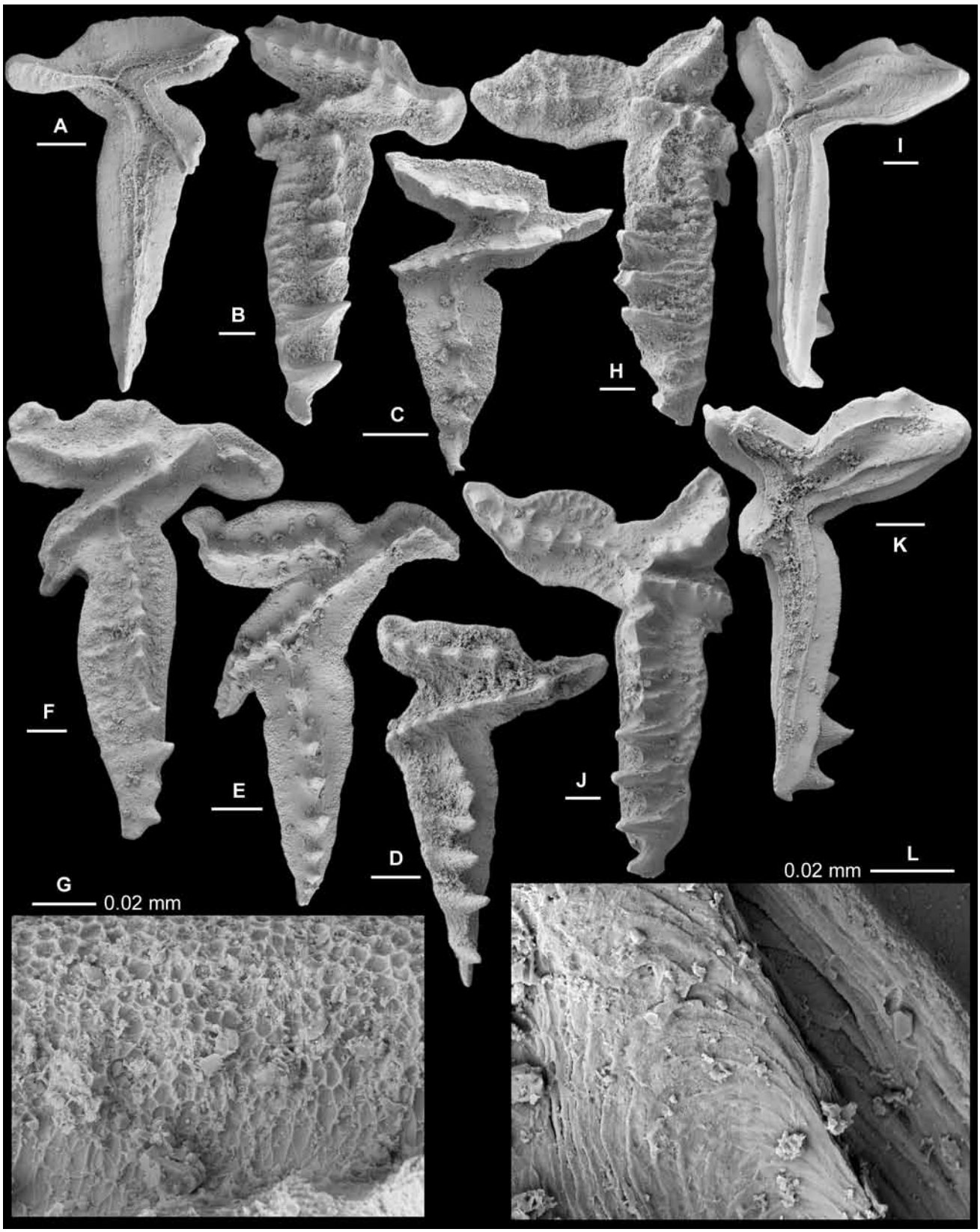

Figure 31. *Yangtzeplacognathus jianyeensis* (An & Ding, 1982). A–G, sinistral Pb element; ***A***, NIGP 153135, AFT-X-K13/44, basal view (IY165-008); ***B***, NIGP 153136, AFT-X-K13/44, upper view (IY165-001); ***C***, NIGP 153137, AFT-X-K13/44, juvenile, upper view (IY165-015); ***D***, NIGP 153138, AFT-X-K13/42, upper view (IY164-009); ***E***, NIGP 153139, AFT-X-K13/41, upper view (IY164-004); ***F–G***, NIGP 153140, AFT-X-K13/40, F, upper view (IY163-038), G, upper view, close up showing fine reticular surface structure (IY163-039). H–L, dextral Pb element; ***H***, NIGP 153141, AFT-X-K13/44, upper view (IY165-002); ***I***, NIGP 153142, AFT-X-K13/44, basal view (IY165-007); ***J***, NIGP 153143, AFT-X-K13/43, upper view (IY164-010); ***K–L***, NIGP 153144, AFT-X-K13/40, K, basal view (IY163-041), L, basal view, close up showing lamellar surface structure (IY163-042). Scale bars 100 μm, unless otherwise indicated.

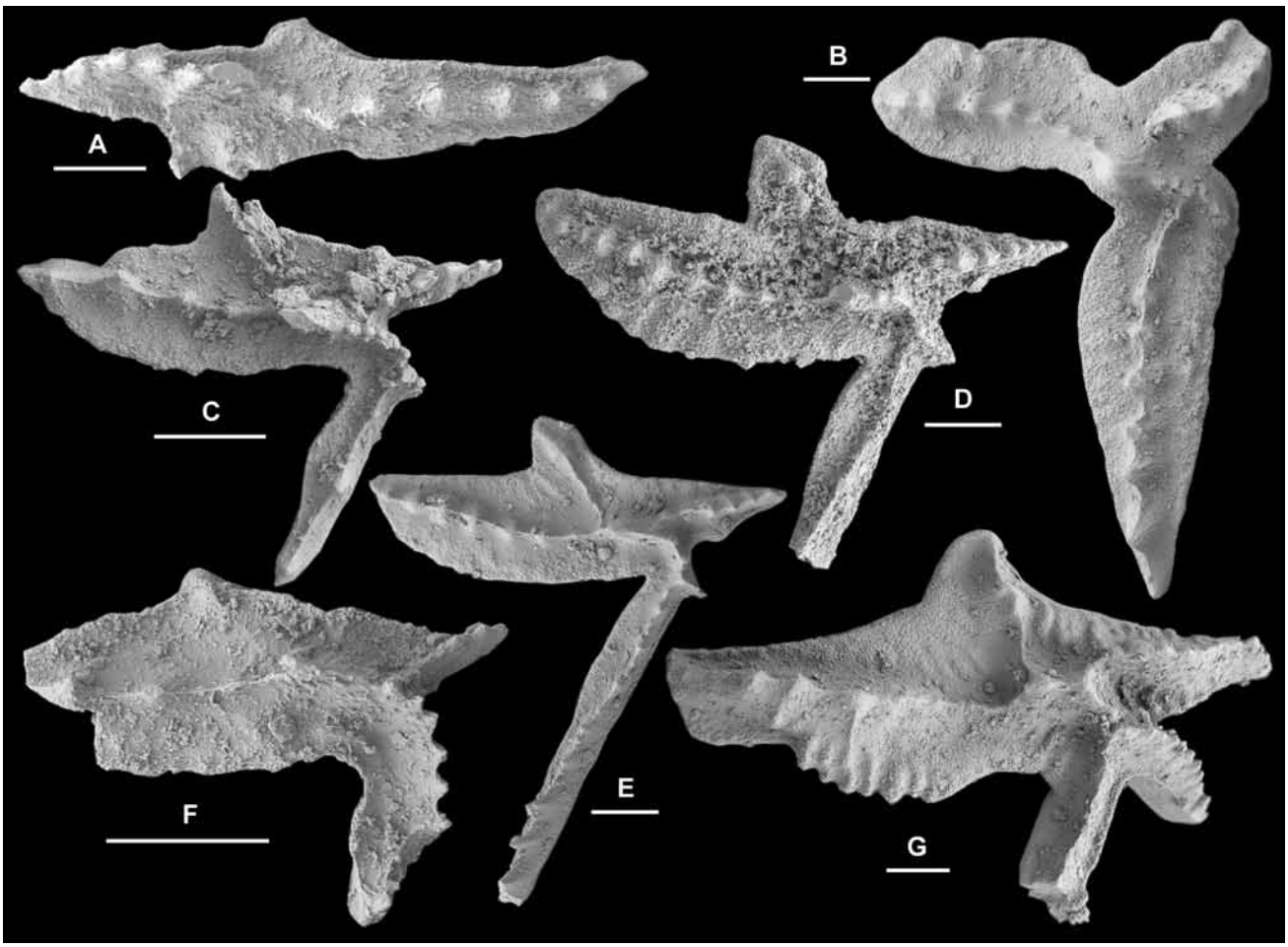

Figure 32. *Yangtzeplacognathus protoramosus* (Chen, Chen & Zhang, 1983). ***A***, sinistral Pa element, NIGP 153145, Nj378, upper view (IY153-018). ***B***, dextral Pb element, NIGP 153146, AFT-X-K13/40, upper view (IY163-040). C–G, dextral Pa element; ***C***, NIGP 153147, Nj378, upper view (IY153-017); ***D***, NIGP 153148, AFT-X-K13/44, upper view (IY165-014); ***E***, NIGP 153149, AFT-X-K13/43, upper view (IY164-023); ***F***, NIGP 153150, Nj378, upper view (IY153-021); ***G***, NIGP 153151, AFT-X-K13/44, upper view (IY165-013). Scale bars 100 µm.

Yangtzeplacognathus jianyeensis (An & Ding, 1982)

Figs 30A–L, 31A–L

Polyplacognathus miaopoensis An *et al*., 1981: pl. 1, fig. 25 (*nomen nudum*); Zeng *et al*., 1983: pl. 12, fig. 26; An *et al.*, 1985: 44–45, *partim* only pl. 18, figs 13–14, non figs 8, 15 = *Y. protoramosus*; Ni & Li, 1987: pl. 55, fig. 6, pl. 59, fig. 36.

Eoplacognathus cf. *reclinatus* (Fåhraeus).–Ni, 1981: pl. 1, fig. 32.

Polyplacognathus jianyeensis An & Ding, 1982: 9, pl. 3, figs 1–7; An & Xu, 1984: pl. 3, figs 18–19; An *et al*., 1985: pl. 18, figs 16–18.

Eoplacognathus ramosus Chen *et al*., 1983: 135, pl. 1, figs 1–4.

Eoplacognathus jianyeensis (An & Ding).–Chen & Zhang, 1984a: 329, pl. 1, figs 5–7, 12–14, 17–18, pl. 2, figs 3–4; Chen & Zhang, 1984b: 127, pl. 1, figs 30–33; An, 1987: 149, pl. 27, figs 1–7, 9–10; Chen & Zhang, 1989: 220, pl. 2, figs 26–29; Ding *et al*. *in* Wang, 1993: 175, pl. 31, figs 1–9; Wang & Zhou, 1998: *partim* only pl. 1, figs ?3, 10, non figs 5, 7–8 = *Y. protoramosus;* Dong & Wang, 2006: 149, pl. 7, figs 2, 5–6.

Eoplacognathus protoramosus Chen, Chen & Zhang.–Xiong *et al*., 2006: pl. 1, fig. 13.

Yangtzeplacognathus jianyeensis (An & Ding).–Zhang, 1998b: 28, fig. 5M–S, fig. 6C, fig. 11C3, fig. 13; Zhang, 1998c: 99, pl. 19, figs 1–4 (*cum syn*.).

Material. 176 specimens from 12 samples (see Tables 1–2).

Remarks. Zhang (1998b) provided detailed description of this species as consisting of sinistral and dextral Pa (stelliplanate) and Pb (pastiniplanate) elements. It is characterized by the Pb element having four processes including a very short, narrow and downwardly-bent anterior process.

The nomenclatural history of this species is particularly confused. An & Ding (1982) erected *Polyplacognathus jianyeensis* as consisting of sinistral and dextral Pb (ambalodiform) and a Pa (polyplacognathiform) elements, with the type material recovered from the Datianba Formation of Tangshan, Jiangsu Province. *Polyplacognathus miaopoensis* was introduced into the literature without diagnosis or description as a *nomen nudum* by illustration of a designated holotype (sinistral Pb element) recovered from the Miaopo Formation of Xingtan, Hubei Province (An *et al*., 1981, pl. 1, fig. 25). Later, An *et al.* (1985, p. 44) provided the diagnosis and description for *Eoplacognathus miaopoensis* based on the Pb element only, indicating that its Pa element was not recovered at the time, but in the illustration they also included a dextral Pa element (An *et al*., 1985, pl. 18, fig. 8), which is actually referable to *Y. protoramosus* (see Zhang, 1998b, p. 25). Thus An *et al.* (1985) not only considered *E. miaopoensis* and

P. jianyeensis to represent separate species, but also to belong to different genera. Chen *et al*. (1983) proposed *Eoplacognathus ramosus* as consisting of sinistral and dextral Pa (polyplacognathiform) and Pb (ambalodiform) elements based on type material from the Datianba Formation of Tangshan, near Nanjing (same type locality as that of *Y. jianyeensis* and *Y. protoramosus*), and regarded *P. miaopoensis* as an invalid senior synonym (*nomen nudum*) of *E. ramosus*. An (1987) revised *Y. jianyeensis* as a species of *Eoplacognathus* by regarding both *P. miaopoensis* and *E. ramosus* as synonymous, but followed the original definition given by An & Ding (1982) without differentiation of the sinistral and dextral Pa elements in the species apparatus as Chen *et al*. (1983) had documented.

Based on a collection of over 200 specimens from central China, Zhang (1998b) revised *Y. crassus* as the type species of the new genus *Yangtzeplacognathus*, consisting of unpaired markedly dissimilar sinistral and dextral Pa (stelliplanate) and Pb (pastiniplanate) elements, and distinguished it from other species of *Yangtzeplacognathus* by having Pb elements with four processes.

Yangtzeplacognathus protoramosus (Chen, Chen & Zhang, 1983)

Fig. 32A–G

Eoplacognathus protoramosus Chen, Chen & Zhang, 1983: 135–136, pl. 1, figs 7–10; An, 1987: 149–150, pl. 27, figs 11–13, 17–18; Ding *et al*. in Wang, 1993: 175, *partim*, only pl. 32, figs 1–6 (*cum syn.*).

Yangtzeplacognathus protoramosus (Chen, Chen & Zhang).–Zhang, 1998c: 25–27, fig. 5E–L, fig. 6B, fig. 12 (*cum syn.*).

Eoplacognathus miaopoensis An *et al*.–An *et al*., 1985: 44–45, *partim* only pl. 18, figs 8, 15.

Eoplacognathus jianyeensis (An & Ding).–Wang & Zhou, 1998: *partim* only pl. 1, figs 5, 7–8.

Eoplacognathus foliaceus (Fåhraeus).–Wang, 2001: 352, pl. 1, fig. 9.

Material. 24 specimens from eight samples (see Tables 1–2).

Remarks. Chen *et al*. (1983) erected *E. protoramosus* as consisting of sinistral and dextral Pa (polyplacognathiform) and Pb (ambalodiform) elements based on material from the Datianba Formation of Tangshan, near Nanjing, and regarded it as the most distinctive species defining their *E. protoramosus* Subzone in the upper part of the *P. serra* Zone. Zhang (1998c) indicated that this species had a stratigraphic range limited to the upper part of *P. serra* Zone in South China, but in the collections from the Dawangou section it has also been reported from the basal part of the Kanling Formation (Sandbian, *anserinus* Zone). The figured dextral Pb element (Fig. 32B) from the base of the Kanling Formation (sample AFT-X-K13/40) is identical with the specimen illustrated by Zhang (1998c, fig. 5J, fig. 12F) representing the late form of this species. In the Dawangou section *Y. protoramosus* is relatively uncommon, but extends well into the *anserinus* Zone. Zhao *et al*. (2006, p. 196) also recorded *Y. protoramosus* in the *anserinus* Zone at Lunnan in the Tarim Basin.

ACKNOWLEDGMENTS. YYZ's study was supported by the CAS/SAFEA International Partnership Program for Creative Research Teams. Part of the material studied in this contribution was collected by ZHW during 1987 with the support of a State Scientific Research Project on the correlation of the Phanerozoic strata in the Tarim Basin. Field work and collecting in the Tarim Basin during 2008 and processing of half of each sample was undertaken with the support of research grants to YDZ (2008ZX05008-001–001). Prof. Zhang Shiben from Petrol China is thanked for his guidance in the field work in 2008. Gary Dargan (formerly of Geological Survey of New South Wales, Londonderry) assisted with acid leaching and residue separation of the remaining half of each sample collected in 2008. Dr Viive Viira from Estonia is thanked for providing the senior author with her valuable monograph and for useful discussions on the type specimens of *Polonodus clivosus*. Scanning electron microscope photographs were prepared in the Electron Microscope Unit of the Australian Museum (Sydney). J. Repetski and R. L. Ethington are thanked for their careful and constructive reviews of the manuscript. IGP publishes with permission of the Executive Director, NSW Office of Resources and Energy.

References

Abaimova, G. P. 1971. New Early Ordovician conodonts from the southeastern part of the Siberian Platform. *Paleontological Journal* 1971(4): 486–493.

Agematsu, S., K. Sashida, S. Salyapongse, and A. Sardsud. 2006. Ordovician conodonts from the Thong Pha Phum area, western Thailand. *Journal of Asian Earth Sciences* 26:49–60. doi:10.1016/j.jseaes.2004.09.009

Agematsu, S., K. Sashida, S. Salyapongse, and A. Sardsud. 2007. Ordovician conodonts from the Satun area, southern peninsular Thailand. *Journal of Paleontology* 81(1):19–37. doi:10.1666/0022-3360(2007)81[19:OCFTSA]2.0.CO;2

Agematsu, S., K. Sashida, and A. B. Ibrahim. 2008a. Biostratigraphy and paleobiogeography of Middle and Late Ordovician conodonts from the Langkawi Islands, northwestern Peninsular Malaysia. *Journal of Paleontology* 82(5):957–973. doi:10.1666/07-058.1

Agematsu, S., K. Sashida, and A. Sardsud. 2008b. Reinterpretation of Early and Middle Ordovician conodonts from the Thong Pha Phum area, western Thailand, in the context of new material from western and northern Thailand. *Paleontological Research* 12(2):181–194. doi:10.2517/1342-8144(2008)12[181:ROEAMO]2.0.CO;2

Albanesi, G. L., and G. Ortega. 2003. Advances on conodont-graptolite biostratigraphy of the Ordovician System of Argentina. In *Aspects of the Ordovician System of Argentina, Serie Correlación Geológica,* ed. F. G. Aceñolaza, vol. 16, pp. 143–165. INSUGEO, Tucumán.

Albanesi, G. L., M. A. Hünicken, and C. R. Barnes. 1998. Bioestratigrafía, biofacies y taxonomia de conodontes de las secuencias ordovícicas del Cerro Porterillo, Precordillera central de San Juan, R. Argentina. *Actas de la Academia Nacional de Ciencias* 12:1–249.

An, T. X. 1981. Recent progress in Cambrian and Ordovician conodont biostratigraphy of China. *Geological Society of America Special Paper* 187:209–226.

An, T. X. 1987. *Early Palaeozoic Conodonts from South China*. Peking University Publishing House, Beijing, 238 pp. (in Chinese with English abstract).

An, T. X., and L. S. Ding. 1982. Preliminary studies and correlations on Ordovician conodonts from the Ningzhen Mountains, China. *Acta Petroleum Sinica* 3(4):1–11 (in Chinese).

An, T. X., and L. S. Ding. 1985. Ordovician conodont biostratigraphy in Hexian, Anhui Province. *Geological Review* 31:1–12 (in Chinese with English abstract).

An, T. X., and B. Z. Xu. 1984. Ordovician System and conodonts of Tungshan and Xianning, Hubei. *Acta Scientiarum Naturalium Universitatis Pekinensis* 1984(5):73–87 (in Chinese with English abstract).

An, T. X., and S. C. Zheng. 1990. *The Conodonts of the Marginal Areas around the Ordos Basin, North China*. Science Press, Beijing. 199 pp. (in Chinese with English abstract).

An, T. X., G. Q. Du, Q. Q. Gao, X. B. Chen, and W. T. Li. 1981. Ordovician conodont biostratigraphy of the Huanghuachang area of Yichang, Hubei. In *Selected Papers of the First Symposium of the Micropalaeontological Society of China*, Micropalaeontological Society of China, ed., Science Press, Beijing, 105–113 (in Chinese).

An, T. X., F. Zhang, W. D. Xiang, Y. Q. Zhang, W. H. Xu, H. J. Zhang, D. B. Jiang, C. S. Yang, L. D. Lin, Z. T. Cui, and X. C. Yang. 1983. *The Conodonts of North China and the Adjacent Regions*. Science Press, Beijing, 223 pp. (in Chinese with English abstract).

An, T. X., G. Q. Du, and Q. Q. Gao. 1985. *Ordovician conodonts from Hubei*. Geological Publishing House, Beijing, 64 pp. (in Chinese with English abstract).

Armstrong, H. A. 1997. Conodonts from the Ordovician Shinnel Formation, southern Uplands, Scotland. *Palaeontology* 40:763–797.

Armstrong, H. A. 2000. Conodont micropalaeontology of mid-Ordovician aged limestone clasts from Lower Old Red Sandstone conglomerates, Lanark and Strathmore basins, Midland Valley, Scotland. *Journal of Micropalaeontology* 19:45–59. doi:10.1144/jm.19.1.45

Bagnoli, G., and S. Stouge. 1997. Lower Ordovician (Billingenian–Kunda) conodont zonation and provinces based on sections from Horns Udde, north Öland, Sweden. *Bollettino della Società Paleontologica Italiana* 35:109–163.

Barnes, C. R., and M. L. S. Poplawski. 1973. Lower and Middle Ordovician conodonts from the Mystic Formation, Québec, Canada. *Journal of Paleontology* 47:760–790.

Bauer, J. A. 1987. Conodonts and conodont biostratigraphy of the McLish and Tulip Creek formations (Middle Ordovician) of south-central Oklahoma. *Oklahoma Geological Survey, Bulletin* 141:1–55.

Bauer, J. A. 1990. Stratigraphy and conodont biostratigraphy of the upper Simpson Group, Arbuckle Mountains, Oklahoma. In *Early to Middle Paleozoic Conodont Biostratigraphy of the Arbuckle Mountains, Southern Oklahoma,* ed. S. M. Ritter. *Oklahoma Geological Survey Guidebook* 27:39–46.

Bauer, J. A. 1994. Conodonts from the Bromide Formation (Middle Ordovician), south-central Oklahoma. *Journal of Paleontology* 68:358–376.

Bauer, J. A. 2010. Conodonts and conodont biostratigraphy of the Joins and Oil Creek Formations, Arbuckle Mountains, South-central Oklahoma. *Oklahoma Geological Survey Bulletin* 150:1–44.

Bednarczyk, W. S. 1998. Ordovician conodont biostratigraphy of the Polish part of the Baltic syneclise. In *Proceedings of the Sixth European Conodont Symposium (ECOS VI)*, ed. H. Szaniawski. *Palaeontologia Polonica* 58:107–121.

Bergström, S. M. 1962. Conodonts from the Ludibundus Limestone (Middle Ordovician) of the Tvären area (S. E. Sweden): *Arkiv för Mineralogi och Geologi* 3(1):1–61.

Bergström, S. M. 1971. Conodont biostratigraphy of the Middle and Upper Ordovician of Europe and Eastern North America. *Geological Society of America Memoir* 127:83–157.

Bergström, S. M. 1983. Biogeography, evolutionary relationships, and biostratigraphic significance of Ordovician platform conodonts. *Fossils and Strata* 15:35–58.

Bergström, S. M. 1988. On Pander's Ordovician conodonts: distribution and of the *Prioniodus elegans* fauna in Baltoscandia. *Senckenbergiana lethaea* 69:217–251.

Bergström, S. M. 1990. Biostratigraphic and biogeographic significance of Middle and Upper Ordovician conodonts in the Girvan succession, south-west Scotland. *Courier Forschungsinstitut Senckenberg* 118:1–43.

Bergström, S. M. 2007. Middle and Upper Ordovician conodonts from the Fågelsång GSSP, Scania, southern Sweden. *GFF* 129:77–82. doi:10.1080/11035890701292077

Bergström, S. M., and Z. H. Wang. 1998. Biostratigraphic significance of the Ordovician conodont *Eoplacognathus crassus* Chen & Zhang, 1993. *GFF* 120:91–93. doi:10.1080/11035899801201091

Bergström, S. M., J. Riva, and M. Kay. 1974. Significance of conodonts, graptolites, and shelly faunas from the Ordovician of Western and North-central Newfoundland. *Canadian Journal of Earth Sciences* 11:1625–1660. doi:10.1139/e74-163

Bergström, S. M., S. C. Finney, X. Chen, and Z. H. Wang. 1999. The Dawangou section, Tarim Basin (Xinjiang Autonomous Region), China: potential as global stratotype for the base of the *Nemagraptus gracilis* Biozone and the base of the global Upper Ordovician Series. *Acta universitatis Carolinae—Geologica* 43(1/2):69–71.

Bergström, S. M., S. C. Finney, X. Chen, C. Pålsson, Z. H. Wang, and Y. Grahn. 2000. A proposed global boundary stratotype for the base of the Upper Series of the Ordovician System: The Fågelsång section, Scania, southern Sweden. *Episodes* 23(3):102–109.

Bergström, S. M., W. D. Huff, M. R. Saltzman, D. R. Kolata, and S. A. Leslie. 2004. The greatest volcanic ash falls in the Phanerozoic: trans-Atlantic relations of the Ordovician Millbrig and Kinnekulle K-bentonites. *The Sedimentary Record* December: 4–8.

Bischoff, G., and D. Sannemann. 1958. Unterdevonische Conodonten aus dem Frankenwald. *Notizblatt Hessiches Landesamt Bodenforschung* 86:87–110.

Branson, E. B., and M. G. Mehl. 1933. Conodont studies. *University of Missouri Studies* 8:1–349.

Bradshaw, L. E. 1969. Conodonts from the Fort Peña Formation (Middle Ordovician), Marathon Basin, Texas. *Journal of Paleontology* 42:1137–1168.

Burrett, C., B. Stait, and J. Laurie. 1983. Trilobites and microfossils from the Middle Ordovician of Surprise Bay, southern Tasmania, Australia. *Association of Australasian Palaeontologists, Memoir* 1:177–193.

Cai, C. F., K. K. Li, M. Anlai, C. M. Zhang, Z. M. Xu, R. H. Worden, G. H. Wu, B. S. Zhang, and L. X. Chen. 2009. Distinguishing Cambrian from Upper Ordovician source rocks: evidence from sulfur isotopes and biomarkers in the Tarim Basin. *Organic Geochemistry* 40:755–768. doi:10.1016/j.orggeochem.2009.04.008

Chen, M. J., and J. H. Zhang. 1984a. On two evolutionary continuums of conodonts in the Middle Ordovician. *Journal of Nanjing University (Natural Science)* 1984–2:327–334 (in Chinese with English abstract).

Chen, M. J., and J. H. Zhang. 1984b. Middle Ordovician conodonts from Tangshan, Nanjing. *Acta Micropalaeontologica Sinica* 1:120–137 (in Chinese with English abstract).

Chen, M. J., and J. H. Zhang. 1989. Ordovician conodonts from the Shitai region, Anhui. *Acta Micropalaeontologica Sinica* 6(3):213–228 (in Chinese with English abstract).

Chen, M. J., Y. T. Chen, and J. H. Zhang. 1983. Ordovician conodont sequence in Nanjing Hills. *Journal of Nanjing University, Natural Sciences* 1983(1):129–139 (in Chinese with English abstract).

Chen, X., and S. M. Bergström, eds. 1995. The base of the *austrodentatus* Zone as a level for global subdivision of the Ordovician System. *Palaeoworld* 5:1–117.

Chen, X., J. Y. Rong, X. F. Wang, Z. H. Wang, Y. D. Zhang, and R. B. Zhan. 1995. Correlation of the Ordovician rocks of China: charts and explanatory notes. *International Union of Geological Sciences, Publication* 31:1–104.

Chen, X., Y. D. Zhang, S. M. Bergström, and H. F. Xu. 2006. Upper Darriwilian graptolite and conodont zonation in the global stratotype section of the Darriwilian stage (Ordovician) at Huangnitang, Changshan, Zhejiang, China. *Palaeoworld* 15:150–170.
doi:10.1016/j.palwor.2006.07.001

Chen, X., S. M. Bergström, Y. D. Zhang, D. Goldman, and Q. Chen. 2011. Upper Ordovician (Sandbian–Katian) graptolite and conodont zonation in the Yangtze region, China. *Earth and Environmental Science Transactions of the Royal Society of Edinburgh* 101:1–24.

Chen, X., D. Goldman, S. A. Leslie, and N. A. Williams. 2008. Ordovician Dawangou section, Tarim Basin, western Xinjiang, China and its implication for biogeography. *Geological Society of America Abstracts with Programs* 40(5):85.

Chen, X., Y. D. Zhang, Y. Li, J. X. Fan, P. Tang, Q. Chen, and Y. Y. Zhang, (in press). A correlation of the Ordovician black organic rocks from the Tarim Basin and its peripheral regions. *Science China (Earth Sciences)*.

Clark, D. L., W. C. Sweet, S. M. Bergström, G. Klapper, R. L. Austin, F. H. T. Rhodes, K. J. Müller, W. Ziegler, M. Lindström, J. F. Miller, and A. G. Harris. 1981. Conodonta. In *Treatise on Invertebrate Paleontology, part W, Miscellanea, supplement 2*, ed. R. A. Robison. Geological Society of America, Boulder and University of Kansas, Lawrence, 202pp.

Cooper, B. J. 1976. Multielement conodonts from the St. Clair Limestone (Silurian) of southern Illinois. *Journal of Paleontology* 50(2):205–217.

Cooper, B. J. 1981. Early Ordovician conodonts from the Horn Valley Siltstone, central Australia. *Palaeontology* 24:147–183.

Ding, L. S. 1987. Preliminary probes into Ordovician conodont biostratigraphy from the Kunshan area, Jiangsu, China. In *Symposium on petroleum stratigraphy and palaeontology* (1987), 41–53, 375–380, Geological Publishing House, Beijing (in Chinese with English abstract).

Dong, D. Y., and W. Wang. 2006. *The Cambrian—Triassic Conodont Faunas in Yunnan, China—Correlative Biostratigraphy and the Study of Palaeobiogeographic Province of Conodont*. Yunnan Science and Technology Press, Kunming, 347 pp. (in Chinese with English summary).

Drygant, D. M. 1974a. Simple conodonts from the Silurian and lowermost Devonian. *Paleontologicheskiy Sbornik* 10:64–69.

Drygant, D. M. 1974b. New Middle Ordovician conodonts from North-western Volyn. *Paleontologicheskiy Sbornik* 11:54–58.

Du, P. D., Z. X. Zhao, Z. B. Huang, Z. J. Tan, C. Wang, Z. L. Yang, G. Z. Zhang, and J. N. Xiao. 2005. Discussion on four conodont species of *Histiodella* from Tarim Basin and their stratigraphic implication. *Acta Micropalaeontologica Sinica* 22(4):357–369.

Duan, J. Y. 1990. Ordovician conodonts from northern Jiangsu and indices of their colour alteration. *Acta Micropalaeontologica Sinica* 7(1):19–41 (in Chinese with English abstract).

Dzik, J. 1976. Remarks on the evolution of Ordovician conodonts. *Acta Palaeontologica Polonica* 21:395–455.

Dzik, J. 1978. Conodont biostratigraphy and paleogeographical relations of the Ordovician Mójcza Limestone (Holy Cross Mts., Poland). *Acta Palaeontologica Polonica* 23:51–72.

Dzik, J. 1994. Conodonts of the Mójcza Limestone. *Palaeontologia Polonica* 53:43–128.

Ethington, R. L., and D. L. Clark. 1964. Conodonts from the El Paso Formation (Ordovician) of Texas and Arizona. *Journal of Paleontology* 38:685–704.

Ethington, R. L., and D. L. Clark. 1982. Lower and Middle Ordovician conodonts from the Ibex area, western Millard County, Utah. *Brigham Young University, Geological Studies* 28(2):1–160.

Fåhraeus, L. E. 1966. Lower Viruan (Middle Ordovician) conodonts from the Gullhögen Quarry, Southern Central Sweden. *Sveriges Geologiska Undersökning* C 610:1–40.

Fåhraeus, L. E. 1970. Conodont-based correlations of Lower and Middle Ordovician strata in western Newfoundland. *Geological Society of America Bulletin* 81:2061–2076.
doi:10.1130/0016-7606(1970)81[2061:CCOLAM]2.0.CO;2

Fåhraeus, L. E. 1982a. Recognition and redescription of Pander's (1856) *Scolopodus* (form) species—constituents of multi-element taxa (Conodontophorida, Ordovician). *Geologica et Palaeontologica* 16:19–28.

Fåhraeus, L. E. 1982b. Allopatric speciation and lineage zonation exemplified by the *Pygodus serrus—P. anserinus* transition (Conodontophorida, Ordovician). *Newsletters on Stratigraphy* 11(1):1–7.

Fåhraeus, L. E., and D. R. Hunter. 1981. Paleoecology of selected conodontophorid species from the Cobbs Arm Formation (Middle Ordovician), New World Island, north-central Newfoundland. *Canadian Journal of Earth Sciences* 18:1653–1665.
doi:10.1139/e81-153

Fåhraeus, L. E., and D. R. Hunter. 1985. Simple-cone conodont taxa from the Cobbs Arm Limestone (Middle Ordovician), New World Island, Newfoundland. *Canadian Journal of Earth Sciences* 22:1171–1182.
doi:10.1139/e85-120

Ferretti, A., and E. Serpagli. 1999. Late Ordovician conodont faunas from southern Sardinia, Italy: bistratigraphic and paleogeographic implications. In *Studies on Conodonts—Proceedings of the Seventh European Conodont Symposium, Bologna-Modena, 1998*, ed. E. Serpagli. *Bollettino della Società Paleontologica Italiana* 37(2–3):215–236.

Gao, Q. Q. 1991. *Conodonts.* In *Sinian to Permian stratigraphy and Palaeontology of the Tarim Basin II, Keping-Bachu area*. Xinjiang Petroleum Administration Bureau and the Jianghan Petroleum Administration Bureau, ed, Petroleum Industry Press, Beijing, 125–149 (in Chinese with English abstract).

Graves, R. W., and S. Ellison. 1941. Ordovician conodonts of the Marathon Basin, Texas. *University of Missouri, School of Mines and Metallurgy, Bulletin of the Technical Series* 14:1–26.

Hadding, A. R. 1913. Undre dicellograptusskiffern i Skåne jämte några därmed ekvivalenta bildningar. *Lunds Universitets Årsskrift, Ny Följd, Afdelning 2*, 9(15):1–90.

Harris, A. G., S. M. Bergström, R. L. Ethington, and R. J. Ross Jr. 1979. Aspects of Middle and Upper Ordovician conodont biostratigraphy of carbonate facies in Nevada and southeast California and comparison with some Appalachian successions. *Brigham Young University Geology Studies* 26:7–43.

Harris, A. G., J. A. Dumoulin, J. E. Repetski, and C. Carter. 1995. Correlation of Ordovician rocks of Northern Alaska. In *Ordovician Odyssey: short Papers for the Seventh International Symposium on the Ordovician System,* ed. J. D. Cooper, M. L. Droser, and S. C. Finney. Fullerton, Calif., Pacific Section Society for Sedimentary Geology (SEPM), Book 77:21–26.

Harris, R. W. 1962. New conodonts from Joins (Ordovician) Formation of Oklahoma. *Oklahoma Geology Notes* 22:199–211.

Hamar, G. 1964. Conodonts from the lower Middle Ordovician of Ringerike. *Norsk Geologisk Tidsskrift* 44:243–292.

Hamar, G. 1966. Preliminary report on conodonts from the Oslo-Asker and Ringerike districts. *Norsk Geologisk Tidsskrift* 46:27–83.

He, D. F., X. Y. Zhou, C. J. Zhang, and X. F. Yang. 2007. Tectonic types and evolution of Ordovician proto-type basins in the Tarim region. *Chinese Science Bulletin* 52 (supp. 1):164–177.
doi:10.1007/s11434-007-6010-z

Henningsmoen, G. 1948. The Tretaspis Series of the Kullatorp core. In *Deep boring through Ordovician and Silurian strata at Kinnekulle, Vestergötland*, ed. B. Waern, P. Thorslund, and G. Henningsmoen. *Bulletin of the Geological Institution of the University of Uppsala* 32:374–432.

Heredia, S., S. Peralta, and M. Beresi. 2005. Darriwilian conodont biostratigraphy of the Las Chacritas Formation, Central Precordillera (San Juan Province, Argentina). *Geologica Acta* 3(4):385–394.

Hints, O., and J. Nõlvak. 1999. Proposal for the lower boundary-stratotype of the Keila Regional Stage (Upper Ordovician). *Proceedings of the Estonian Academy of Sciences, Geology* 48:158–169.

Huang, B. C., R. X. Zhu, Y. Otofuji, and Z. Y. Yang. 2000. The Early Paleozoic paleogeography of the North China block and the other major blocks of China. *Chinese Science Bulletin* 45(12):1057–1065.
doi:10.1007/BF02887174

Huff, W. D., S. M. Bergström, and D. R. Kolata. 1992. Gigantic Ordovician volcanic ash falls in North America and Europe: biological, tectonomagmatic, and event-stratigraphic significance. *Geology* 20:875–878.
doi:10.1130/0091-7613(1992)020<0875:GOVAFI>2.3.CO;2

Ji, Z. L., and C. R. Barnes. 1994. Lower Ordovician conodonts of the St. George Group, Port au Port Peninsula, western Newfoundland, Canada. *Palaeontographica Canadiana* 11:1–149.

Johnston, D. I., and C. R. Barnes. 2000. Early and Middle Ordovician (Arenig) conodonts from St. Pauls Inlet and Martin Point, Cow Head Group, western Newfoundland, Canada. 2. Systematic paleontology. *Geologica et Palaeontologica* 34:11–87.

Kennedy, D. J., C. R. Barnes, and T. T. Uyeno. 1979. A Middle Ordovician conodont faunule from the Tetagouche Group, Camel Back Mountain, New Brunswick. *Canadian Journal of Earth Sciences* 16:540–551.
doi:10.1139/e79-049

Lamont, A., and M. Lindström. 1957. Arenigian and Llandeilian cherts identified in the Southern Uplands of Scotland by means of conodonts, etc. *Transactions of the Edinburgh Geological Society* 17:60–70.

Landing, E. 1976. Early Ordovician (Arenigian) conodont and graptolite biostratigraphy of the Taconic allochthon, eastern New York. *Journal of Paleontology* 50:614–646.

Lee, H. Y. 1975. Conodonten aus dem unteren und mittleren Ordovizium von Nordkorea. *Palaeontographica Abteilung A* 150:161–186.

Lehnert, O. 1995. Ordovizische Conodonten aus der Präkordillere Westargentiniens: Ihre Bedeutung für Stratigraphie und Paläogeographie. *Erlanger Geologische Abhandlungen* 125:1–193.

Lehnert, O., S. M. Bergström, M. Keller, and O. Bordonaro. 1999. Ordovician (Darriwilian-Caradocian) conodonts from the San Rafael Region, west-central Argentina: biostratigraphic, paleoecologic, and paleogeographic implications. In *Studies on Conodonts—Proceedings of the Seventh European Conodont Symposium, Bologna-Modena, 1998,* ed. E. Serpagli, *Bollettino della Società Paleontologica Italiana* 37(2–3):199–214.

Leslie, S. A. 2000. Mohawkian (Upper Ordovician) conodonts of eastern North America and Baltoscandia. *Journal of Paleontology* 74(6):1122–1147.
doi:10.1666/0022-3360(2000)074<1122:MUOCOE>2.0.CO;2

Leslie, S. A., and O. Lehnert. 2005. Middle Ordovician (Chazyan) sea-level changes and the evolution of the Ordovician conodont genus *Cahabagnathus* Bergström, 1983. *Journal of Paleontology* 79(6):1131–1142.
doi:10.1666/0022-3360(2005)079[1131:MOCSCA]2.0.CO;2

Li, Z. X., and C. M. Powell. 2001. An outline of the palaeogeographic evolution of the Australasian region since the beginning of the Neoproterozoic. *Earth-Science Reviews* 53:237–277.
doi:10.1016/S0012-8252(00)00021-0

Lindström, M. 1955a. Conodonts from the lowermost Ordovician strata of south-central Sweden. *Geologiska Föreningens i Stockholm Förhandlingar* 76:517–604.

Lindström, M. 1955b. The conodonts described by A. R. Hadding, 1913. *Journal of Paleontology* 29(1):105–111.

Lindström, M. 1964. *Conodonts*. Amsterdam: Elsevier Publishing Company.

Lindström, M. 1971. Lower Ordovician conodonts of Europe. In *Symposium on Conodont Biostratigraphy,* ed. W. C. Sweet, and S. M. Bergström. *Geological Society of America, Memoir* 127:21–61.

Löfgren, A. 1978. Arenigian and Llanvirnian conodonts from Jämtland, northern Sweden. *Fossils and Strata* 13:1–129.

Löfgren, A. 1990. Non-platform elements of the Ordovician conodont genus *Polonodus*. *Paläontologische Zeitschrift* 64(3/4):245–259.

Löfgren, A. 1994. Arenig (Lower Ordovician) conodonts and biozonation in the eastern Siljan District, central Sweden. *Journal of Paleontology* 68:1350–1368.

Löfgren, A. 1998. Apparatus structure of the Ordovician conodont *Decoriconus peselephantis* (Lindström 1955). *Paläontologische Zeitschrift* 72(3/4):337–350.

Löfgren, A. 2000. Early to early Middle Ordovician conodont biostratigraphy of the Gillberga quarry, northern Öland, Sweden. *GFF* 122:321–338.
doi:10.1080/11035890001224321

Löfgren, A. 2003. Conodont faunas with *Lenodus variabilis* in the upper Arenigian to lower Llanvirnian of Sweden. *Acta Palaeontologica Polonica* 48:417–436.

Löfgren, A. 2004. The conodont fauna in the Middle Ordovician *Eoplacognathus pseudoplanus* Zone of Baltoscandia. *Geological Magazine* 141(4):505–524.
doi:10.1017/S0016756804009227

Löfgren, A. 2006. An *Oistodus venustus*-like conodont species from the Middle Ordovician of Baltoscandia. *Paläontologische Zeitschrift* 80(1):12–21.

Löfgren, A., and T. J. Tolmacheva. 2003. Taxonomy and distribution of the Ordovician conodont *Drepanodus arcuatus* Pander, 1856, and related species. *Paläontologische Zeitschrift,* 77(1):203–221.

Löfgren, A., and J. H. Zhang. 2003. Element association and morphology in some Middle Ordovician platform-equipped conodonts. *Journal of Paleontology* 77(4):721–737.
doi:10.1666/0022-3360(2003)077<0721:EAAMIS>2.0.CO;2

McCracken, A. D. 1989. *Protopanderodus* (Conodontata) from the Ordovician Road River Group, northern Yukon Territory, and the evolution of the genus. *Geological Survey of Canada Bulletin* 388:1–39.

McCracken, A. D. 1991. Middle Ordovician conodonts from the Cordilleran Road River Group, northern Yukon Territory, Canada. In *Ordovician to Triassic Conodont Paleontology of the Canadian Cordillera,* ed. M. J. Orchard, and A. D. McCracken. *Geological Survey of Canada, Bulletin* 417:41–63.

McHargue, T. R. 1982. Ontogeny, phylogeny, and apparatus reconstruction of the conodont genus *Histiodella*, Joins Fm., Arbuckle Mountains, Oklahoma. *Journal of Paleontology* 56:1410–1433.

Mellgren, J., and M. E. Eriksson. 2006. A model of reconstruction for the oral apparatus of the Ordovician conodont genus *Protopanderodus* Lindström, 1971. *Transactions of the Royal Society of Edinburgh: Earth Sciences* 97:97–112.
doi:10.1017/S0263593300001425

Molnar, P., and P. Tapponnier. 1975. Cenozoic tectonics of Asia: effects of a continental collision. *Science* 189:419–426.
doi:10.1126/science.189.4201.419

Moskalenko, T. A. 1973. Conodonts of the Middle and Upper Ordovician of the Siberian Platform. *Akademiy Nauk SSSR, Sibirskoe Otdelinie, Trudy Instituta Geologii i Geofiziki* 137:1–143.

Ni, S. Z. 1981. Discussion on some problems of Ordovician stratigraphy by means of conodonts in eastern part of Yangtze Gorges Region. In *Selected papers on the 1st Convention of Micropalaeontological Society of China*. Micropalaeontological Society of China, ed., Science Press, Beijing, 127–134 (in Chinese).

Ni, S. Z., and Z. H. Li. 1987. Conodonts. In *Biostratigraphy of the Yangtze Gorge area 2:Early Palaeozoic Era*, ed. X. F. Wang, S. Z. Ni, Q. L. Zeng, G. H. Xu, T. M. Zhou, Z. H. Li, L. W. Xiang, and C. G. Lai, Geological Publishing House, Beijing, p. 386–447, 549–555, 619–632 (in Chinese with English abstract).

Nicoll, R. S. 1980. Middle Ordovician conodonts from the Pittman Formation, Canberra, ACT. *BMR Journal of Australian Geology & Geophysics* 5:150–153.

Nicoll, R. S. 1990. The genus *Cordylodus* and a latest Cambrian-earliest Ordovician conodont biostratigraphy. *BMR Journal of Australian Geology & Geophysics* 11:529–558.

Nicoll, R. S. 1992. Analysis of conodont apparatus organisation and the genus *Jumudontus* (Conodonta), a coniform-pectiniform apparatus structure from the Early Ordovician. *BMR Journal of Australian Geology & Geophysics* 13:213–228.

Norford, B. S., D. E. Jackson, and G. S. Nowlan. 2002. Ordovician stratigraphy and faunas of the Glenogle Formation, southeastern British Columbia. *Geological Survey of Canada, Bulletin* 569:1–77.

Nowlan, G. S. 1981. Some Ordovician conodont faunules from the Miramichi Anticlinorium, New Brunswick. *Geological Survey of Canada, Bulletin* 345:1–35.

Nowlan, G. S. 1983. Biostratigraphic, paleogeographic, and tectonic implications of Late Ordovician conodonts from the Grog Brook Group, northwestern New Brunswick. *Canadian Journal of Earth Sciences* 20:651–671.
doi:10.1139/e83-060

Nowlan, G. S., and J. G. Thurlow. 1984. Middle Ordovician conodonts from the Buchans Group, central Newfoundland, and their significance for regional stratigraphy of the Central Volcanic Belt. *Canadian Journal of Earth Sciences* 21:284–296.
doi:10.1139/e84-031

Orchard, M. J. 1980. Upper Ordovician conodonts from England and Wales. *Geologica et Palaeontologica* 14:9–44.

Ortega, G., G. L. Albanesi, and S. E. Frigerio. 2007. Graptolite-conodont biostratigraphy and biofacies of the Middle Ordovician Cerro Viejo succession, San Juan Precordillera, Argentina. *Palaeogeography, Palaeoclimatology, Palaeoecology* 245:245–263.
doi:10.1016/j.palaeo.2006.02.023

Ortega, G., G. L. Albanesi, A. L. Banchig, and G. L. Peralta. 2008. High resolution conodont-graptolite biostratigraphy in the Middle-Upper Ordovician of the Sierra de La Invernada Formation (Central Precordillera, Argentina). *Geologica Acta* 6(2):161–180.

Ottone, E. G., G. L. Albanesi, G. Ortega, and G. D. Holfeltz. 1999. Palynomorphs, conodonts and associated graptolites from the Ordovician Los Azules Formation, Central Precordillera, Argentina. *Micropaleontology* 45(3):225–250.
doi:10.2307/1486135

Pan, Y. S., W. M. Zhou, R. H. Xu, D. A. Wang, Y. Q. Zhang, Y. W. Xie, T. E. Chen, and H. Luo. 1996. Geological characteristics and evolution of the Kunlun Montains region during the Early Paleozoic. *Science in China (Series D)* 39(4):337–347.

Pander, C. H. 1856. *Monographie der fossilen Fische des Silurischen Systems der Russisch-Baltischen Gouvernements*. 91 p., Akademie der Wissenschaften, St. Petersburg.

Percival, I. G., E. J. Morgan, and M. M. Scott. 1999. Ordovician stratigraphy of the northern Molong Volcanic Belt: new facts and figures. *Geological Survey of New South Wales, Quarterly Notes* 108:8–27.

Percival, I. G., and Y. Y. Zhen. 2007. Darriwilian conodonts of Eastern Australia: biostratigraphy and biogeographic distribution. In *Proceedings of the Tenth International Symposium on the Ordovician System, The Third International Symposium on the Silurian System, and IGCP 503 Annual Meeting, June, 2007, Nanjing*, ed. J. Li, J.-X. Fan and I. Percival. *Acta Palaeontologica Sinica* 46 (Supplement), pp. 387–392.

Pickett, J. W., and I. G. Percival. 2001. Ordovician faunas and biostratigraphy in the Gunningbland area, central New South Wales. *Alcheringa* 25:9–52.
doi:10.1080/03115510108619212

Podhalańska, T. 1979. Middle Ordovician biozones in the Łeba Elevation, NW Poland. *Bulletin de l'Académie Polonaise des Sciences. Série des Sciences de la Terre* 26(3–4):221–227.

Pohler, S. M. L. 1994. Conodont biofacies of Lower to lower Middle Ordovician megaconglomerates, Cow Head Group, Western Newfoundland. *Geological Survey of Canada, Bulletin* 459:1–71.

Pohler, S. M. L., and M. J. Orchard. 1990. Ordovician conodont biostratigraphy, western Canadian Cordillera. *Geological Survey of Canada Paper* 90–15:1–37.

Pyle, L. J., and C. R. Barnes. 2001. Conodonts from the Kechika Formation and Road River Group (Lower to Upper Ordovician) of the Cassiar Terrane, northern British Columbia. *Canadian Journal of Earth Sciences* 38:1378–1401.
doi:10.1139/e01-033

Pyle, L. J., and C. R. Barnes. 2002. *Taxonomy, evolution, and biostratigraphy of conodonts from the Kechika Formation, Skoki Formation, and Road River Group (Upper Cambrian to Lower Silurian), Northeastern British Columbia*. 227pp., NRC Research Press, Ottawa.

Pyle, L. J., and C. R. Barnes. 2003. Conodonts from a platform-to-basin transect, Lower Ordovician to Lower Silurian, northeastern British Columbia, Canada. *Journal of Paleontology* 77(1):146–171.
doi:10.1666/0022-3360(2003)077<0146:CFAPTB>2.0.CO;2

Rasmussen, J. A. 1991. Conodont stratigraphy of the Lower Ordovician Huk Formation at Slemmestad, southern Norway. *Norsk Geologisk Tidsskrift* 71:265–288.

Rasmussen, J. A. 2001. Conodont biostratigraphy and taxonomy of the Ordovician shelf margin deposits in the Scandinavian Caledonides. *Fossils and Strata* 48:1–180.

Rhodes, F. H. T. 1953. Some British Lower Palaeozoic conodont faunas. *Philosophical Transactions of the Royal Society of London, Series B, Biological Sciences* 237:261–334.
doi:10.1098/rstb.1953.0005

Sergeeva, S. P. 1963. Conodonts from the Lower Ordovician of the Leningrad region. *Paleontologicheskiy Zhurnal, Akademiya Nauk SSSR* 2:93–108.

Sergeeva, S. P. 1974. Some new conodonts from the Ordovician deposits of Leningrad region. *Paleontologičeskij sbornik* 2:79–84.

Serpagli, E. 1974. Lower Ordovician conodonts from Precordilleran Argentina (Province of San Juan). *Bollettino della Società Paleontologica Italiana* 13:17–98.

Simes, J. E. 1980. Age of the Arthur Marble: conodont evidence from Mount Owen, northwest Nelson. *New Zealand Journal of Geology and Geophysics* 23(4):529–532.

Smith, M. P. 1991. Early Ordovician conodonts of east and north Greenland. *Meddelelser om Grønland, Geoscience* 26:1–81.

Stouge, S. 1984. Conodonts of the Middle Ordovician Table Head Formation, western Newfoundland. *Fossils and Strata* 16:1–145.

Stouge, S., and G. Bagnoli. 1990. Lower Ordovician (Volkhovian-Kundan) conodonts from Hagudden, northern Öland, Sweden. *Palaeontographia Italica* 77:1–54.

Stouge, S., and G. Bagnoli. 1999. The suprageneric classification of some Ordovician prioniodontid conodonts. In *Studies on Conodonts—Proceedings of the Seventh European Conodont Symposium, Bologna-Modena, 1998*, ed. E. Serpagli. *Bollettino della Società Paleontologica Italiana* 37(2–3):145–158.

Sweet, W. C. 1988. *The Conodonta: Morphology, Taxonomy, Paleoecology, and Evolutionary History of a Long-Extinct Animal Phylum*. 212pp. Clarendon Press, Oxford.

Sweet, W. C. 2000. Conodonts and biostratigraphy of Upper Ordovician strata along a shelf to basin transect in central Nevada. *Journal of Paleontology* 74(6):1148–1160.
doi:10.1666/0022-3360(2000)074<1148:CABOUO>2.0.CO;2

Sweet, W. C., and S. M. Bergström. 1962. Conodonts from the Pratt Ferry Formation (Middle Ordovician) of Alabama. *Journal of Paleontology* 36:1214–1252.

Sweet, W. C., R. L. Ethington, and C. R. Barnes. 1971. North American Middle and Upper Ordovician conodont faunas. *Geological Society of America Memoir* 127:163–193.

Tolmacheva, T. J. 2006. Apparatus of the conodont *Scolopodus striatus* Pander, 1856 and a re-evaluation of Pander's species of *Scolopodus*. *Acta Palaeontologica Polonica* 51:247–260.

Trotter, J. A., and B. D. Webby. 1994. Upper Ordovician conodonts from the Malongulli Formation, Cliefden Caves area, central New South Wales. *AGSO Journal of Australian Geology & Geophysics* 15(4):475–499.

van Wamel, W. A. 1974. Conodont biostratigraphy of the Upper Cambrian and Lower Ordovician of north-western Öland, south-eastern Sweden. *Utrecht Micropalaeontological Bulletins* 10:1–125.

Viira, V. 1967. Ordovician conodont succession in the Ohesaare core. *Eesti NSV teaduste Akadeemia Toimetised, Keemia Geoloogia* 16(4):319–329.

Viira, V. 1974. *Konodonty ordovika Pribaltiki* (Ordovician conodonts of the east Baltic). 142 pp., Tallinn ("Valgus").

Viira, V. 2008. Conodont biostratigraphy in the Middle-Upper Ordovician boundary beds of Estonia. *Eastonian Journal of Earth Sciences* 57(1):23–38.
doi:10.3176/earth.2008.1.03

Viira, V. 2011. Lower and Middle Ordovician conodonts from the subsurface of SE Estonia and adjacent Russia. *Estonian Journal of Earth Sciences* 60(1):1–21.
doi:10.3176/earth.2011.1.01

Viira, V., A. Löfgren, S. Mägi, and J. Wickström. 2001. An Early to Middle Ordovician succession of conodont faunas at Mäekalda, northern Estonia. *Geological Magazine* 138(6):699–718.
doi:10.1017/S0016756801005945

Wang, C. Y., ed. 1993. *Conodonts of the Lower Yangtze Valley — an index to biostratigraphy and organic metamorphic maturity*. Science Press, Beijing, 326 pp. (in Chinese with English summary).

Wang, Q. M., T. Nishidai, and M. P. Coward. 1992. The Tarim basin, NW China: formation and aspects of petroleum geology. *Journal of Petroleum Geology* 15(1):5–34.
doi:10.1111/j.1747-5457.1992.tb00863.x

Wang, Q., P. Z. Zhang, J. T. Freymueller, R. Bilham, K. M. Larson, X. Lai, X. Z. You, Z. J. Niu, J. C. Wu, Y. X. Li, J. N. Liu, Z. Q. Yang, and Q. Z. Chen. 2001. Present-day crustal deformation in China constrained by global positioning system measurements. *Science* 294:574–577.
doi:10.1126/science.1063647

Wang, Y. J., J. F. Cheng, and Y. D. Zhang. 2008. New radiolarian genera and species of Heituao Formation (Ordovician) in the Kuruktag Region, Xinjiang. *Acta Palaeontologica Sinica* 47(4):393–404 (in Chinese with English Abstract).

Wang, Z. H. 2001. Ordovician conodonts from Kalpin of Xinjiang and Pingliang of Gansu across the base of Upper Ordovician Series. *Acta Micropalaeontologica Sinica* 18(4):349–363.

Wang, Z. H., and K. Q. Lou. 1984. Late Cambrian and Ordovician conodonts from the marginal areas of the Ordos Platform, China. *Bulletin of Nanjing Institute of Geology and Palaeontology, Academia Sinica* 8:237–304 (in Chinese with English abstract).

Wang, Z. H., and T. R. Zhou. 1998. Ordovician conodonts from western and northeastern Tarim and their significance. *Acta Palaeontologica Sinica* 37(2):173–193.

Wang, Z. H., and S. M. Bergström. 1999a. Conodonts across the base of the Darriwilian Stage in South China. *Acta Micropalaeontologica Sinica* 16(4):325–350 (in Chinese with English abstract).

Wang, Z. H., and S. M. Bergström. 1999b. Conodont-graptolite biostratigraphic relations across the base of the Darriwilian Stage (Middle Ordovician) in the Yangtze Platform and the JCY area in Zhejiang, China. In *Studies on Conodonts—Proceedings of the Seventh European Conodont Symposium, Bologna-Modena, 1998*, ed. E. Serpagli. *Bollettino della Società Paleontologica Italiana* 37(2–3):187–198.

Wang, Z. H., and Y. P. Qi. 2001. Ordovician conodonts from drillings in the Taklimakan desert, Xinjiang, NW China. *Acta Micropalaeontologica Sinica* 18(2):133–148.

Wang, Z. H., S. M. Bergström, and H. R. Lane. 1996. Conodont provinces and biostratigraphy in Ordovician of China. *Acta Palaeontologica Sinica* 35(1):26–59.

Wang, Z. H., Y. P. Qi, and S. M. Bergström. 2007. Ordovician conodonts of the Tarim region, Xinjiang, China: occurrence and use as palaeoenvironment indicators. *Journal of Asian Earth Sciences* 29:832–843.
doi:10.1016/j.jseaes.2006.05.007

Webby, B. D., F. Paris, M. L. Droser, and I. G. Percival, eds. 2004. *The great Ordovician biodiversification event*. Columbia University Press, New York, 484 pp.

Webers, G. F. 1966. The Middle and Upper Ordovician conodont faunas of Minnesota. *Minnesota Geological Survey Special Publication* 4:1–123.

Windley, B. F., M. B. Allen, C. Zhang, Z. Y. Zhao, and G. R. Wang. 1990. Paleozoic accretion and Cenozoic redeformation of the Chinese Tien Shan Range, central Asia. *Geology* 18:128–131.
doi:10.1130/0091-7613(1990)018<0128:PAACRO>2.3.CO;2

Xiong, J. F., T. Wu, and D. S. Ye. 2006. New advances on the study of Middle-Late Ordovician conodonts in Bachu, Xinjiang. *Acta Palaeontologica Sinica* 45(3):359–373 (in Chinese with English abstract).

Yao, Y. G., and K. J. Hsü. 1994. Origin of the Kunlun Mountains by arc-arc and arc-continent collisions. *The Island Arc* 3:75–89.
doi:10.1111/j.1440-1738.1994.tb00096.x

Zeng, Q. L., S. Z. Ni, G. H. Xu, T. M. Zhou, X. F. Wang, Z. H. Li, C. G. Lai, and L. W. Xiang. 1983. Subdivision and correlation on the Ordovician in the eastern Yangtze Gorges, China. *Bulletin of the Yichang Institute of Geology & Mineral Resources, Chinese Academy of Geological Sciences* 6:1–68.

Zhang, J. H. 1997. The Lower Ordovician conodont *Eoplacognathus crassus* Chen & Zhang, 1993. *GFF* 119:61–65.

Zhang, J. H. 1998a. The Ordovician conodont genus *Pygodus*. In *Proceedings of the sixth European conodont Symposium (ECOS VI),* ed. H. Szaniawski. *Palaeontologia Polonica* 58:87–105.

Zhang, J. H. 1998b. Four evolutionary lineages of the Middle Ordovician conodont family Polyplacognathidae. *Meddelanden från Stockholms Universitets Institution för Geologi och Geokemi 298* (Paper 5):1–35.

Zhang, J. H. 1998c. Conodonts from the Guniutan Formation (Llanvirnian) in Hubei and Hunan Provinces, south-central China. *Stockholm Contributions in Geology* 46:1–161.

Zhang, J. H. 1998d. Review of the Ordovician conodont zonal index *Eoplacognathus suecicus* Bergström. *Meddelanden från Stockholms Universitets institution för geologi och geokemi* 298 (Paper 6):1–16.

Zhang, J. H., and Chen, M. J. 1992. Evolutionary trends and stratigraphic significance of *Periodon*. *Acta Micropalaeontologica Sinica* 9(4):391–396 (in Chinese with English abstract).

Zhang, Y. D., X. Chen, G. H. Yu, D. Goldman, and X. Liu. 2007. *Ordovician and Silurian rocks of northwest Zhejiang and northeast Jiangxi provinces, SE China*, 189 pp, University of Science and Technology of China Press, Hefei.

Zhao, S. Y., T. X. An, H. R. Qiu, S. L. Wan, and H. Ding. 1984. Conodonts. In *Palaeontological Atlas of North China, Volume III, Micropalaeontology*, ed. Tianjing Institute of Geology and Mineral Resources, 857 pp, Geological Publishing House, Beijing (in Chinese).

Zhao, X., R. S. Coe, S. A. Gilder, and G. M. Frost. 1996. Palaeomagnetic constraints on the palaeogeography of China: implications for Gondwanaland. *Australian Journal of Earth Sciences* 43:643–672.
doi:10.1080/08120099608728285

Zhao, Z. J., Z. X. Zhao, and Z. B. Huang. 2006. Ordovician conodont zones and sedimentary sequences of the Tarim Basin, Xinjiang, NW China. *Journal of Stratigraphy* 30(3):193–203 (in Chinese with English abstract).

Zhao, Z. X., and G. Z. Zhang. 1991. Subsurface Ordovician conodonts and stratigraphy of the Tarim Basin. Pp. 64–74 in *Papers on petroleum exploration in the Tarim Basin*. Science, Technology and Health Publishing House of Xinjiang, Ulumuqi (in Chinese with English abstract).

Zhao, Z. X., G. Z. Zhang, and J. N. Xiao. 2000. *Paleozoic stratigraphy and conodonts in Xinjiang*. 340 pp., Petroleum Industry Press, Beijing (in Chinese with English Abstract).

Zhen, Y. Y., and B. D. Webby. 1995. Upper Ordovician conodonts from the Cliefden Caves Limestone Group, central New South Wales, Australia. *Courier Forschungsinstitut Senckenberg* 182:265–305.

Zhen, Y. Y., and I. G. Percival. 2004a. Middle Ordovician (Darriwilian) conodonts from allochthonous limestones in the Oakdale Formation of central New South Wales, Australia. *Alcheringa* 28:77–111.
doi:10.1080/03115510408619276

Zhen, Y. Y., and I. G. Percival. 2004b. Middle Ordovician (Darriwilian) conodonts from the Weemalla Formation, south of Orange, New South Wales. *Memoirs of the Association of Australasian Palaeontologists* 30:153–178.

Zhen, Y. Y., and J. W. Pickett. 2008. Ordovician (Early Darriwilian) conodonts and sponges from west of Parkes, central New South Wales. *Proceedings of the Linnean Society of New South Wales* 129:57–82.

Zhen, Y. Y., and R. S. Nicoll. 2009. Biogeographic and biostratigraphic implications of the *Serratognathus bilobatus* fauna (Conodonta) from the Emanuel Formation (Early Ordovician) of the Canning Basin, Western Australia. *Records of the Australian Museum* 61(1):1–30.
doi:10.3853/j.0067-1975.61.2009.1520

Zhen, Y. Y., B. D. Webby, and C. R. Barnes. 1999. Upper Ordovician conodonts from the Bowan Park succession, central New South Wales, Australia. *Geobios* 32(1):73–104.
doi:10.1016/S0016-6995(99)80084-9

Zhen, Y. Y., I. G. Percival, and J. R. Farrell. 2003a. Late Ordovician allochthonous limestones in Late Silurian Barnby Hills Shale, central western New South Wales. *Proceedings of the Linnean Society of New South Wales* 124:29–51.

Zhen, Y. Y., I. G. Percival, and B. D. Webby. 2003b. Early Ordovician conodonts from far western New South Wales, Australia. *Records of the Australian Museum* 55(2):169–220.
doi:10.3853/j.0067-1975.55.2003.1383

Zhen, Y. Y., I. G. Percival, and B. D. Webby. 2004a. Early Ordovician (Bendigonian) conodonts from central New South Wales, Australia. *Courier Forschungsinstitut Senckenberg* 245:39–73.

Zhen, Y. Y., I. G. Percival, and B. D. Webby. 2004b. Conodont faunas from the Mid to Late Ordovician boundary interval of the Wahringa Limestone Member (Fairbridge Volcanics), central New South Wales. *Proceedings of the Linnean Society of New South Wales* 125:141–164.

Zhen, Y. Y., I. G. Percival, A. Löfgren, and J. B. Liu. 2007. Drepanoistodontid conodonts from the Early Ordovician Honghuayuan Formation of Guizhou, South China. *Acta Micropalaeontologica Sinica* 24(2):125–148.

Zhen, Y. Y., Y. D. Zhang, and I. G. Percival. 2009a. Early Sandbian (Late Ordovician) conodonts from the Yenwashan Formation, western Zhejiang, South China. *Alcheringa* 33:133–161.
doi:10.1080/03115510902844160

Zhen, Y. Y., I. G. Percival, R. A. Cooper, J. E. Simes, and A. J. Wright. 2009b. Darriwilian (Middle Ordovician) conodonts from Thompson Creek, Nelson Province, New Zealand. *Memoir of the Association of Australasian Palaeontologists* 37:25–53.

Zhong, D. 1990. Conodonts. 144–154, 243–247. In *Sinian to Permian Stratigraphy and Palaeontology of the Tarim Basin, Xinjiang Volume I—Kuruktag Area*, ed. South Xinjiang Petroleum Prospecting Corporation, Xinjiang Petroleum Administration Bureau, and the Institute of Petroleum and Geosciences, Dian-Qian-Gui Petroleum Prospecting Bureau. Nanjing University Press, Nanjing (in Chinese).

Zhong, D., and Y. X. Hao. 1990. Ordovician System. 40–104. In *Sinian to Permian stratigraphy and palaeontology of the Tarim Basin, Xinjiang Volume I—Kuruktag Area*, ed. South Xinjiang Petroleum Prospecting Corporation, Xinjiang Petroleum Administration Bureau, and the Institute of Petroleum and Geosciences, Dian-Qian-Gui Petroleum Prospecting Bureau. Nanjing University Press, Nanjing (in Chinese).

Zhou, D. K., T. R. Zhou, and P. Wang. 1991. Division of geological ages of Qiulitag Group in northeastern Tarim. In *Research of petroleum geology of northern Tarim Basin in China*, ed. R. X. Jia, pp. 37–43. China University of Geoscience Press, Wuhan (in Chinese with English abstract).

Zhou, Z. Y., and P. J. Chen, eds. 1990. *Biostratigraphy and Geological Evolution of Tarim*. 366 pp, Science Press, Beijing (in Chinese).

Zhou, Z. Y., and P. J. Chen, eds. 1992. *Biostratigraphy and Geological Evolution of Tarim*. 399 pp, Science Press, Beijing.

Zhou, Z. Y., and H. L. Lin. 1995. *Stratigraphy, Paleogeography and Plate-tectonics of Northwest China*. 299 pp, Nanjing University Press, Nanjing (in Chinese).

Zhylkaidarov, A. 1998. Conodonts from Ordovician ophiolites of central Kazakhstan. *Acta Palaeontologica Polonica* 43(1): 53–68.

Ziegler, W., ed. 1974. *Catalogue of Conodonts,* vol. 2. 403 pp. (Schweizerbart'sche Verlagsbuchhandlung, Stuttgart).

Addendum

While this paper was in review, it came to the attention of the authors that a paper by Stouge *et al*., presented to the 11th International Symposium on the Ordovician System, gave a slightly different biostratigraphic zonation for the early to middle Darriwilian part of the Dawangou and Yangjikan sections. Without detail of the stratigraphic ranges of the critical species of conodonts, and systematic descriptions of the fauna, it is not possible at this point to discuss the relation between the biostratigraphic scheme outlined by Stouge *et al*. (2011), and our interpretation.

Stouge, S., P. D. Du, and Z. X. Zhao. 2011. Middle Ordovician (Darriwilian) global conodont zonation based the Dawangou and Saergan formations of the western Tarim region, Xinjiang Province, China. In *Ordovician of the World*, ed. J. C. Gutiérrez-Marco, I. Ràbano & D. García-Bellido. Spain. *Cuadermos del Museo Geominero, 14.* Instituto Geológico y Minero de España, Madrid, pp. 581–586.